Cement and Concrete Research 173 (2023) 107301

Contents lists available at ScienceDirect

Cement and Concrete Research

journal homepage: www.elsevier.com/locate/cemconres

# Carbonation mechanisms and kinetics of lime-based binders: An overview

Carlos Rodriguez-Navarro *, Teodora Ilić, Encarnación Ruiz-Agudo, Kerstin Elert

*Dept. Mineralogy and Petrology, University of Granada, Fuentenueva s/n, 18002 Granada, Spain*

ARTICLE INFO

*Keywords:*
Mortar
Carbonation
Kinetics
Acceleration
Reaction
Amorphous material
Pore solution
Microstructure
$Ca(OH)_2$
$CaCO_3$

ABSTRACT

The reaction of slaked lime with atmospheric $CO_2$ in the presence of humidity leads to the formation of cementing carbonate phases in traditional aerial lime mortars and plasters. This carbonation reaction also affects the setting and degradation of hydraulic lime mortars and modern cement. Here, we present an overview of the existing knowledge on carbonation of lime-based binders, which are experiencing a revival as compatible material for the conservation of the built heritage and new sustainable construction. First, the carbonation reaction is defined and its importance in a range of technical and natural processes is outlined. This sets the ground for presenting a review of existing mechanistic models for the carbonation of lime-based materials, including the recent interface-coupled dissolution-precipitation model, and the understanding of carbonation in terms of non-classical crystallization theory. Kinetics models and experimental results for carbonation of lime-based binders (crystals and powder, as well as mortars/plasters) and its acceleration are presented and discussed. Finally, conclusions and future research directions are indicated.

## 1. Introduction

Carbonation refers to the reaction of a mineral including mono or divalent metal cations with $CO_2$ to form a solid carbonate phase. In the case of lime-based binders, carbonation is defined as the reaction of an alkaline-earth metal hydroxide with (atmospheric) $CO_2$, resulting in the crystallization of a carbonate phase as follows:

$$M(OH)_2 + CO_2 = MCO_3 + H_2O \quad (1)$$

where M is either $Ca^{2+}$ or $Mg^{2+}$. This is a highly exothermic reaction ($\Delta H = +74$ kJ mol$^{-1}$ for the case of $Ca(OH)_2$ carbonation) that spontaneously takes place under Earth surface *P-T* conditions [1].

Carbonation is largely responsible for the setting and hardening of lime-based binders used in old and modern constructions (Fig. 1a). It is the main process responsible for strength development of aerial lime binders, both calcitic (high-calcium) and dolomitic (or magnesian) limes [2,3]. Carbonation also occurs to a significant extent in hydraulic limes [4,5], where the main setting and strengthening mechanism is however the hydration of calcium silicate (and aluminate) phases (i.e., natural hydraulic limes), or the reaction of portlandite ($Ca(OH)_2$) with a pozzolanic material (i.e., artificial hydraulic limes or ancient Roman concrete, i.e., *Opus caementicium*), forming a matrix of calcium silicate (and aluminate) hydrate phases (CSH, CAH, CASH) [6–10].

Carbonation is also a common and thoroughly studied process in Portland cement [11–17]. On the one hand, the highly alkaline pH reached during the hydration of cement can lead to the early precipitation of $CaCO_3$, which aids in early strength gain [18]. Accelerated carbonation curing of concrete is thus considered as an effective means for gaining early strength while at the same time contributing to $CO_2$ sequestration [19–21]. On the other hand, portlandite, CSH and ettringite ($Ca_6Al_2(SO_4)_3(OH)_{12}{\cdot}26H_2O$) formed upon cement hydration can undergo carbonation when the set and hardened cement is exposed to atmospheric $CO_2$ or carbonate-bearing fluids [15,22–24]. Such a secondary carbonation process can be highly deleterious, resulting in the degradation (cracking and spalling) of cement and concrete structures, particularly in the case of reinforced concrete, as the reaction results in a pH decrease from ~12.5 in uncarbonated cement, to ≤10 in carbonated cement, facilitating corrosion of the steel reinforcing elements [25]. Corrosion products with high molar volume generate internal stresses and cause cracking of the cover concrete aligned in the direction of reinforcing iron bars. Fig. 1b shows a dramatic example of such a degradation.

Carbonation of cement can result in the formation of deleterious, highly soluble alkali carbonate salts such as trona ($Na_3(CO_3)(HCO_3){\cdot}2H_2O$), natrite ($Na_2CO_3$), thermonatrite ($Na_2CO_3{\cdot}H_2O$), natron ($Na_2CO_3{\cdot}10H_2O$), kalicinite ($KHCO_3$) and potash ($K_2CO_3$). Alkalis (Na and K) are commonly present as impurities in cement clinker, and upon chemical weathering (dissolution) of set cement, such alkalis can be

* Corresponding author.
*E-mail address:* carlosrn@ugr.es (C. Rodriguez-Navarro).

https://doi.org/10.1016/j.cemconres.2023.107301
Received 17 March 2023; Accepted 3 August 2023
Available online 17 August 2023

leached [26]. The resulting alkali-rich, high-pH pore solutions foster the dissolution and hydration of atmospheric $CO_2$, forming $CO_3^{2-}$-rich solutions and leading to the precipitation of Na and K (along with Ca) carbonates. While formation of secondary $CaCO_3$ might have a protective effect [26], crystallization of alkali carbonates within the pore system of cement or adjacent building materials such as stone or bricks can produce substantial damage. It is recognized that sodium carbonates are, along with sodium sulfates, the most deleterious salts affecting building materials [27,28] as they are able to precipitate at relatively high supersaturations, resulting in high crystallization pressures, typically higher than the tensile strength of most building materials [29–34]. As an example, Fassina et al. [35] report degradation of marble at the S. M[a] dei Miracoli church in Venice due to the crystallization of sodium carbonate associated with the improper use of (chemically and mechanically incompatible) Portland cement during a conservation intervention. Problems like this one, which underline the incompatibility and deleterious effects of the use of modern cement in the conservation of the built heritage, have contributed to the revival of traditional lime-based binders for the conservation of ancient masonry [3,36,37].

Carbonation has been demonstrated to be an effective mechanism for the setting and hardening of low-lime calcium silicate cements [13,38,39]. As opposed to traditional hydration setting and hardening of high-lime calcium silicates (i.e., belite, $2CaO{\cdot}SiO_2$, and alite, $3CaO{\cdot}SiO_2$) in Portland cement (which takes place following a dissolution-precipitation process, see Juilland et al. [40]), low-lime cements include non-hydraulic phases such as wollastonite ($CaSiO_3$) and/or rankinite ($Ca_3Si_2O_7$) that react with $CO_2$ (at relatively high $CO_2$ pressure and *T*) to form calcium carbonates plus silica that provide a compact and mechanically sound structure [38,39,41]. This class of cements with reduced carbon footprint might find numerous applications, such as the fabrication of pre-cast concrete elements or the sealing of $CO_2$ injection wells during geologic carbon sequestration (GCS) [42].

Due to its importance in cementitious materials, especially in cement, carbonation has been experimentally studied and quantified using a range of analytical techniques [43]. Among them, we can list thermogravimetric analysis coupled to differential scanning calorimetry (TGA-DSC), differential thermal analysis (DTA), and X-ray diffraction (XRD), which enable to measure the content of $CaCO_3$ along a carbonation profile. A simple and widely used method to evaluate the progress of the carbonation front with depth involves phenolphthalein spraying on freshly cut mortars specimens. Other techniques are, for instance, scanning electron microscopy (SEM), optical microscopy, Raman spectroscopy, and micro-computed X-ray tomography (micro-CT) [43,44]. All of them have been used to analyze the carbonation of lime mortars and plasters [45–47].

From an environmental perspective, carbonation is of global significance as it contributes to the draw-down of atmospheric $CO_2$ and the regulation of Earth's climate over geologic timescales ($>10^6$ years) [48,49]. Carbonation takes place in nature following Earth's surface chemical weathering of primary silicates including divalent metals such as $Ca^{2+}$, $Mg^{2+}$ or $Fe^{2+}$. This is the case of minerals such as olivine ($FeMgSiO_4$), serpentine ($Mg_3Si_2O_5(OH)_4$), pyroxenes ($MgSiO_3$, $CaSiO_3$, $FeSiO_3$), and Ca-plagioclase ($CaAl_2Si_2O_4$), which upon reaction with $CO_2$ in an aqueous environment result in the precipitation of carbonate phases such as calcite ($CaCO_3$), hydrated magnesium carbonates (at low *T*) or magnesite ($MgCO_3$) (at high *T*) or siderite ($FeCO_3$) (under conditions of low oxygen fugacity), and $SiO_2$ or other secondary aluminosilicate phases [50,51]. The overall carbonation of primary silicates is given by the following Urey-type reaction [51,52]:

$$(Mg, Ca, Fe)_xSi_yO_{x+2y-t}(OH)_{2t} + xCO_2 = x(Mg, Ca, Fe)CO_3 + ySiO_2 + tH_2O \quad (2)$$

Such a natural process contributes to the safe and stable geological mineral storage of C on the Earth surface and subsurface for millions of years. This type of reaction has drawn significant attention in the last few decades because carbonation of primary silicates has emerged as a technology for both in situ and ex situ mineral carbon capture and storage (CCS) aimed at reducing anthropogenic $CO_2$ emission and the draw-down of the concentration of atmospheric $CO_2$, a greenhouse gas claimed responsible for the on-going global warming [53,54]. Related to CCS, the search for more sustainable ways to dispose industrial alkaline wastes have led to their use as supplementary cementitious materials in cement as well as for mineral carbon capture [55]. It has been recently


**Fig. 1.** Lime carbonation: positive and negative effects. a) Masonry structure of the XIIth century Colegiata of Santillana del Mar (Spain) built using sandstone blocks and aerial lime mortar; b) the deleterious effect of delayed carbonation of a reinforced concrete structure (II World War submarine bunker Valentine, Bremen, Germany). Massive loss of concrete scales associated with steel bar corrosion upon carbonation is observed, along with carbonate efflorescence/encrustation (white stains). See detail in inset.

estimated that carbonation of Ca- and Mg-rich alkaline industrial residues such as fly ash, cement kiln dust, steel slag, and red mud can result in the permanent and safe storage of about 200–300 Mt of $CO_2$ annually by forming Ca and/or Mg carbonates [56]. Such waste materials (also including carbide lime and paper mill sludge) are of high interest for their potential use as additives (e.g., pozzolanic additives) or as $Ca(OH)_2$ sources for lime-based binders, enabling to reduce the carbon footprint of the cement industry. Also, low *T* direct air capture of $CO_2$ using CaO and/or $Ca(OH)_2$ for carbonation/decarbonation cycling is drawing attention in recent years [57].

Due to its many technological applications and environmental implications, the carbonation reaction has been extensively studied, not just in the case of cement, but also in the case of lime-based building materials (e.g., refs. [1,36,45,47,58–75]), which are experiencing a revival, especially in the field of heritage conservation due to their high compatibility with ancient structures [3,37,76–78]. However, despite significant recent progress, there are still several aspects of the mechanism and kinetics of carbonation that are not well understood.

Here we present a general overview of the carbonation of lime-based binders, focusing both on the mechanism(s) underlying this reaction, as well as its kinetics. Particular attention is paid to the understanding of carbonation in terms of the recently proposed non-classical crystallization theory. We also pay attention to the interface-coupled dissolution-precipitation (ICDP) model for mineral replacement reactions [71] to explain how, from a mechanistic point of view, carbonation takes place at the individual portlandite crystal level. Additionally, we focus here on progress made regarding the better understanding of this reaction and its implications in the performance of lime mortars and plasters. Finally, general conclusions about the mechanism and kinetics of carbonation of lime-based binders, as well as possible research directions to further advance the understanding of the carbonation of lime mortars and plasters, and the optimization of this fundamental process are outlined.

## 2. Carbonation within the frame of the lime cycle

Lime mortars and plasters have been used for decorative and building purposes since the origin of pyrotechnology in the Levant ca. 10,000–12,000 BCE [79–82]. Lime was the binder of choice until the invention of Portland cement back in the XIX century, which phased-out lime as the primary binder in building and construction [3,83]. In recent decades, however, lime-based binders have experienced a revival as compatible and more environmentally friendly materials, as compared with Portland cement, for the conservation of the built heritage and are finding applications in modern sustainable construction [37,84,85]. The preparation and setting/hardening of lime-based binders involve a series of sequential steps collectively known as the lime cycle [2,3,37,72], schematically shown in Fig. 2 for the case of calcitic lime and in Fig. 3 for dolomitic lime. Below, we present a brief overview of the main features of each step of the lime cycle.

### 2.1. Calcination

The first step of the lime cycle involves the calcination of carbonate rocks. If the calcined rock is a limestone or a calcitic marble, i.e., basically made of calcite, the material resulting from its calcination is CaO (quicklime), produced via the reaction,

$$CaCO_3 = CaO + CO_2 \quad (3)$$

This is a highly-endothermic, solid-state topotactic reaction, which starts (under atmospheric *P*) at ~600 °C [86] and is typically performed in lime kilns at *T* between 750 and 900 °C [2,3]. In contrast, if the carbonate rock used for calcination is a dolostone (made up of dolomite, $CaMg(CO_3)_2$), the reaction progresses according to what is commonly known as "two-step calcination" via the reactions [87],

$$CaMg(CO_3)_2 = MgO + CaCO_3 + CO_2 \quad (4)$$

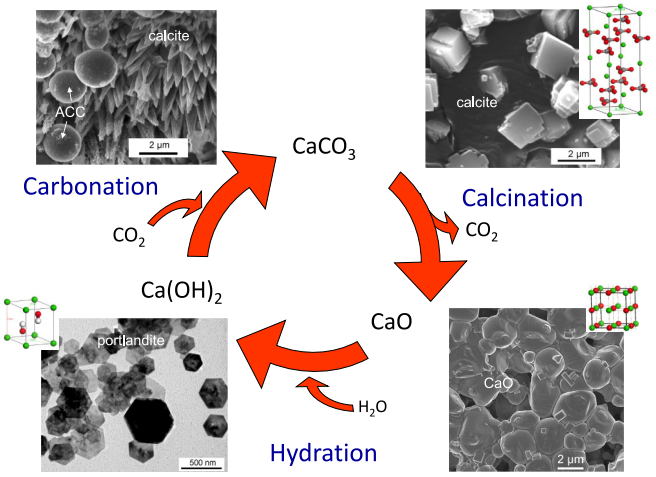


**Fig. 2.** The lime cycle of calcitic lime. Modified from [72].

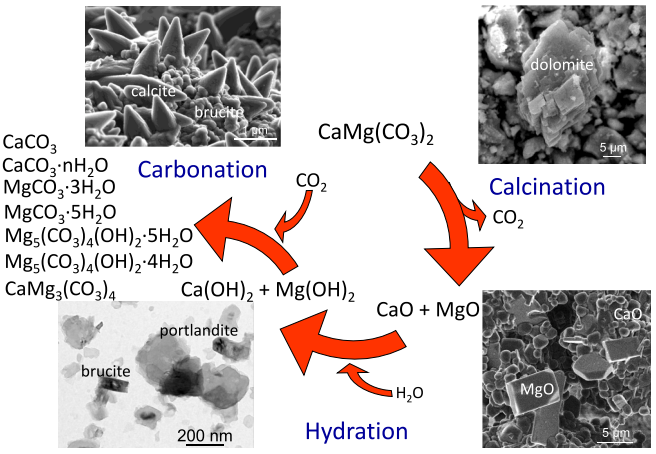


**Fig. 3.** The lime cycle of dolomitic lime. Note that the cycle is not closed, because the end-product of carbonation is not the starting dolomite, but a full range of calcium and magnesium carbonate phases.

$$CaCO_3 = CaO + CO_2 \quad (5)$$

Note, however, that Rodriguez-Navarro et al. [72] have demonstrated that this reaction involves the initial decomposition of dolomite at relatively low *T* (~500 °C) into a mixed Ca—Mg oxide, which rapidly undergoes spinodal decomposition into CaO plus MgO. The newly formed CaO is highly reactive and re-carbonates in the kiln (via a gas-solid reaction) to form $CaCO_3$ that further decomposes at a higher *T* into CaO and $CO_2$. In contrast, the newly formed MgO is less reactive towards $CO_2$, which prevents its re-carbonation, so that it only experiences further growth (sintering) as *T* increases during calcination. This decomposition mechanism has profound effects on the reactivity of the resulting oxides (i.e., highly reactive CaO and poorly reactive MgO), and determines the properties of the products obtained in the subsequent steps of the (dolomitic) lime cycle. Note that industrially, the products of the calcination of dolomite rocks are known as "dolime", and in some cases the dolomitic lime cycle is known as the "dolime cycle" [88].

There is also the possibility of using rocks made of magnesite for the preparation of magnesian limes [88]. These rocks, however, are rare, as compared with limestones, calcitic and dolomitic marble, or dolostones. Nonetheless pure magnesian limes can be produced by the calcination of for instance, magnesite-rich bodies in serpentinite rock outcrops or magnesite marble, via the reaction,

$$MgCO_3 = MgO + CO_2 \quad (6)$$

### 2.2. Hydration or slaking

The second step of the lime cycle involves the hydration (or slaking) of the oxide(s) to form either portlandite in the case of calcitic limes, or portlandite plus brucite $Mg(OH)_2$ in the case of dolomitic limes, via the following reactions:

$$CaO + H_2O = Ca(OH)_2 \quad (7)$$

$$MgO + H_2O = Mg(OH)_2 \quad (8)$$

Hydration is a highly exothermic process which can be performed by adding to the oxide an amount of water slightly in excess of the stoichiometric amount or adding a significantly higher amount of water than the stoichiometric amount. In the first case the hydrated lime forms a more or less dry powder, whereas in the second case, lime putty (a dispersion of portlandite crystals in water) is obtained [2,89]. Powder lime, also known as dry hydrated lime, can be readily bagged and is the main product of current industrial lime production, typically performed using steam hydrators [2]. Conversely, lime putties were the most common traditional products used in construction since the origins of pyrotechnology [3]. One of the main advantages of the use of slaked lime putties is the fact that their rheological properties and reactivity improve upon long term storage under water. This so-called "aging" process results in the development of sub-micrometer sized plate-like portlandite crystals [89] that are highly reactive (i.e., have a high specific surface area) and impart a high plasticity to the lime paste [90]. In turn, drying is avoided (as it occurs during the preparation of a dry hydrate) thereby preventing detrimental particle coarsening via drying-induced irreversible oriented aggregation [91].

### 2.3. Carbonation

The third, and final, step of the lime cycle involves the carbonation of Ca and/or Mg hydroxides to form calcium and/or magnesium carbonates. This way the end-product of the cycle is similar (compositionally, but not texturally/structurally) to the starting phase(s) in the uncalcined raw carbonate rock used to produce lime. However, this is only (partially) true in the case of calcitic limes, as the end-product is typically calcite, the same mineral present in the starting limestone or calcitic marble. It is, however, not true in the case of dolomitic limes (see below).

#### 2.3.1. Phases formed upon carbonation

In the case of calcitic lime, the stable end-product of carbonation is calcite [36,69,73]. However, other anhydrous metastable polymorphs have been observed to develop during the carbonation of portlandite [75,92]. Indeed, one interesting aspect of the carbonation of calcitic lime mortars and plasters is the formation of metastable $CaCO_3$ phases. While the Ostwald rule of stages predicts that both vaterite and aragonite could precede the formation of stable calcite [93], it is rather unclear why in some fully carbonated lime mortars and plasters, even in the case of historical buildings, vaterite and aragonite are still present [94–96]. It is likely that in the case of vaterite, its formation and stabilization is due to the presence of organic additives in the original mortar mix [96–98]. It has been widely reported that organics foster the formation and stabilization of vaterite [99]. Conversely, it is observed that in lime mortars without organics vaterite forms (in concentrations $< 5$ wt%) during the early stage of carbonation (both under normal and accelerated carbonation curing conditions) but readily transforms into more stable calcite over time, i.e., weeks or months [92]. However, it is not that clear why aragonite forms and is preserved in lime mortars. The presence of this phase is of special relevance to differentiate (man-made) pyrogenic and (natural) geogenic $CaCO_3$ in archaeological sites. Toffolo [100] has shown that upon hydration of CaO derived either from wood ash or from limestone calcination, the resulting hydrated lime carbonates producing a fraction of aragonite. It could be argued that aragonite forms because of the presence of Mg in the calcined material. It is well-known that Mg inhibits the precipitation of calcite and favors the crystallization of aragonite [101] as it has been observed in the case of dolomitic lime [102]. Toffolo [100], in contrast, has confirmed that aragonite forms in Mg-free lime plasters, suggesting that (likely for kinetic reasons) aragonite precipitates upon carbonation in the highly alkaline and reactive solution derived from the hydration of pyrogenic CaO. Identification of original pyrogenic carbonates in archaeological sites is key not just to disclose the presence of lime plasters and mortars, but also for an accurate $^{14}C$ dating [100].

In the case of dolomitic limes, the end product of carbonation (in addition to Mg-calcite and metastable vaterite and/or aragonite), is not dolomite or magnesite, but a number of hydrated magnesium carbonate and hydroxycarbonate phases such as nesquehonite ($MgCO_3{\cdot}3H_2O$), landsfordite ($MgCO_3{\cdot}5H_2O$), dypingite ($Mg_5(CO_3)_4(OH)_2{\cdot}5H_2O$), artinite ($Mg_2CO_3(OH)_2{\cdot}3H_2O$), giorgiosite ($Mg_5(CO_3)_4(OH)_2{\cdot}5H_2O$), and hydromagnesite ($Mg_5(CO_3)_4(OH)_2{\cdot}4H_2O$), or even a mixed Ca—Mg carbonate such as huntite ($CaMg_3(CO_3)_4$) [102–108]. Neither dolomite nor magnesite forms upon carbonation of dolomitic limes because such phases do not precipitate under standard *P-T* conditions on the Earth surface due to kinetics reasons. This is the root-cause of the so-called "dolomite problem", which is based on the fact that, for yet unknown reasons, dolomite was very common in the geologic past but extremely scarce in the recent geologic record, and its low *T* (abiotic) synthesis in the laboratory has systematically failed [101].

#### 2.3.2. Role of aggregate and additives

For practical building or decorative applications, hydrated limes are typically mixed with an aggregate (carbonatic or silicic in nature) to prepare plasters and mortars once they are mixed with water [77]. Such products are applied in the fresh state by masons either as structural mortars or as finishing plasters or renders. Upon application, they experience drying and their subsequent carbonation. As a result of this reaction, an interconnected microstructure of calcium carbonate crystals forms which is responsible for the strength development of the mortar or plaster [65]. For a full understanding of their carbonation both from a mechanistic and a kinetic point of view, the effects of the mixing water and the aggregate, as well as the binder:aggregate ratio, on the development of the set and hardened mortars or plasters phase composition and (micro)structure (i.e., porosity, pore size distribution, and pore network connectivity) have to be considered [77,109,110].

There is another important aspect to consider when studying the carbonation of lime mortars and plasters: natural (and more recently artificial) organic and inorganic additives or admixtures were/are often added to the lime-based mortars and plasters (either during lime slaking or mortar/plaster preparation) to improve the fresh and set state properties of the mixes [80,111,112]. In ancient Europe, India and other regions, plant extracts, fruit juices, oils, animal fats and even blood or beer were added to slaked lime to improve the properties of mortars and plasters [111,112,113]. Chinese builders traditionally used sticky rice (amylopectin-rich) as additive, which enables the formation of a more compact and durable calcite matrix after carbonation, imparting a high durability to lime mortars [113]. Ethnohistoric, archaeological and analytical evidence shows that pre-Columbian civilizations in Mesoamerica (e.g., ancient Maya and Aztec) used plant extracts to improve the properties of lime mortars, plasters and stuccoes [115–119]. However, how such additives affect the dynamics and kinetics of the carbonation process undergone by the lime binder is not well known, currently being the subject of intensive research.

## 3. Carbonation chemistry

Once a fresh lime paste (i.e., a lime plaster or mortar) is applied in place, it will first undergo drying. According to Van Balen and Van

Gemert [109] this results in an initial strength gain (basically due to capillary forces). During this early stage, incipient carbonation can take place. However, carbonation of the saturated material is very limited because the diffusion rate of $CO_2$ in an aqueous solution is ~10,000 lower than in air [64]. Therefore, only a thin surface layer of the fresh saturated paste will be carbonated during this early stage. Subsequently, upon further drying an accelerated event of carbonation takes place. However, full carbonation may only be reached after long exposure to atmospheric $CO_2$ (months, years or even centuries) [47]. This is so because the carbonation process is complex and includes several rate-limiting steps that control how $CO_2$ is dissolved in the pore water and reach the portlandite crystals surface, how it diffuses through the (saturated or open) pore system of the lime mortar or plaster from the (carbonated) surface to the (uncarbonated) interior, and how the carbonation reaction progresses from the surface of the portlandite crystals to their core through a carbonate product layer [1,69]. To these steps, which can be rate-limiting, it must be added the effect of the diffusion of $H_2O$ product, from the reaction interface out to the external surface of the lime plaster or mortar, followed by its evaporation [109]. Fig. 4 graphically shows these effects.

### 3.1. Reactions and rate-controlling steps

Carbonation of calcium hydroxide involves the chemical reaction between atmospheric carbon dioxide and $Ca(OH)_2$ dissolved in the pore water of the mortar, resulting in the precipitation of calcium carbonate according to the general eq. [47,61]:

$$Ca(OH)_2\ (s) + CO_2\ (g) + H_2O\ (aq) = CaCO_3\ (s) + 2H_2O\ (aq) \quad (9)$$

Note that $H_2O$ is included in the left and right terms of this equation to highlight the crucial role water plays in the reaction (see below). The reaction is exothermic and proceeds spontaneously under standard *P-T* conditions [1].

In the case of dolomitic limes, there are several possible overall carbonation reactions for magnesium hydroxide, such as:

$$Mg(OH)_2 + CO_2 + 2H_2O \rightarrow MgCO_3{\cdot}3H_2O\ (\text{nesquehonite}) \quad (10)$$

$$5Mg(OH)_2 + 4CO_2 \rightarrow Mg_5(CO_3)_4(OH)_2{\cdot}4H_2O\ (\text{hydromagnesite}) \quad (11)$$

$$5Mg(OH)_2 + 4CO_2 + H_2O \rightarrow Mg_5(CO_3)_4(OH)_2{\cdot}5H_2O\ (\text{dypingite}) \quad (12)$$

If we focus on the carbonation reaction of high-Ca lime, the most common in building applications, the overall carbonation reaction in Eq. (9) involves the following steps [1,69,120–122]: (i) continuous dissolution of calcium hydroxide in the pore water with dissociation of $Ca^{2+}$ and $OH^-$ ions (Eq. (13)); (ii) dissolution of gaseous $CO_2$ into the alkaline pore solution to form a loosely hydrated aqueous form (Eq. (14)); (iii) hydration of $CO_2$ with $OH^-$ ions to form carbonic acid ($H_2CO_3$) followed by its (nearly instantaneous) dissociation into bicarbonate ($HCO_3^-$) (Eq. (15)) and carbonate ($CO_3^{2-}$) ions (Eq. (16)) and, finally, (iv) the reaction between $Ca^{2+}$ and $CO_3^{2-}$ ions forming a calcium carbonate precipitate through nucleation and subsequent growth resulting in an interconnected microstructure (Eq. (17)) [1,69,70].

$$Ca(OH)_2\ (s) = Ca^{2+}\ (aq) + 2OH^-\ (aq) \quad (13)$$

$$CO_2\ (g) = CO_2\ (aq) \quad (14)$$

$$CO_2\ (aq) + OH^-\ (aq) = HCO_3^-\ (aq) \quad (15)$$

$$HCO_3^-\ (aq) + OH^-\ (aq) = CO_3^{=}\ (aq) + H_2O\ (aq) \quad (16)$$

$$Ca^{2+}\ (aq) + CO_3^{=}\ (aq) = CaCO_3\ (s) \quad (17)$$

The same equations describe the carbonation of brucite present in dolomitic limes (i.e., replacing Ca with Mg in Eqs. (13) and (17), but considering that the end product is a hydrated phase).

All these reaction steps are interrelated and altering the kinetics of one of them influences the others [69]. The order of these individual reaction steps offers a complex mechanism that is pH-dependent because of its strong effect on the speciation of carbonic species [120,123,124]. At pH > 10, which represents the situation of the pore solution in carbonating lime mortars, $HCO_3^-$ ions can readily form by the direct reaction of carbon dioxide and $OH^-$ ions at a forward reaction rate $8 \times 10^3$ L mol$^{-1}$ s$^{-1}$ (Eq. (15)) [122]. Because the rate of Eq. (16) is faster than that of Eq. (15), and Eq. (17) is known to be instantaneous, Eq. (15) therefore is the rate-controlling step at this highly alkaline pH range. At lower pHs (8 < pH < 10), representative of a more advanced stage of the carbonation reaction, the direct hydration of carbon dioxide with water, $CO_2 + H_2O = H_2CO_3$, and the subsequent dissociation of carbonic acid to form bicarbonate ions, will compete with Eq. (15), whose rate decreases as pH decreases in a carbonate-bicarbonate buffer. At pH < 8, representative of the final stage of the carbonation process, the direct hydration of carbon dioxide with water has a forward reaction rate of $1.1 \times 10^{-3}$ L mol$^{-1}$ s$^{-1}$ at 25 °C, which is six orders of magnitude lower than that of Eq. (15) [122]. This slow reaction leads to the formation of $HCO_3^-$ and $H^+$, making the solution more acidic. As a result, precipitated calcium carbonate may undergo (partial) dissolution at such acidic conditions until the pore solution reaches saturation with respect to $CaCO_3$, thus increasing the pH up to ~8.5–9 [125]. This will enable further restructuring/regrowth of the calcite crystals, which typically change their shape from scalenohedral to rhombohedral [69]. Cizer et al. [69] have shown that the high $[Ca^{2+}]/[CO_3^{2-}]$ ratio during the early carbonation of lime plasters favors the formation of calcite crystals with scalenohedral morphology. However, upon further progress of the carbonation reaction, such crystals tend to evolve into rhombohedral shaped calcite crystals via a dissolution-reprecipitation process [69]. Such a morphological evolution can have a significant impact on the structure and physical-mechanical properties of the set and hardened lime mortars [92].

In general terms, and irrespectively of the pH, the slow conversion of carbon dioxide into $HCO_3^-$ is the rate-controlling step of the carbonation reaction [123,124,126] and significantly limits the yield of the overall reaction.

### 3.2. Solid-state vs. through-solution reaction: the role of $H_2O$

There is another critical rate-limiting factor during carbonation of $Ca(OH)_2$: water availability. It has been known for more than a century that little or no carbonation of portlandite takes place in dry or very low relative humidity (RH = $100(pH_2O/pH_2O_{sat})$, where $pH_2O$ and $pH_2O_{sat}$ are the partial pressure of water under actual and saturation conditions, respectively) conditions at room *T* [127]. This observation suggests that the formation of $CaCO_3$ during portlandite carbonation is a through-solution process at room *T* [61,128]. It has been shown, however, that in nominally dry (RH < 0.01 %), low $pCO_2$ and room *T* conditions, powder $Ca(OH)_2$ can undergo carbonation by physisorption of $CO_2$ followed by chemisorption, with further progress of the reaction catalyzed by product $H_2O$ [129]. Yet, Potinga et al. [129] state that water molecules present in the system would already be physisorbed on portlandite crystals to kick-start the carbonation process. In any case, the authors reported that the carbonate yield under such dry conditions was almost negligible. Shih et al. [62] and Montes-Hernandez et al. [130] also pointed to the autocatalytic role of $H_2O$ released during the carbonation reaction. In all these cases carbonation was assumed to be a gas-solid reaction, that is, a solid-state reaction, which might be relevant in terms of reaction rate for the carbonation of $Ca(OH)_2$ at high *T* (>200 °C) when ion mobility is sufficiently rapid as to facilitate substitution of $OH^-$ by $CO_3^{2-}$, resulting in a change of $d_{001}$-spacing of portlandite and the progress of carbonation [131]. A solid-state model, however, does not explain why a few adsorbed monolayers of $H_2O$ on portlandite particles are necessary to enable the progress of carbonation at room *T* at a significant rate [132], because the presence of water is not

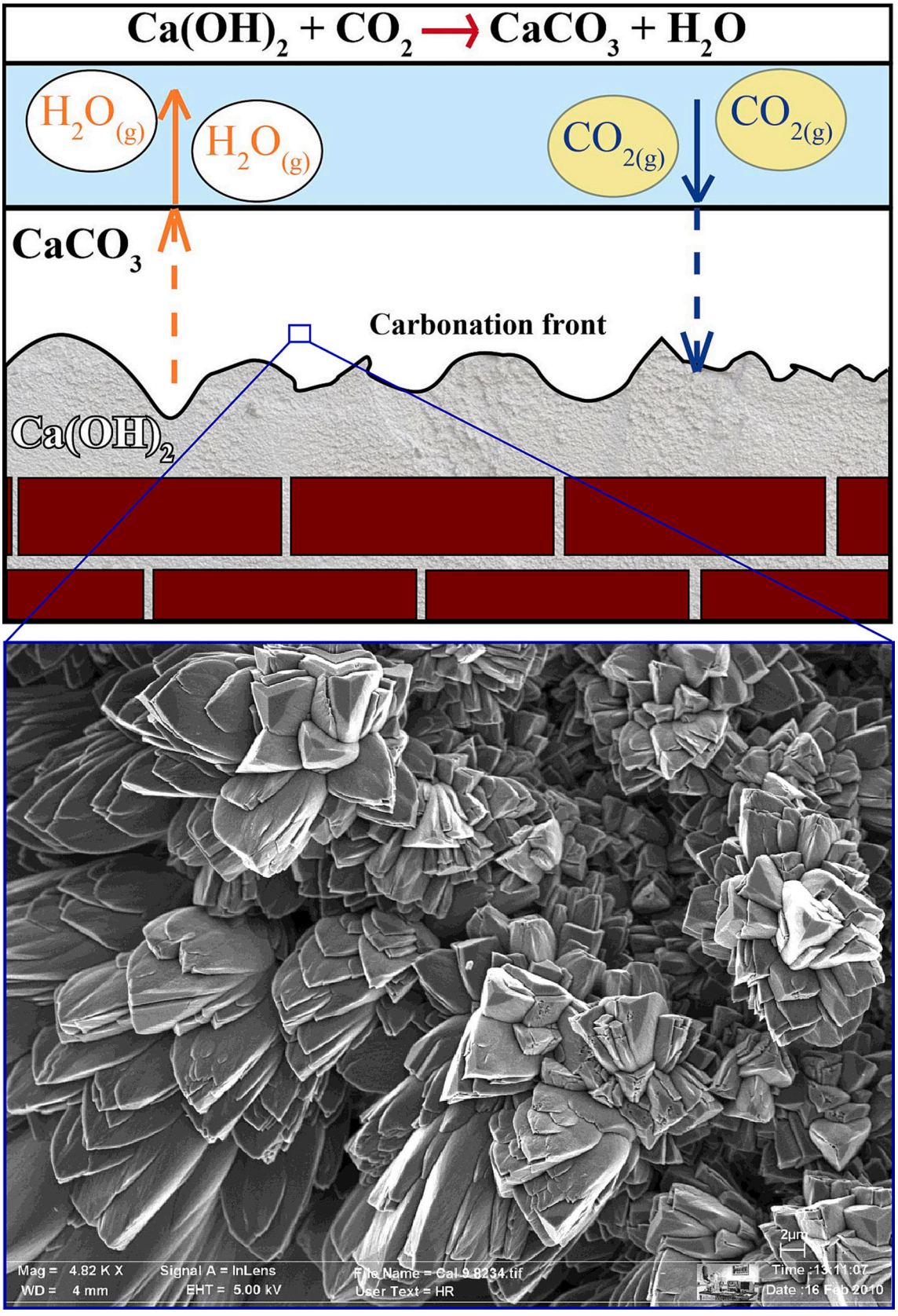


**Fig. 4.** The carbonation of lime plasters: Scheme of the progress of the carbonation front across a lime render. Note the counter diffusion of $CO_2$ (reactant) and $H_2O$ (product). The FESEM photomicrograph shows a detail of the calcite crystals structure formed after carbonation of $Ca(OH)_2$.

required during a solid-state reaction. Conversely, water is critical during a reaction involving dissolution followed by or coupled to precipitation [133]. Further analyses have clearly demonstrated that, indeed, for carbonation of $Ca(OH)_2$ at room *P-T* conditions to progress at a significant rate, the presence of $H_2O$ even in very low quantities (i.e., adsorbed monolayers) is required [75,132]. Water adsorbed on portlandite enables its (partial) dissolution according to Eq. (13). As a result, $CO_2$ can readily dissolve and hydrate forming bicarbonate and carbonate ions in the high pH aqueous solution in contact with the portlandite substrate, thus enabling $CaCO_3$ precipitation. Note, however, that the high-*T* (>200 °C) carbonation of $Ca(OH)_2$, as well as CaO, which has been thoroughly studied both from a mechanistic and kinetic point of view due to its relevance for $CO_2$ mineral capture and thermochemical energy storage, is considered a true gas-solid (solid-state) reaction [134–136].

In the following sections we will further explore the mechanism of carbonation involving dissolution, with a focus on the carbonation of $Ca(OH)_2$ (and $Mg(OH)_2$) at room *T* and atmospheric $pCO_2$, conditions most relevant for the setting and hardening of lime-based binders.

## 4. Carbonation mechanism: a non-classical crystallization view

The actual mechanism resulting in the conversion of Ca (or Mg) hydroxide into a product carbonate phase has been the subject of extensive research. Early studies on the carbonation of hydrated lime are summarized by Boynton [2], and more recent ones are presented in refs. [1,10,36,37,45,47,64–75,77,102]. They focused on the analysis of the reaction of Ca (or Mg) hydroxide with $CO_2$ in an aqueous solution, observing the evolution of the reaction and determining the product phases. Yet, it is not fully clear how the carbonate phase nucleates and grows in such an aqueous solution.

### 4.1. Carbonation and classical nucleation theory

It has been commonly assumed that carbonation leads to the direct precipitation of a particular crystalline carbonate phase, typically stable calcite in the case of high calcium lime plasters [2]. Nucleation and growth of this product phase is explained in terms of classical nucleation theory (CNT), which is rooted on the seminal works by Gibbs [137,138], further developed by Volmer and Weber [139] and Becker and Döring [140], among others, for the specific case of the nucleation of a solid phase from solution. According to CNT the formation of a solid in a solution is a first-order phase transition occurring once an aggregate or cluster of monomers (atoms, ions or molecules) that continuously form and disintegrate, reaches a critical size $r_c$, that enables spontaneous growth to a macroscopic size via monomer-by-monomer incorporation into the crystal lattice [141]. For this to happen, a free energy barrier $\Delta G$ must be overcome, which involves two competing factors: the free energy consumption needed for the creation of a new surface, $\Delta G_s$, and the energy released by the formation of the bulk solid phase, $\Delta G_v$,

$$\Delta G = \Delta G_v + \Delta G_s = -\frac{\frac{4}{3}\pi r^3}{v_m} kTln\left(\frac{a}{a_c}\right) + 4\pi r^2\gamma \tag{18}$$

where *r* is the size of the cluster, $v_m$ its molar volume, *k* the Boltzmann constant, *T* the temperature, *a* and $a_c$ are the ionic activity in solution and the (equilibrium) ion activity of the newly formed solid phase, respectively, $a/a_c$ is the supersaturation of the system, and γ is the surface energy of the solid phase. Taking the derivative of Eq. (18) and setting it equal to zero, the value of $r_c$, that is, the radius of a nuclei where the surface and volume terms of Gibbs energy are equal, is obtained,

$$r_c = \frac{2v_m\gamma}{kTln\left(\frac{a}{a_0}\right)} \tag{19}$$

This equation shows that the radius of the critical cluster in equilibrium with a supersaturated solution is proportional to its surface energy and inversely proportional to the system's supersaturation and *T*. This means that it is thermodynamically more favorable to nucleate a new phase (with smaller $r_c$) at high rather than at low supersaturation. From Eqs. (18) and (19) the free energy barrier for nucleation, $\Delta G^*$ is given by,

$$\Delta G^* = \frac{16\pi {v_m}^2\gamma^3}{3\left[kTln\left(\frac{a}{a_0}\right)\right]^2} \tag{20}$$

Eq. (20) shows that the free energy barrier varies with the cube of γ, underlining that the surface energy of the crystal nuclei is a critical parameter during nucleation. However, this parameter is very difficult to determine with accuracy, limiting the applicability of CNT [141,142].

Fig. 5 shows the evolution of $\Delta G$ considering a CNT scenario (i.e., calculated using Eq. (18) and considering the variation of cluster size as the reaction coordinate), evidencing that there is a maximum, $\Delta G^*$, given by Eq. (20), that must be overcome for the system to reach the minimum free energy, represented by the stable crystalline product phase. Note that Eqs. (19) and (20) are directly applicable for homogeneous nucleation. In most cases, and particularly for the case of lime carbonation, there are however pre-existing surfaces that favor heterogeneous nucleation resulting in lower values of $\Delta G^*$ than those determined for homogeneous nucleation [143–145].

### 4.2. Carbonation in the light of non-classical crystallization theory

CNT shows that there is a high energy barrier for the nucleation of a solid phase to occur. However, there is the possibility of reaching the energy minima of the system without necessarily overcoming the energy barrier determined by CNT using Eq. (20). As shown by Fig. 5, if the transition from the solution to the stable crystalline phase proceeds via a series of (meta)stable states, it is possible to bypass such a high nucleation barrier [146,147]. This possibility, which considers crystallization not just under thermodynamic but also under kinetic control [146], is at the root of the so-called non-classical crystallization (NCC) theory.

The CNT view of crystal formation is currently challenged by an increasing body of theoretical, computational, and experimental studies disclosing alternative crystallization processes and routes, including the existence of stable pre-nucleation clusters (PNC) [148], liquid [149,150] and solid amorphous precursor phases [74,75,119,151,152] during the pre- and post-nucleation stages. Moreover, it has been shown that growth of a newly formed solid phase (amorphous or crystalline) does not necessarily progress via monomer addition as predicted by CNT. It can take place via the addition or aggregation of nanoparticles (amorphous or crystalline), including oriented-aggregation (OA) and mesocrystal formation [152]. All these processes are considered as "non-classical" crystallization routes, which are schematically presented in Fig. 6.

NCC plays a crucial role in the formation of carbonates, being particularly relevant for the case of lime-based binders undergoing carbonation. Gebauer et al. [148] demonstrated that the formation of $CaCO_3$ is preceded by the formation of "stable prenucleation clusters" (PNCs) with size below the critical radius (<1–2 nm). Upon aggregation, such clusters, which are described as "dynamically ordered liquid-like oxyanion polymers" (DOLLOPs) [153], can lead to liquid-liquid phase separation forming highly hydrated liquid-like entities, which upon water exclusion and densification result in the formation of an amorphous solid: amorphous calcium carbonate (ACC) [154]. Note that the formation of an amorphous solid precursor does not fit within the classical CNT crystallization picture where densification and long-range order must emerge simultaneously during precipitation [155].

ACC in turn can undergo growth and/or aggregation before transformation into a more stable crystalline phase. Controversy exists, however, regarding how such an amorphous-to-crystalline transition

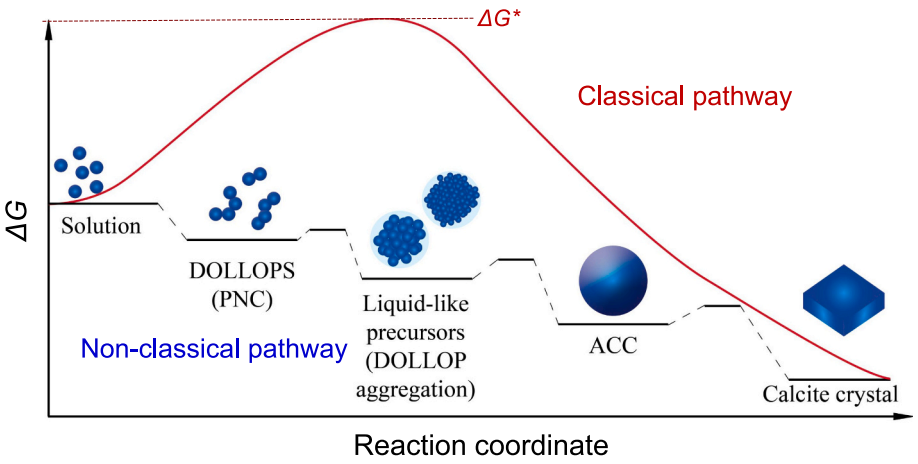


**Fig. 5.** Free energy landscape for crystallization pathways under thermodynamic (classical pathway) and kinetic control (solution → DOLLOP/PNCs → ACC→ stable crystal). The free energy barrier for nucleation depends on whether the system follows the classic pathway (red line) according to CNT, or the non-classical pathway (black line) according to NCC. (For interpretation of the references to color in this figure legend, the reader is referred to the web version of this article.)

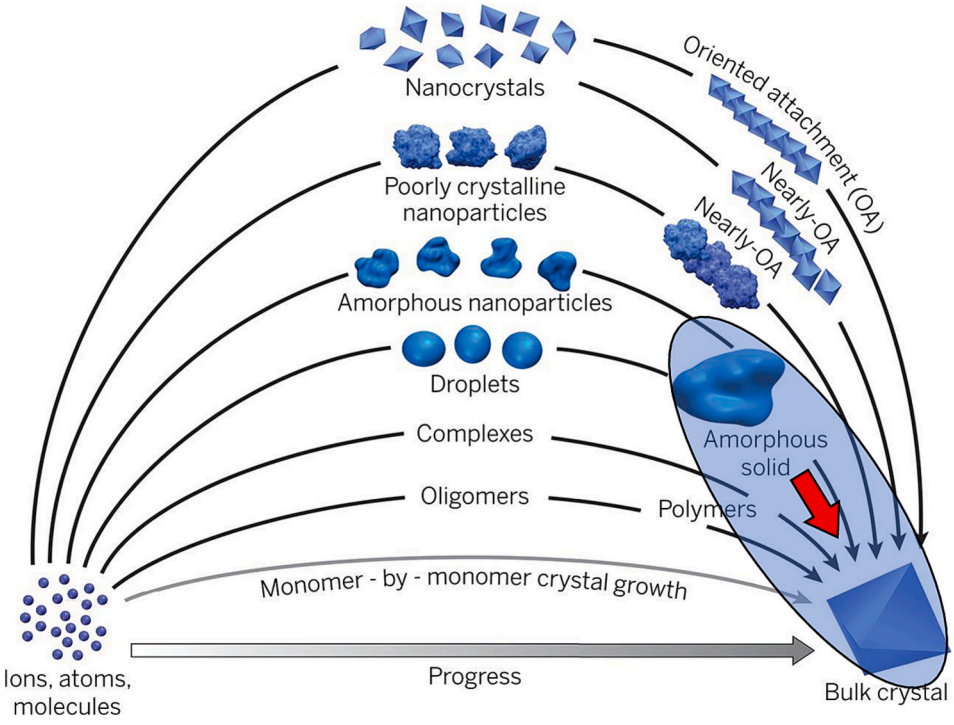


**Fig. 6.** Classical vs. nonclassical crystallization: Possible alternative routes for the formation of a crystalline phase and its growth via classical (grey arrowed lines) and non-classical crystallization (solid black arrowed curves). The route involving an amorphous precursor (most relevant for lime carbonation) is indicated (red arrow). (For interpretation of the references to color in this figure legend, the reader is referred to the web version of this article.)
Reprinted from [152], with permission by AAAS.

takes place in solution or in humid air [74,75]. In an aqueous solution, it has been reported that the easiest and energetically favored mode of transformation would be the dissolution of ACC and the subsequent nucleation and growth of a crystalline $CaCO_3$ phase [74,156]. Conversely, at high *T*, where ion diffusion within a solid is favored, ACC transforms into calcite (at $T \sim 330$ °C) via a solid-state mechanism [157]. However, at low *T*, in the absence of a bulk aqueous solution, for instance upon exposure to humidity or under (nearly) dry conditions (i.e., condition relevant for lime-binder carbonation), it is unclear how this transformation takes place. Two schools of thought exist. One proposes that ACC can transform into any of the $CaCO_3$ anhydrous polymorphs (vaterite, aragonite or calcite) via a solid-state mechanism [157,158]. The other school of thought proposes that ACC can transform into a crystalline phase via an ICDP mechanism [74,133]. In this latter case there is an adsorbed aqueous fluid at the ACC-atmosphere interface saturated with respect to ACC. Because ACC is more soluble than any anhydrous $CaCO_3$ polymorph, this aqueous film will be supersaturated with respect to any one of these crystalline phases, enabling their precipitation and the subsequent replacement of ACC as the dissolution of the parent phase (ACC) and the precipitation front advances to the core of this amorphous phase [74,75]. Because of the tight coupling between dissolution of ACC and precipitation of a crystalline $CaCO_3$ phase, a pseudomorphic replacement takes place [74].

The general observation that in the $CO_2$-CaO-$H_2O$ system (as well as in the $CO_2$-MgO-$H_2O$ system), crystallization of calcium (or magnesium) carbonate phases is non-classical [74,75,152,159] has direct and profound consequences for the carbonation of lime mortars and plasters, as well as for any carbonation reaction.

It has been unambiguously demonstrated that carbonation of Ca$(OH)_2$ proceeds via a NCC pathway [1,69,73,75,160]. After reaction of dissolved and hydrated $CO_2$ in a saturated Ca$(OH)_2$ solution, the systems follows a downhill energy landscape where PNCs first form, giving way

to the nucleation and growth of ACC (after a dense liquid precursor), and its transformation into crystalline $CaCO_3$ (Fig. 5). Phases formation and transition(s) follow the Ostwald rule of stages with the sequence (from less to most stable phases): ACC → vaterite → aragonite → calcite [74,75].

Such a NCC pathway is not limited to a (super)saturated $Ca(OH)_2$ solution in contact with atmospheric $CO_2$, thus representing the initial carbonation of a freshly prepared lime mortar or plaster (i.e., fully or partially saturated). The same sequence of events has been observed in dry $Ca(OH)_2$ powders [75] and dry lime pastes [69] exposed to a sufficiently high RH as to enable adsorption of water on the surface of the portlandite particles [132] and the formation of ACC.

Gillott [59] was the first to report on the presence of X-ray amorphous calcium carbonate following carbonation of $Ca(OH)_2$ crystals, which was responsible for the exothermic band at 310 °C (determined by differential thermal analysis) corresponding to the transformation of ACC into crystalline calcite. More recent transmission electron microscopy (TEM) studies have shown that portlandite exposed to atmospheric $CO_2$ in a humid environment starts to dissolve, typically at the center of the (001) faces of the crystals where a high defect density leads to more reactive surfaces [75]. Subsequently, a pseudomorphic replacement of the remaining portlandite hexagonal plates by ACC takes place via an ICDP mechanism [133] as shown in Fig. 7a–c [75]. ACC can also precipitate as individual spherical particles or as aggregates in the bulk (highly alkaline) solution formed upon dissolution of portlandite (Fig. 7d–f). As the transformation continues, ACC undergoes dissolution while anhydrous crystalline $CaCO_3$ phases form. The resulting precipitates include metastable vaterite (Fig. 8a) and aragonite (Fig. 8b), as well as the final stable calcite product (Fig. 8c–d). Importantly, the initial calcite crystals display scalenohedral form (Fig. 8c) and, over time, in the presence of humidity, they transform into calcite crystals with rhombohedral form (Fig. 8d) [69].

As an alternative for the formation of ACC as a precursor to crystalline $CaCO_3$ phases during the carbonation of $Ca(OH)_2$, Matsushita et al. [161] proposed the formation of an amorphous hydroxycarbonate precursor with formula $Ca_{1+x}CO_3(OH)_{2x}{\cdot}yH_2O$ ($x > 0.05$, $y = 0.6$–$0.8$) based on a X-ray photoelectron spectroscopy (XPS) study. Further studies by Wang et al. [162] confirmed that at high pH conditions, relevant for the carbonation of $Ca(OH)_2$, the formation of an amorphous basic calcium carbonate (ABCC) takes place. It is therefore quite possible that rather than ACC, ABCC is the relevant amorphous phase preceding the formation of crystalline $CaCO_3$ in lime-binders undergoing carbonation.

In the case of dolomitic limes, recent results by Oriols et al. [102] reveal that the carbonation of calcium hydroxide also involves the formation of amorphous and metastable crystalline phases prior to the formation of stable crystalline ones. Furthermore, the authors show that magnesium, which is known to play a role in the stabilization of ACC [163], delays the formation of crystalline calcium carbonates. Yet, while the authors demonstrate that the carbonation of $Mg(OH)_2$ saturated solutions involves the formation of an amorphous magnesium carbonate (AMC) phase, they do not show whether the carbonation of $Mg(OH)_2$ crystals in the dolomitic slaked lime paste also follows the same non-classical pathway observed for the carbonation of $Ca(OH)_2$ crystals. However, $Mg(OH)_2$ crystals have been observed to undergo carbonation via a NCC route involving the formation of amorphous magnesium

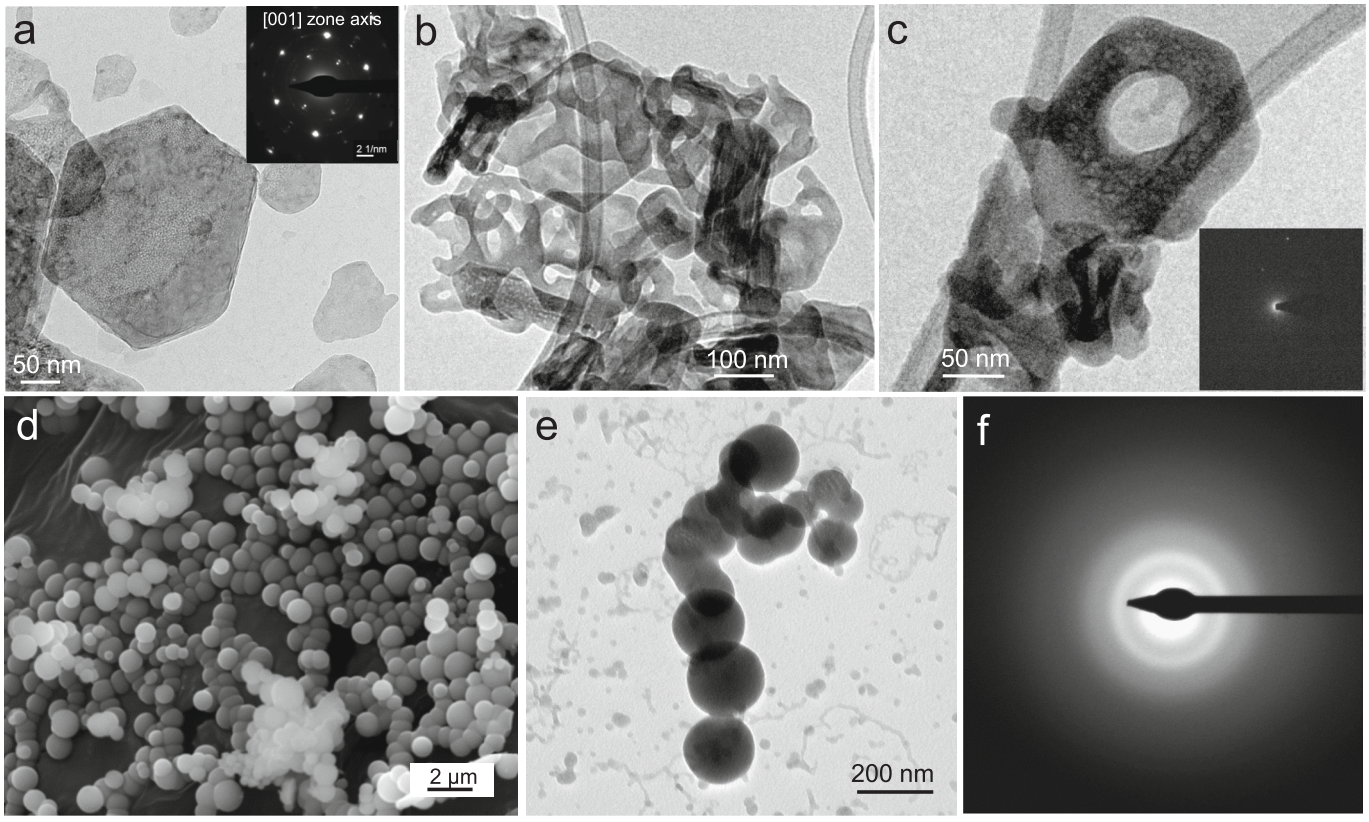


**Fig. 7.** Metastable amorphous precursor $CaCO_3$ phases formed during carbonation of $Ca(OH)_2$. TEM images of portlandite crystals before carbonation (a) and after carbonation in air at room *T* and 80 % RH for 3 h (b). Note the hollow cores indicative of the dissolution of parent hydroxide crystals; c) detail of the hollow core structure, identified as amorphous ACC (see absence of diffraction spots in the SAED pattern in inset), which pseudomorphically replaced portlandite via an interface-coupled dissolution-precipitation reaction; d) FESEM photomicrograph of ACC nanoparticles formed following carbonation in air of a saturated $Ca(OH)_2$ solution; e) TEM image of ACC nanoparticles formed in a saturated $Ca(OH)_2$ solution exposed to atmospheric $CO_2$; f) SAED pattern of the ACC nanoparticles in (e). The diffuse rings are indicative of the amorphous nature of ACC nanoparticles.
Figure parts a) to c) reprinted from [75] with permission by RSC.

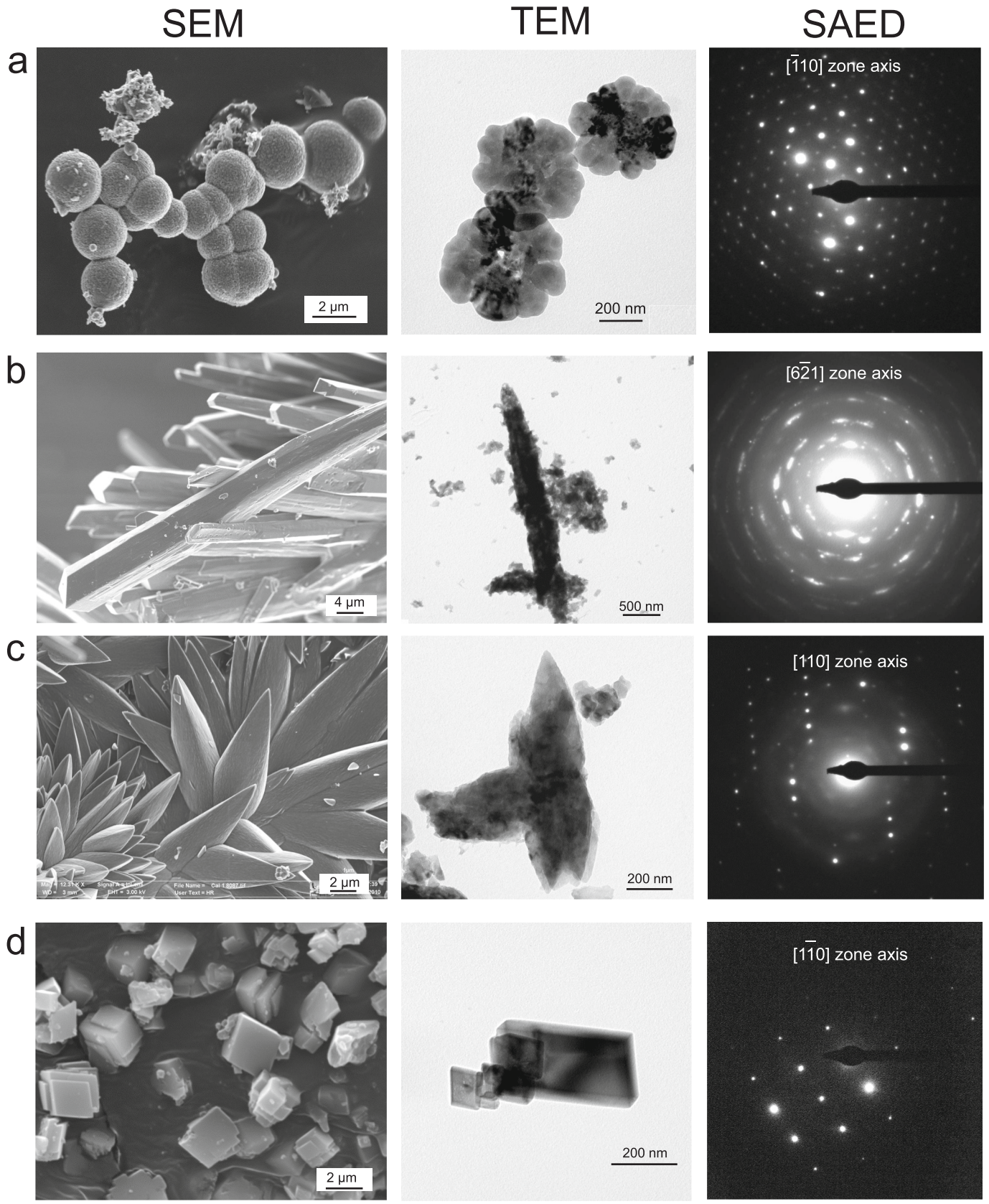


**Fig. 8.** FESEM and TEM observations of crystalline $CaCO_3$ phases formed after ACC following carbonation of $Ca(OH)_2$. a) Spherulitic vaterite structures identified by their TEM-SAED pattern (right); b) spindle-like aragonite structures (SAED pattern on the right, showing arced diffraction spots confirming its mesocrystal structure); c) scalenohedral calcite (SAED pattern on the right); d) rhombohedral calcite (formed after scalenohedral calcite) (SAED pattern on the right).

carbonate (AMC) on the brucite surface prior to the crystallization of nesquehonite [159,164]. It so appears that irrespectively of the reactant alkaline earth metal hydroxide, NCC is the ruling mechanism during carbonation.

In summary, recent research has shown that the carbonation of calcitic (and dolomitic) limes is non-classic. As a result, the formation of amorphous and crystalline (metastable) precursors prior to the formation of the stable carbonate phases must be considered when modeling the kinetics of carbonation (see below) and interpreting the evolution of the physical-chemical, structural/textural and mechanical properties of lime plasters and mortars undergoing carbonation.

### 4.3. Carbonation mechanism at the nanoscale: a NCC view

Nanoscale investigations of the carbonation process within the frame of NCC have been recently performed. One important aspect was to elucidate how the calcite crystals formed upon carbonation of $Ca(OH)_2$ could further grow in the presence of ACC precursor nanoparticles. Rodriguez-Navarro et al. [165] performed in situ atomic force microscopy (AFM) analysis of the grow of calcite crystals in the presence of a saturated $Ca(OH)_2$ solution. It was observed that after an initial dissolution of the calcite substrate and the corresponding release of $Ca^{2+}$ and $CO_3^{2-}$ ions, supersaturation with respect to ACC was rapidly achieved, leading to the precipitation of ACC nanoparticles. Remarkably, in situ AFM imaging showed that the newly formed ACC nanoparticles attached to the (104) faces of the calcite substrate in an ordered manner, contributing to layer growth via advancement of macrosteps formed by the attached ACC nanoparticles (Fig. 9a). Upon further aging, the ACC nanoparticles converted into calcite, preserving the overall rhombohedral morphology of the calcite substrate. These results demonstrate that ACC nanoparticles actively contribute to the growth of calcite via a non-classical attachment mechanism that mimics at the nanoscale the growth mechanism observed at the atomic scale during classical crystal growth, that is, the incorporation at kink and steps of growth units (atoms, ions, or molecules) of sub-nanometer dimensions. Ultimately, this colloidal-like nanoparticle growth mechanism, schematically depicted in Fig. 9b, would contribute to the rapid growth of calcite (and likely aragonite and vaterite) during the carbonation of portlandite (and, possibly, brucite) linking the formation of ACC observed during lime mortar carbonation, to the actual development of the cementing $CaCO_3$ crystals. Interestingly, such a non-classical growth mechanism involving attachment of ACC nanoparticles leads to a nanogranular structure in the final calcite crystals, which is preserved if organics additives are present [165,166]. The organics prevent fusion of nanoparticles during the transformation of ACC into crystalline $CaCO_3$ (Fig. 9c–d). The presence of a nanogranular structure in calcite formed following carbonation of portlandite may thus aid in the identification of organics addition in ancient lime mortars and plasters.

It is currently unknown if the growth of hydrated magnesium carbonate phases formed upon carbonation of dolomitic limes also takes place via this non-classic colloidal attachment mechanism. Further research is warranted to explore this possibility.

## 5. Carbonation kinetics

The carbonation of lime mortars and plasters is recognized as a slow process with sluggish kinetics. This view is supported by analytical results of lime mortars and plasters in some ancient buildings still showing incomplete carbonation. Marchese [167] reported that 12th century non-hydraulic lime-based mortars in mosaics at the Museum of the Duomo in Salerno (Italy) included uncarbonated amorphous (or poorly crystalline) $Ca(OH)_2$. These results were, however, challenged by Newton and Sharp [168]. Nonetheless, further evidence has shown that a fraction of $Ca(OH)_2$ in lime mortars can remain uncarbonated for long periods of time, typically months or years [36], and even centuries [47,169]. XRD and TGA/DTA analyses performed by Adams et al. [169] confirmed the presence of significant amounts of uncarbonated portlandite in 13th–14th century mortars collected from Salisbury

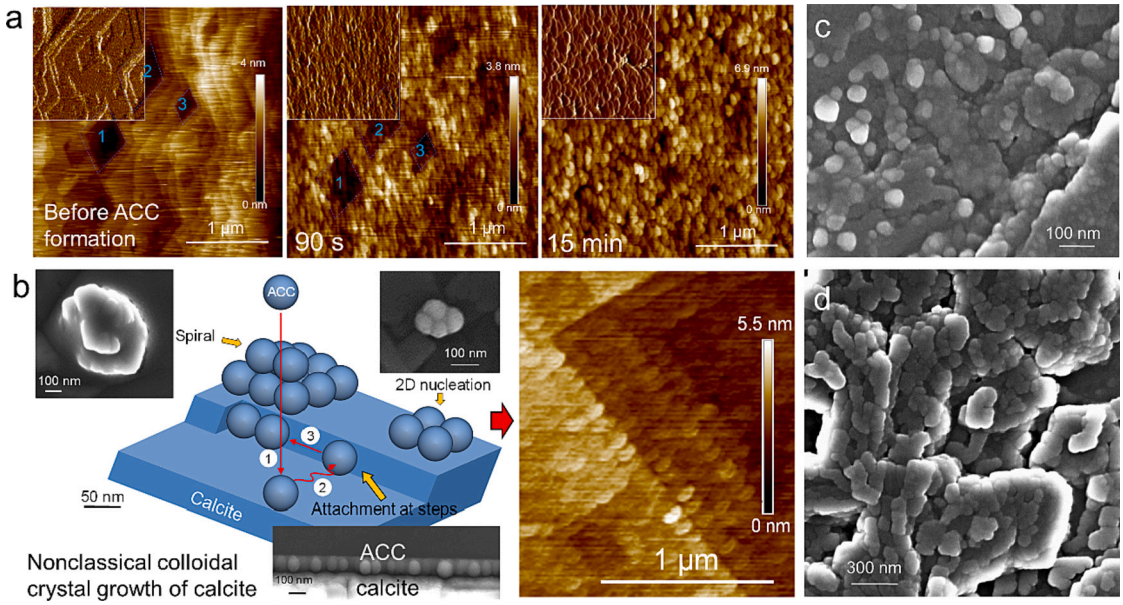


**Fig. 9.** Non-classical growth of calcite via attachment of ACC nanoparticles. a) Time sequence of AFM deflection images (topographic images in insets) showing the attachment of ACC nanoparticles onto (104) calcite in the AFM fluid cell. Note how they arrange in an orderly manner following the contour of calcite rhombohedral pits (1, 2 and 3) (90 s after injection of a saturated $Ca(OH)_2$ solution) and fully cover the calcite surface after 15 min; b) model for the growth of calcite via attachment of ACC nanoparticles. Attachment can lead to growth spirals or 2D islands. If attachment occurs at a step, nanoparticles first adsorb on the terrace (1), migrate to macrosteps (2) and finally to kinks (3). The result is the ordered attachment of ACC nanoparticles along specific calcite crystallographic directions, as shown in the AFM deflection image on the right; c) and d) FESEM images of calcite crystals overgrown via the attachment of ACC nanoparticles formed in the presence of polyacrylate. Once ACC particles transformed into crystalline calcite, the surface overgrowth preserved the nanogranular structure imprinted by the ACC precursor particles.
Modified from [165] with permission by ACS.

Cathedral, UK. Uncarbonated $Ca(OH)_2$ in mortars ca. 800 years old present in the meters-thick walls of the Civic Tower of Pavia (Italy) has been claimed to be partly responsible for its collapse in 1989 [170]. Regarding the identification of uncarbonated $Ca(OH)_2$ fractions in ancient lime mortars and plasters, studies on the (nano)structural features of carbonated lime plasters show lattice distortion in calcite that has been associated with the presence of uncarbonated $Ca(OH)_2$, not easily detected using conventional spectroscopic or XRD analysis [171]. This suggests that the presence of uncarbonated $Ca(OH)_2$ in ancient air lime mortars and plasters might be more common than previously thought. As a result of the observed partial carbonation, the ultimate strength of aerial lime mortars and plaster might not be reached, even after several years. The slow carbonation kinetics might compromise the stability of masonry structures including lime-binders, at least in the short term, and possibly in the long term too. But may also help increase the durability of ancient lime mortars and plasters, as the uncarbonated $Ca(OH)_2$ can contribute to the self-healing of fractures (it might also improve the plastic behavior of the mortar/plaster) [37,172]. Fractures would enable an easier access of $CO_2$ (and $H_2O$) to the uncarbonated areas, enabling precipitation of $CaCO_3$ that could seal the fractures. This self-healing effect has been claimed to contribute to the high durability of ancient Roman concrete prepared using the so-called hot mixing technology [173].

In the case of dolomitic limes, it has been observed that the carbonation of $Mg(OH)_2$ is even slower than that of $Ca(OH)_2$ [174,175]. Lanas et al. [174] observed that while after 1-year exposure to atmospheric $CO_2$ full carbonation of $Ca(OH)_2$ was achieved in dolomitic lime mortars, a negligible fraction of $Mg(OH)_2$ had carbonated. It is not known why brucite shows such a slow rate of carbonation as compared with portlandite. In fact, the mechanisms and kinetics of carbonation of $Mg(OH)_2$ crystals in dolomitic limes have not been thoroughly studied, although some progress has been made recently [102].

In this respect, it is important to indicate that $Mg(OH)_2$ can form in situ within calcitic lime mortars when a dolomitic aggregate is used. The reaction between $Ca(OH)_2$ and dolomite results in the formation of calcite plus brucite [176],

$$Ca(OH)_2 + MgCa(CO_3)_2 = Mg(OH)_2 + 2CaCO_3 \quad (21)$$

Typically, porous calcite reaction rims around partially replaced dolomite grains are observed in lime mortars with dolomite aggregate [177]. Because the carbonation of the resulting $Mg(OH)_2$ is so slow, there is the possibility of its leaching ($Mg(OH)_2$ being a relatively soluble phase) and the creation of porosity in the mortar, ultimately leading to degradation.

Another important consideration regarding the very slow kinetics of the carbonation of dolomitic (or magnesian) limes is the fact that the uncarbonated $Mg(OH)_2$ crystals are prone to react with pollutant (acid) gases such as $SO_2$, resulting in the formation of highly deleterious soluble salts such as epsomite ($MgSO_4{\cdot}7H_2O$) and/or hexahydrite ($MgSO_4{\cdot}6H_2O$) [106]. A similar sulfation process might also occur in the case of the relatively soluble hydrated magnesium carbonate phases formed upon carbonation of brucite in dolomitic mortars or lime mortars with a dolomite aggregate suffering a dedolomitization reaction (Eq. (21)). Note that calcitic lime mortars, once carbonated, can also experience sulfation in polluted environments forming calcium sulfate salts. However, the effects of the crystallization of calcium sulfate phases are much less dramatic than those due to the crystallization of magnesium sulfates [27,106,178].

### 5.1. Kinetics models

Considering the implications of the above-described effects, much research has been dedicated to understanding the kinetics of lime carbonation to determine rate controlling steps and rate constants, Arrhenius parameters, and reaction model(s) best fitting the observed kinetics. Although it is now recognized that, under the prevailing low $T$ and $pCO_2$ conditions during standard application of lime mortars, carbonation involves a dissolution-precipitation process [1,65,75], the kinetic models used for the analysis of this reaction are based on solid-state reactions, summarized in Table 1 [86,179]. Despite this apparent inconsistency, such models have been successfully applied for the kinetic analysis of the carbonation process, yet with disparate results [75,80–183]. It should be kept in mind, however, that while they can yield accurate kinetic parameters, the mechanistic interpretation of the carbonation reaction using a particular kinetic model is not straight forward.

The rate ($k$) of a solid-state reaction, that is $d\alpha/dt$, can be generally described by,

$$k = \frac{d\alpha}{dt} = Ae^{-\left(\frac{E_a}{RT}\right)} f(\alpha) \quad (22)$$

where A is the pre-exponential (frequency) factor, $E_a$ is the apparent activation energy, $T$ is absolute temperature, R is the gas constant, $t$ is time, $f(\alpha)$ is the reaction model, and α is the fractional conversion defined here by,

$$\alpha = \frac{X_0 - X_t}{X_0} \quad (23)$$

where $X_0$ and $X_t$ are the amount of reactant phase at time 0 and at time $t$. The Arrhenius parameters are A, $E_a$ and the kinetic model $f(\alpha)$ [179]. They can be obtained from isothermal kinetic data by applying the above rate law (Eq. (22)). For convenience, the integral form of Eq. (22)

**Table 1**
Rate equations for the analysis of the kinetics of solid-state reactions.

| Rate model | | f(α) = 1/k dα / dt | g(α) = kt |
|---|---|---|---|
| 1. Sigmoid α-T curves | (a) Prout-Tompkins's Eq. (B1) | $\alpha(1-\alpha)$ | $1-(1-\alpha)$ |
| 1.1 Nucleation and nuclei growth | (a) Random nucleation—Avrami-Erofeev Eq. (I) (A2) | $2(1-\alpha)[-\ln(1-\alpha)]^{1/2}$ | $[1-\ln(1-\alpha)]^{1/2}$ |
| | (b) Random nucleation—Avrami-Erofeev Eq. (II) (A3) | $3(1-\alpha)[-\ln(1-\alpha)]^{2/3}$ | $[1-\ln(1-\alpha)]^{1/3}$ |
| | (c) Random nucleation—Avrami-Erofeev Eq. (III) (A4) | $4(1-\alpha)[-\ln(1-\alpha)]^{3/4}$ | $[1-\ln(1-\alpha)]^{1/4}$ |
| 2. Acceleratory α-T curves | (a) Exponential law (E1) | α | ln α |
| 3. Deceleratory α-T curves | | | |
| 3.1 Reaction order | (a) Zero order (F0/R1) | 1 | α |
| | (b) First order—Unimolecular decay (F1) | $(1-\alpha)$ | $-\ln(1-\alpha)$ |
| | (c) Second order (F2) | $(1-\alpha)^2$ | $[1/(1-\alpha)]-1$ |
| | (d) Third order (F3) | $(1-\alpha)^3$ | $(1/2)[1-\alpha)^{-2}-1]$ |
| 3.2 Diffusion mechanism | (a) One dimensional transport (D1) | $0.5\,\alpha^{-1}$ | $\alpha^2$ |
| | (b) 2D transport (cylindrical geometry) (D2) | $[-\ln(1-\alpha)]^{-1}$ | $((1-\alpha)\ln(1-\alpha))+\alpha$ |
| | (c) 3D diffusion, spherical symmetry—Jander Eq. (D3) | $1.5(1-\alpha)^{2/3}[1-(1-\alpha)^{1/3}]^{-1}$ | $(1-(1-\alpha)^{1/3})^2$ |
| | (d) 3D diffusion, spherical symmetry—Ginstling-Brounshtein Eq. (D4) | $1.5[(1-\alpha)^{-1/3}-1]^{-1}$ | $1-(2/3)\alpha-(1-\alpha)^{2/3}$ |
| 3.3 Phase-boundary reaction | (a) 2D (cylindrical geometry) (R2) | $2(1-\alpha)^{1/2}$ | $1-(1-\alpha)^{1/2}$ |
| | (b) 3D (spherical geometry) (R3) | $3(1-\alpha)^{2/3}$ | $1-(1-\alpha)^{1/3}$ |

is used to determine Arrhenius parameters,

$$g(\alpha) = Ae^{-\left(\frac{E_a}{RT}\right)}t \quad (24)$$

where $g(\alpha)$ is defined by,

$$g(\alpha) = \int_0^{\alpha} \frac{d\alpha}{f(\alpha)} \quad (25)$$

Experimental data representing the variation of α with carbonation time $t$ can be fitted to the integral form $g(\alpha)$ of the different models in Table 1. The best fitting model is thus selected as the most appropriate kinetic model for this reaction. Such a best-fitting kinetic model can be used for the determination of the rate constant $k$, and Arrhenius parameters. It can also provide some insights on the mechanistic model best describing a particular reaction. However, as indicated above, a particular mechanistic model deduced from the kinetic analysis, cannot be considered as the "actual" mechanism of any reaction. Additional tests and analyses are necessary to properly determine the "actual" reaction mechanism.

### 5.2. Kinetics of $Ca(OH)_2$ carbonation: rate-controlling steps

Any model describing the kinetics of a reaction such as carbonation (assumed to be a gas-solid reaction) needs to consider the contribution of several "resistances" corresponding to reactant/by-product mass transfer and chemical reaction. In general, for the relevant systems considered here, the following resistances, which can eventually become the rate-controlling steps of a carbonation reaction, are [62,69]: (1) mass transfer and diffusion of the gas towards and within the interparticle pores (for powder samples) or porous structure (pastes and mortars); (2) adsorption/hydration of the gas in aqueous surface films or pore solution; (3) diffusion of the dissolved/hydrated gas to the solid-liquid interface; (4) dissolution of the solid at the solid-liquid interface; (5) surface reaction; (6) diffusion of reactant (and counter-diffusion of by-product) through the solid product layer. The influence of heat transfer on the kinetics of such a gas-solid reaction must also be considered because the carbonation reaction is highly exothermic. However, only when speeding up the reaction significantly (e.g., by forced carbonation in high $pCO_2$ conditions) significant heat transfer takes place [61].

The kinetics (and mechanism) of $Ca(OH)_2$ carbonation in solution (aqueous phase or aqueous dispersion) have been extensively studied due to the relevance of this process in the synthesis of precipitated calcium carbonate (PCC), which has important industrial applications (e.g., as filler for plastics, drugs, paper, rubber, paints) [74,130,184–186].

Carbonation of $Ca(OH)_2$ slurries via injection of $CO_2$ for PCC production involves the formation of metastable precursor phases both amorphous (ACC) and crystalline (vaterite and aragonite) and their partial or complete transformation into stable calcite [184–186]. The same applies for the homogeneous precipitation of $CaCO_3$ in solution [74,93,156,187–189]. The main parameters controlling the kinetics of $CaCO_3$ formation and solid phase evolution/polymorph selection are pH, $T$, $[Ca^{2+}]/[CO_3^{2-}]$, supersaturation, $pCO_2$ (i.e., concentration of $CO_2$ in the gaseous phase, typically expressed in %), gas pressure $P$, and the presence of impurities or additives, both organic (e.g., polycarboxylates) or inorganic (e.g., phosphate or magnesium ions) [1].

In contrast, little research has focused on the understanding of the kinetics and mechanisms of $Ca(OH)_2$ crystals/powders carbonation in air at room $T$, conditions that are most relevant during the setting and hardening of lime mortars and plasters [1,64,71]. So far, it has been experimentally shown that parameters such as RH, $T$, reactant size and surface area, and $pCO_2$, in addition to impurities/additives, affect the carbonation rate and polymorph selection [62,64,75,130,132,182,190].

As indicated above, it is generally recognized that RH plays a critical role in determining the rates of $Ca(OH)_2$ carbonation in air at low $T$. Carbonation rates close to zero have been reported for RH < 8 %, exponentially increasing with RH [62]. Beruto and Botter [132] indicated that at RH > 70 % carbonation rates increase exponentially due to multilayer water adsorption. The authors argued that adsorbed liquid-like water played a catalytic role in this reaction, considered as a gas-liquid-solid reaction. Such an effect was directly observed at the nanoscale by Yang et al. [191] during the carbonation of portlandite crystal in air using AFM. The authors showed the formation of nanogranular $CaCO_3$ precipitates on the (001) basal plane of portlandite, presumably ACC, only when RH ≥ 30 % (no precipitates formed at lower RH). Water vapor sorption isotherms on both calcite and portlandite experimentally obtained by Beruto et al. [65] demonstrated that portlandite was more hydrophilic than calcite. As a result, portlandite experienced multilayer $H_2O$ adsorption at RH > 70 % favoring calcium carbonate precipitation. Because the latter phase was less hydrophilic, carbonation rates tended to reduce as the carbonation degree increased. Dheilly et al. [190] pointed out that at a high RH (≫30 %), $Ca(OH)_2$ could dissolve in the adsorbed water film, and such a highly alkaline film would foster $CO_2$ adsorption and its subsequent hydration to form carbonate ions (i.e., Eqs. (14) and (15)), ultimately facilitating $CaCO_3$ precipitation onto portlandite [62]. Note, however, that using Raman spectroscopy Dubina et al. [192] demonstrated the formation of ACC on $Ca(OH)_2$ powders (after CaO hydration) at lower RH values of 10–20 % (80 °C). The study by Pesce et al. [193] using $^{18}O$ isotope-labeled $Ca(OH)_2$ unambiguously demonstrated that, at the molecular level, carbonation in air involves the dissolution of reactant hydroxide and atmospheric $CO_2$ in an aqueous-film formed on portlandite crystals. Remarkably, the isotopic fingerprint of newly formed carbonates showed that a significant fraction of oxygen came from portlandite, demonstrating that $OH^-$ groups from the latter phase are directly involved in the hydration of $CO_2$ via Eq. (15). The authors concluded that dissolution of portlandite at the solid-liquid interface was the rate-limiting step for carbonation at such an early stage. At latter stages, the isotopic study showed that most of the oxygen in newly formed carbonates came from $H_2O$ in ambient humidity, suggesting that isotopic re-equilibration was due to dissolution of metastable precursor phases (i.e., ACC, or even ABCC) and precipitation of stable ones (e.g., calcite) following the Ostwald rule of stages [75,189]. Chen et al. [194] performed carbonation of levitated $Ca(OH)_2$ aerosol particles showing that carbonation was only progressing for RH > 70 %, in excellent agreement with the RH at which multilayer water adsorption onto portlandite occurs according to Beruto and Botter [132]. The product $H_2O$ released during portlandite carbonation could in turn self-catalyze further carbonation until completion, or until a product ($CaCO_3$) layer formed that hampered the advancement of the reaction front to the core of portlandite particles. According to Shih et al. [62], who underlined the critical role of $H_2O$ adsorption on portlandite particles, the rate controlling step for carbonation was assumed to be the dissolution of $Ca(OH)_2$ at the water-adsorbed surface layer, as also pointed out by Van Balen [64] and Pesce et al. [193].

A recent study by Park et al. [195] suggests that during the interaction of portlandite and water, there is intercalation of $H_2O$ molecules within the (001) planes of the portlandite crystal lattice, a process that occurs along the ⟨100⟩ directions (Fig. 10a). As a result, an increase in the $d_{001}$-spacing of ~0.39 % (i.e., interplanar distance in the [001] direction) compared to completely dry portlandite samples was detected using XRD (Fig. 10b). This result could have important implications for the carbonation mechanism and kinetics because it leaves in question the rate-determining step of this process. According to the authors the intercalation of water molecules could be the very first step enabling $CO_2$ molecules to interact with the portlandite structure thus triggering initial carbonation along the <100> directions, which according to Ruiz-Agudo et al. [71] display a higher carbonation rate as compared with the [001] direction.

The pioneering study by Aono [58] indicated that for a given exposure time, $t$, the carbonation degree $W_t$ of hydrated lime powder (large

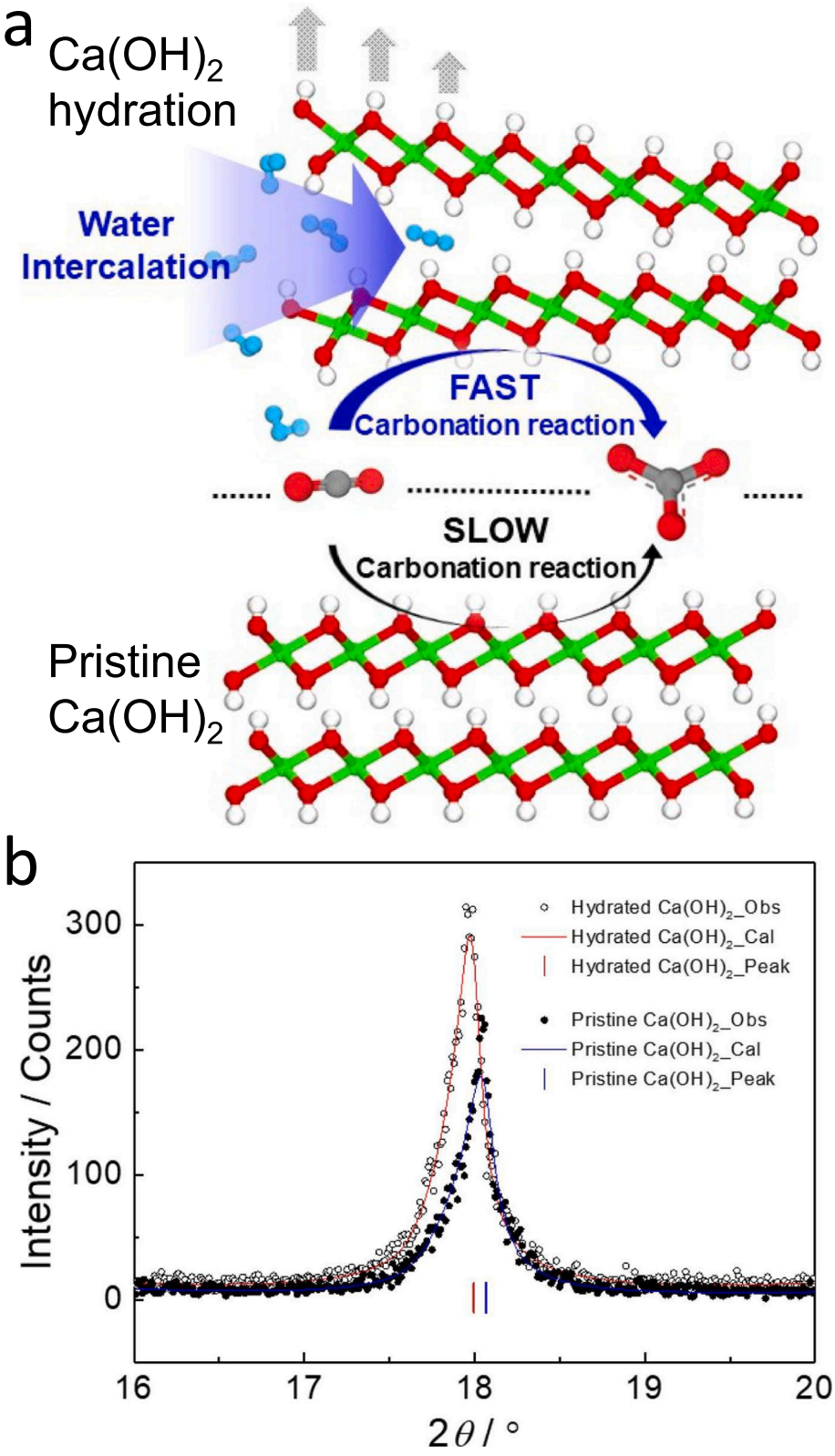


**Fig. 10.** Effect of water molecules intercalation within the portlandite structure on its carbonation kinetics. a) Scheme showing the intercalation of water molecules within the (001) planes of the portlandite structure. This could lead to an acceleration of the carbonation of this phase; b) XRD pattern of the 001 Bragg peak of un-hydrated and hydrated portlandite crystals. Note the left shift in the peak position after hydration, implying an increase in the $d_{001}$-spacing after $H_2O$ intercalation.
Reprinted from [195] with permission by Elsevier.

sample mass of 10 g), revealed an exponential relationship with $CO_2$ concentration, $C$ (i.e., $pCO_2$), given by the following (empirical) equation,

$$W_t = 30\left(1 - e^{-0.0135Ct}\right) \quad (26)$$

where $W_t$ is determined as weight increase following carbonation in a water vapor saturated atmosphere. Although the determination of the carbonation degree by measuring the weight increase might be questionable, as an unknown amount of product water will be absorbed on the carbonated reactant, thus contributing to the value of $W_t$, and the large sample mass might impose diffusion-controlled kinetics, these results could suggest that carbonation rates are dependent on $CO_2$

concentration. Contrary to this common assumption, more recent studies have shown that carbonation rates are independent of $pCO_2$ [1,62,64]. Van Balen [64] demonstrated that the carbonation rate of portlandite powders is zeroth order with respect to $CO_2$ concentration (in the range 15–50 %, at room $T$), suggesting that the controlling factor in the carbonation process might be the dissolution of portlandite at the water-adsorbed surface. As a results, $Ca(OH)_2$ crystals with a higher surface area show a higher carbonation rate (per unit mass of reactant) [64].

Accurate carbonation rates are typically measured using pure $Ca(OH)_2$ powder samples, where transport-limited $CO_2$ supply to reaction sites is negligible. In practice, however, it is observed that the carbonation rate in lime-based mortars and plasters is accelerated by increasing $pCO_2$ [63,92,196]. Such an acceleration is not likely due to an increase in the rate of the actual carbonation reaction, but to the diffusion of $CO_2$ within the pore system of the mortars towards the reaction interface (portlandite-solution interface), which should be faster the higher the $CO_2$ concentration gradient (see below).

### 5.3. *Proposed kinetic models for the carbonation of $Ca(OH)_2$ crystals/ powders*

Several kinetic models for the carbonation of portlandite in air at low $T$ have been proposed. Note that below we refer to pure $Ca(OH)_2$ crystals or powders, not to mortars or plasters. This clarification is important because their carbonation kinetics are different. Carbonation has been described as: (i) a deceleratory (or asymptotic) process displaying no induction time [62,190], which can be fitted to a (pseudo)second order model (F2) eq. [130,186]; (ii) a diffusion-controlled reaction involving 3D diffusion (spherical symmetry) according to the Jander eq. (D3) [180]; (iii) a process that follows sigmoidal-type Avrami-Erofeev kinetics with an induction time before nucleation and growth [181]; (iv) a (pseudo)first order deceleratory reaction (F1) with no induction time and only dependent on the amount of untransformed reactant [75,183]; and (v) a reaction which can be fitted to a boundary nucleation and growth model (BNGM) where the rate depends on the nucleation of particles at the portlandite-solution interface and subsequent growth over the substrate surface (i.e., unreacted portlandite) after coalescence and full coverage [182]. In the general case, the BNGM shows an s-shape α vs. $t$ evolution (i.e., denoting the presence of an induction time). However, in the limiting case scenario, the rate limiting step is the growth of the product surface layer, which is described by first order kinetics (F1). Fig. 11 shows a comparison of α vs. $t$ curve fittings obtained from two of the above-mentioned kinetic models, exemplifying the disparity of models used to fit experimental results. The disagreement among the proposed kinetic (and underlaying mechanistic) models, may lay in the fact that most of the previous studies did not consider the possible role of metastable precursors phases (ACC in particular) in the carbonation process. For instance, quantification of portlandite conversion into $CaCO_3$ using XRD or FTIR neglects the formation of ACC, underestimating the rate of conversion at earlier stages and leading to the assumption of an induction time [1], yielding a s-shaped (e.g., Avrami-Erofeev) kinetic model. However, analysis using TG, which quantifies the full amount of $CaCO_3$ (amorphous plus crystalline) yields no induction time and a (pseudo)first order kinetic model [75]. The choice of one model or the other strongly affects $k$ values (i.e., reaction rates) and Arrhenius parameters.

From the above-mentioned kinetic analyses, Arrhenius parameters are obtained. However, there is a large scattering in their values. Camerini et al. [182] reported apparent activation energy values of ~31–60 kJ $mol^{-1}$ for different types of hydrated limes and nanolimes (i.e., $Ca(OH)_2$ nanoparticles, typically with size < 200 nm, used as alcoholic dispersions for the consolidation of cultural heritage materials [197]). These values contrast with values of activation energy of 6–12 kJ $mol^{-1}$ reported for the dry solid-gas carbonation at relatively high $T$ (>250 °C) of portlandite micrometric aggregates used for acid gas

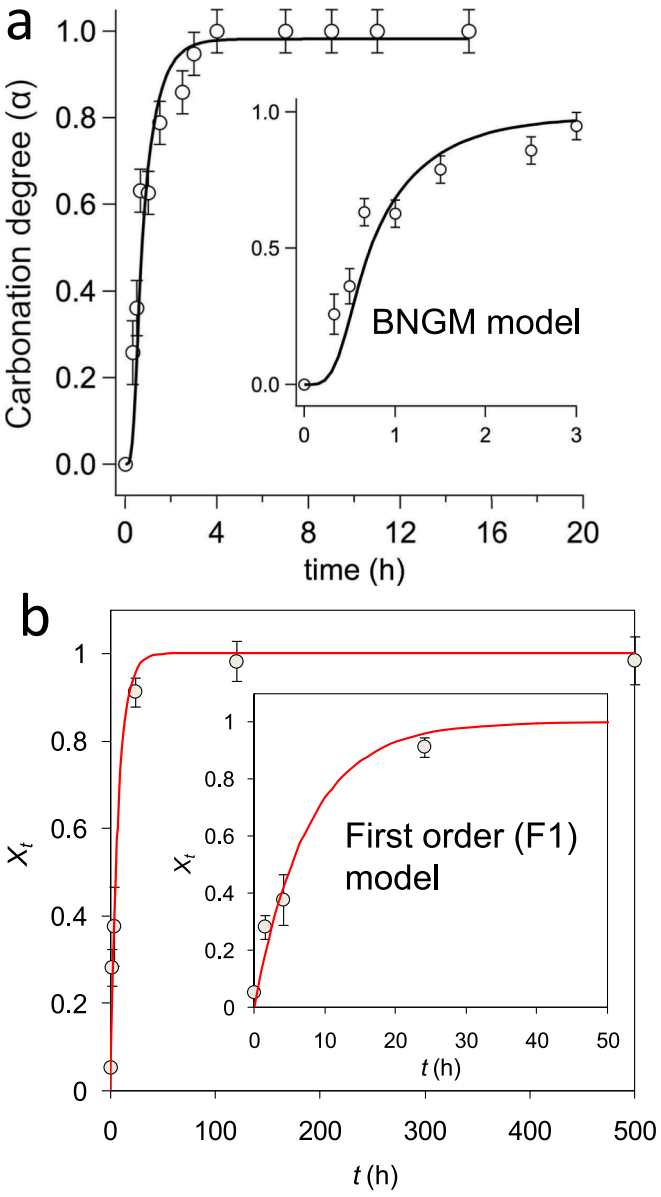


**Fig. 11.** Carbonation degree vs. time for $Ca(OH)_2$ (nano)particles exposed to humid air. Values are fitted to two different kinetic models: a) Boundary nucleation and growth model (BNGM). Reprinted from [182] with permission by Elsevier; and b) first order (F1) model. Reprinted from [75] with permission by RSC.

capture or the value of 7.5 kJ $mol^{-1}$ reported for the carbonation of portlandite at low $T$ using liquid and supercritical $CO_2$ [182,198]. Note, however, that Yu et al. [199] report a higher $E_a$ value of 40 kJ $mol^{-1}$ for the high $T$ (≥500 °C) capture of $CO_2$ by $Ca(OH)_2$ powders forming an intermediate bicarbonate phase ($Ca(HCO_3)_2$) and pointing to a reaction-controlled process. The discrepancy in the obtained $E_a$ values likely reflects that the carbonation mechanism (and/or the rate controlling step) is different in the studied systems (as the experimental conditions are different too). Nonetheless, the relatively high $E_a$ values obtained by Camerini et al. [182] suggest that the carbonation process at room $T$, atmospheric $pCO_2$ and in the presence of humidity (75 % RH), which most closely reflects the carbonation conditions of lime plasters and mortars applied in the field, is reaction-controlled (i.e., surface-controlled), whereas for the lower $E_a$ values reported, carbonation is transport-controlled (i.e., diffusion-controlled) [200]. Interestingly, the values of $E_a$ reported by Camerini et al. [182] are in excellent agreement

with those reported for the dissolution of common silicate and carbonate minerals ($E_a$ values ranging from 35 kJ mol$^{-1}$ for calcite to 75 kJ mol$^{-1}$ for quartz) when dissolution is reaction-controlled [200]. It is thus very likely that, as pointed out by Shih et al. [62], Van Balen [64] (2005), and Pesce et al. [193], the rate controlling step for portlandite carbonation is the actual dissolution of this phase in the aqueous layer adsorbed on its surface.

There is another aspect that needs to be considered when analyzing the kinetics of carbonation of portlandite crystals: the presence of defects. Pisu et al. [183] detected an anomalous Raman emission band at 780 cm$^{-1}$ using near-infrared (NIR) excitation in portlandite crystals, which increased in intensity upon thermal treatment (max. at 200–300 °C). This luminescence effect was associated with the creation of point defects. A kinetic analysis of the carbonation of heat-treated portlandite showed first order kinetics (F1) with faster conversion for the samples annealed at 200–300 °C, i.e., those with the highest defect density. The authors concluded that defects acted as nucleation sites for $CaCO_3$, playing a key role in speeding carbonation in annealed portlandite. These results partially agree with the observations by Rodriguez-Navarro et al. [75] showing that carbonation starts at the center of portlandite (001) faces, where a higher defect density is present (Fig. 8). However, these areas of high defect density do not act as nucleation sites for $CaCO_3$. Instead, being highly reactive, they are the first areas to dissolve, leading to the formation of ACC which eventually transforms into crystalline $CaCO_3$.

## 6. Carbonation kinetics of lime mortars and plasters

The above kinetic studies were performed using samples of pure (typically thin) powders of $Ca(OH)_2$ crystals. In contrast, in the case of a lime plaster or a mortar, where a 3D porous structure exists, carbonation proceeds in three different stages with clearly differentiated kinetic regimes [1].

### 6.1. Carbonation stage 1

During the initial stage, $CO_2$ diffusion to reacting sites (i.e., portlandite surface) is limited due to saturation by capillary water in the porous system of the plaster or mortar [64,109]. The carbonation kinetics of this initial stage are therefore strongly dependent on the drying

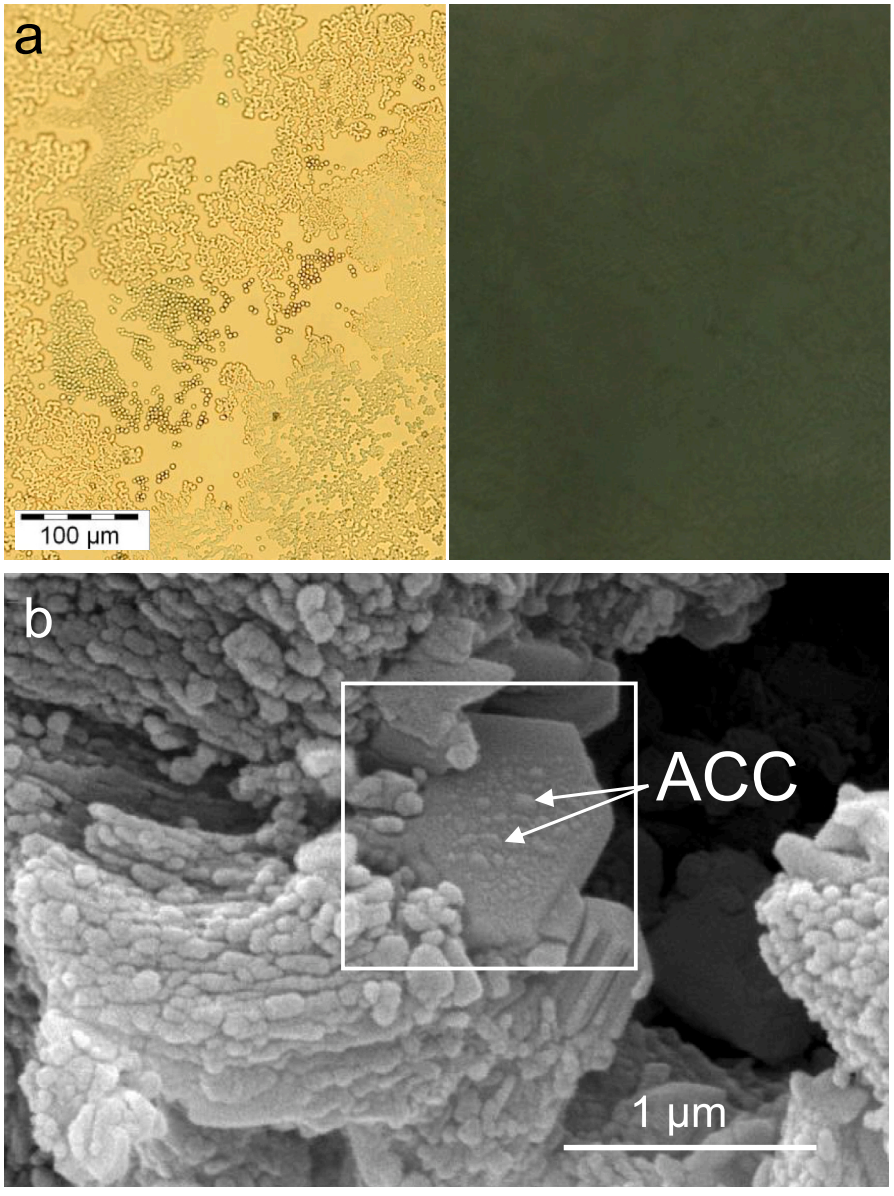


**Fig. 12.** ACC particles formation during carbonation. a) ACC nanoparticles formed at the air-solution interface forming fractal-like aggregates observed under a polarized light microscope. Plane light image (left) and corresponding crossed polars image (right). Note the absence of birefringence under crossed polars, demonstrating the amorphous nature of the particles; b) ACC nanoparticles formed on the surface of portlandite hexagonal plates (squared area) in a lime paste during early carbonation (24 h) in air, at room *T* and 60 % RH.
Part (b) reprinted from [69] with permission by Springer.

rate of the mortar as well as on the rate of $H_2O$ production following Ca$(OH)_2$ carbonation [64]. Carbonation first occurs on the surface of the plaster/mortar where pore solutions saturated with respect to Ca$(OH)_2$ are in direct contact with atmospheric $CO_2$. Rodriguez-Navarro et al. [74] have shown that under these conditions very rapid carbonation takes place via the formation of ACC at the air-solution interface (Fig. 12a). The precipitated ACC undergoes self-organization [201] displaying a fractal-like structure associated with diffusion-limited colloid-aggregation [202]. During this initial stage, the surface of portlandite crystals in the plaster matrix can also start to carbonate, forming an ACC phase. While the smaller, more reactive portlandite crystals could fully dissolve and transform into ACC during this stage, as shown in Fig. 8, ACC can cover the less reactive, larger portlandite crystals (Fig. 12b). This ACC surface covering can hinder further portlandite dissolution [1], explaining why after an initial fast carbonation the rate decreases sharply, leading to a dormant period at the end of stage 1.

### 6.2. Carbonation stage 2

During the second stage, conversion of metastable ACC into stable calcite (or vaterite and/or aragonite) takes place, a phase transition that according to Rodriguez-Navarro et al. [74] occurs via a dissolution/precipitation mechanism. Also, further drying of the mortar paste contributes to creating an open pore network that facilitates $CO_2$ access to reaction sites (i.e., the surface of unreacted portlandite). These two effects trigger another fast carbonation period, until the rate starts to decrease and eventually becomes asymptotic during the following stage 3 [1].

### 6.3. Carbonation stage 3

During the final stage, the overall carbonation rate is reduced as the reaction front moves further away from the surface of the porous plaster or mortar. In this case the reaction is controlled by diffusion of $CO_2$ to the reaction front through the carbonated mortar layer. In turn, the reaction rate is also affected by the counter-diffusion of product $H_2O$ (as water vapor) from the reaction interface towards the exterior of the structure.

### 6.4. An explanation for the transition between stage 2 and 3

While the transition between stage 1 and 2 is explained by the transformation of (partially passivating) ACC formed on Ca$(OH_2)$ crystals into crystalline $CaCO_3$ [1], it is not so clear why/how a transition from stage 2 to stage 3 occurs. As indicated above, the formation of a passivating $CaCO_3$ product layer on the reactant Ca$(OH)_2$ surface has been suggested as a rate limiting effect that could contribute to explaining why the carbonation of portlandite crystals [75,182] as well as lime plasters and mortars shows deceleratory kinetics [61].

Ruiz-Agudo et al. [71] studied at the nanoscale how the carbonation process evolved in the case of portlandite single crystals, providing additional insights on the mechanism of carbonation at the nanoscale and showing that full passivation might not occur. The authors performed a detailed in situ AFM analysis of the dissolution of portlandite single crystals and their subsequent carbonation, complemented by ex situ FESEM and 2DXRD analyses of portlandite single crystals subjected to carbonation in air at room $T$ and 93 % RH. The authors showed that the dissolution and carbonation reactions are strongly anisotropic, taking place at a faster rate along the <100> than along the ⟨001⟩ directions of portlandite. Moreover, it was observed that initial

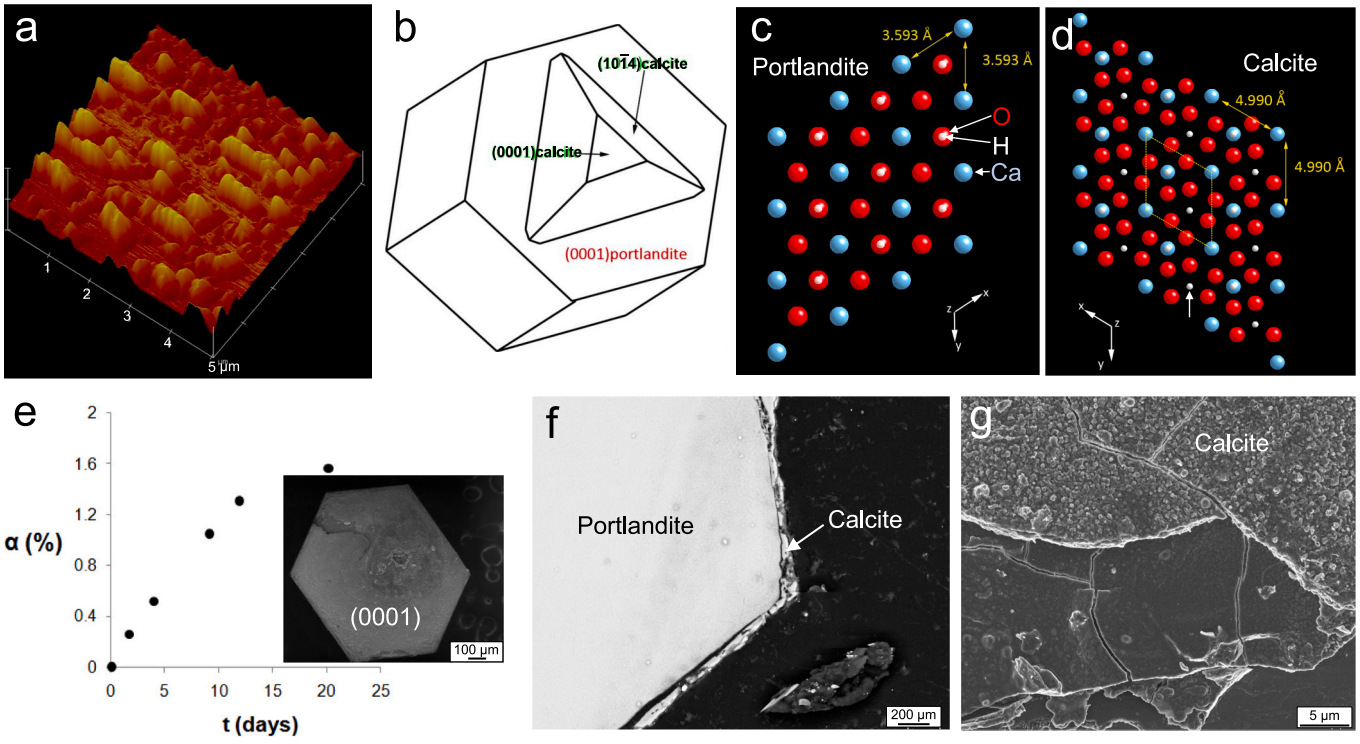


**Fig. 13.** Carbonation of portlandite single crystals. a) Topographic (height) AFM image of the (001) surface of portlandite covered by pyramidal calcite crystals following initial carbonation at 93 % RH in air at room $T$; b) scheme of the formation of calcite on the portlandite (001) basal plane; c) atomic structure of portlandite projected along [001]; d) atomic structure of calcite projected along [001]. Note the similarity of the structures with just a difference in the Ca—Ca bond length of ~20 %, which enables epitaxial crystallization of calcite on portlandite; e) fractional conversion (α) of portlandite into calcite over time (the inset shows and FESEM image of the basal plane of carbonated portlandite); f) FESEM image of a cross-section of partially carbonated portlandite showing the detachment of a thin surface layer of calcite from the {100} faces of portlandite; g) pervasive fracturing in calcite surface layers formed on the basal plane of partially carbonated portlandite. Reprinted from [71] with permission by ACS.

carbonation following dissolution of the (001) faces resulted in the epitaxial precipitation of numerous calcite crystals (most likely after ACC formation) with their *c*-axis parallel to the *c*-axis of portlandite (Fig. 13a). Such crystals nucleated as randomly distributed islands on such surfaces, not forming a continuous carbonate layer. Importantly, 2DXRD analysis showed that the individual calcite crystals displayed a random orientation along their <100> directions (i.e., they were rotated around their *c*-axis). This demonstrated that the formation of calcite on portlandite (001) faces was epitaxial, not topotaxial (and a similar epitaxial effect was expected for the (100) faces). These results also demonstrated that the process did not proceed by a solid-state replacement mechanism, which would be topotaxial. Rather, the reaction involved a tight ICDP mechanism [133]. However, it was postulated that because the transformation of portlandite into calcite implies an increase in volume of ~12 % (i.e., the molar volume of portlandite is 32.81 $cm^3$/mol, and the molar volume of calcite is 36.90 $cm^3$/mol) an impervious (passivating) calcite layer could form eventually. Interestingly, FESEM observation of split sections of partially carbonated portlandite crystals showed fracturing at the carbonate/hydroxide interface, resulting in the detachment of carbonate layers along the (001) planes (Fig. 13b) [71]. This was caused by strain accumulation at this interface associated with the volume increase in the product layer, resulting in stresses high enough to cause the observed fracturing. Fracturing and detachment of carbonated layers exposed fresh portlandite surfaces for carbonation to progress towards the core of the parent phase. This study thus showed that the portlandite crystals were not fully passivated by the carbonate product, in contrast to what was stated by Galan et al. [203] (see below). According to the results by Ruiz-Agudo et al. [71], the transition from stage 2 to 3 is due to the formation of a product layer on the portlandite crystals surface, which does not lead to full passivation. The latter explains why during stage 3 the carbonation rate does not reach a zero value if a fraction of uncarbonated portlandite still persists [1]. Ultimately, Ruiz-Agudo et al. [71] showed that even though the carbonate product layer did not result in full passivation, it acted as a diffusional barrier, inducing an exponential reduction of the carbonation rate over time (Fig. 13e).

Galan et al. [203] also observed epitaxial films of $CaCO_3$ on mm-sized portlandite crystals subjected to carbonation at room *T* in laboratory air as well as 100 % $CO_2$ atmosphere under variable RH conditions (25 to 90 %). By performing dissolution tests, the authors concluded that the $CaCO_3$ surface shells formed at 75 % RH were passivating, but those formed at 90 % RH were not. It seems likely that at 90 % RH, the adsorbed water layer was too thick to enable a pseudomorphic replacement via a tightly coupled ICDP process (i.e., $CaCO_3$ could nucleate both in the bulk aqueous films as well as at the portlandite-solution interface), so a non-continuous permeable calcite layer developed. Conversely at 75 % RH, the few adsorbed $H_2O$ monolayers facilitated a tightly coupled ICDP process (i.e., $CaCO_3$ nucleation only occurred at the portlandite-solution interface), resulting in a pseudomorphic replacement, and yielding a non-porous impervious product surface layer. It is interesting to consider two aspects of the study by Galan et al. [203]: (i) while the carbonate shell formed around the portlandite crystals reduced the dissolution rate of the unreacted $Ca(OH)_2$, it is unclear whether this shell would be able to fully passivate the hydroxide against further carbonation, and (ii), what is more important, the thickness of the calcium carbonate shell formed on mm-sized portlandite crystals reached values of up to ~100 μm after 6 months carbonation in air (laboratory conditions). Considering that $Ca(OH)_2$ crystals in slaked lime typically have sizes up to a few micrometers [36,91], complete carbonation of such crystals under standard conditions (room *T*, atmospheric $pCO_2$ and medium-high ~75 % RH) can be expected within a few weeks. In conclusion, and in contrast to what has been stated by several researchers regarding the carbonation of $Ca(OH)_2$ [12,203,204], we can state that the slow kinetics of lime binders' carbonation, leading to the observed incomplete carbonation of old (medieval) mortars and plasters is not due to a full passivation effect by the carbonate product layer formed on portlandite crystals, but rather to other(s) rate-controlling process(es) that will be discussed below.

### 6.5. Carbonation stages in dolomitic lime mortars

The previous discussion refers to portlandite crystals in high calcium lime pastes, plasters, and mortars based on the large body of published research. In contrast, little information exists on the kinetics of the carbonation of brucite in dolomitic limes. Nonetheless, there are some experimental results on the carbonation of this hydroxide indicating that, as in the case of portlandite, negligible carbonation occurs in the absence of water, because carbonation takes place via a dissolution-precipitation mechanism [164]. Precipitation of a poorly crystalline carbonate phase in the early stages of the reaction does not significantly hinder brucite dissolution, as the carbonate coating remains sufficiently permeable, but Harrison et al. [164] postulate that the conversion of this phase to substantially less porous, crystalline nesquehonite could result in passivation of the brucite surface. However, no experimental proof for the later has been presented. In any case, there is no reason to exclude the possibility of the existence of three distinct stages during the carbonation of the $Mg(OH)_2$-component of dolomitic limes as observed for the case of the $Ca(OH)_2$-component. Yet it is expected that the carbonation of the portlandite component in dolomitic limes will be affected by $Mg^{2+}$ ions in the pore solution. As indicated above, $Mg^{2+}$ is known to stabilize ACC [163], which would likely prolong the dormant period of stage 1, as the conversion of ACC into crystalline (Mg)calcite will be delayed.

### 6.6. Key parameters affecting carbonation rates

Studies on the carbonation kinetics of cementitious materials focused mostly on Portland cement, but in some cases, they also dealt with lime plasters and mortars. These studies show that there are three main factors affecting the overall carbonation rates: (i) *T*, (ii) RH, and (iii) $CO_2$ concentration [17,62,205]. Other factors that have a less pronounced effect on the carbonation rate are the pressure of the reacting gas, grain size and surface area, and porosity and pore-size distribution [206]. Below we focus on the evaluation of the three main factors affecting carbonation rates.

#### 6.6.1. Temperature

The solubility of portlandite decreases with increasing *T* [2,61]. Such a retrograde solubility means that there will be less $Ca^{2+}$ in solution (from $Ca(OH)_2$ dissolution) to react with dissolved $CO_2$ as *T* increases. Similarly, the solubility of $CO_2$ is inversely proportional to *T* [61], and there will be less dissolved $CO_2$ at high *T* than at low *T*. Thus, lower carbonation rates are expected as *T* increases [17]. Conversely, carbonation of portlandite shows Arrhenius behavior (see previous section). This means that the reaction rate will increase with *T*. Similarly, an increase in *T* will also increase the diffusion rate of reactant and product species (i.e., $CO_2$ and $H_2O$) thereby speeding up carbonation. It follows that there should be an optimal *T* at which these two opposite effects balance out, resulting in a maximum carbonation rate. In the case of cement, increasing rates of carbonation are observed with increasing *T* (for constant RH conditions) up to ~60 °C, which marks an inflection point in the carbonation rate [17]. It is expected that such an inflection point would also exist in the case of aerial lime mortars. For the latter case, however, this inflection point has not been determined, although Van Balen and Van Gemert [109] state that the optimum carbonation speed is found at ~20 °C. There is another important factor to consider: increased *T* (leading to lower RH for a given $pH_2O$) will speed up the evaporation of water from the carbonating lime mortar. If the evaporation rate is too high, premature drying might occur, stopping the carbonation process. Conversely, if *T* is too low, the evaporation rate would be lower, and product $H_2O$ might accumulate in the pores, hampering $CO_2$ diffusion and reducing the carbonation rate.

Sanchez-Moral et al. [207] explored the effect of *T* on the kinetics of lime mortars carbonation, and observed faster and more thorough carbonation upon curing in air at 17 °C than at 30 °C. In contrast, their thermodynamic simulation using the geochemical computer code PHRQPITZ showed that the carbonation rate should be higher at the higher *T*. The authors claimed that the slower carbonation at the higher *T* was due to rapid crystallization of numerous small calcite crystals blocking surface pores, which led to a reduction in the diffusion rate of $CO_2$ and did not occur at the lower *T*. It follows that the effect of *T* on carbonation rates is not as simple or predictable as previously thought, and further research is necessary to better understand the effect of this variable on the carbonation of lime plasters.

#### 6.6.2. Humidity

As indicated above, water is critical for the progress of the carbonation reaction and will be very slow at very low RH. The rate of carbonation will also be minimum at very high RH, when capillary condensation occurs inside the pore system of the mortar [109]. In the latter case, the excess water will hamper diffusion of $CO_2$ to the reaction sites. As a result, an optimal intermediate RH value must exist which maximizes the carbonation rate. According to Van Balen and Van Gemert [109] this optimal RH ranges from 40 to 80 % for lime mortars. In the case of cement, and in good agreement with the previous RH values, maximum carbonation rates are observed at RH ranging from 50 to 70 % [17].

#### 6.6.3. $CO_2$ concentration

$CO_2$ concentration (i.e., $pCO_2$) appears to be a ruling factor determining carbonation rates both in aerial lime mortars [77] as well as in cement [17].

Carbonation rates of lime mortars and plaster increase with $pCO_2$. Nevertheless, very high $CO_2$ concentrations (i.e., 100 % [$CO_2$]) can result in extremely fast heat release by the highly exothermic carbonation reaction. As a result, premature drying might take place, hampering further carbonation [61]. Numerous studies show, however, that a less extreme increase in $CO_2$ concentration (5–20 % [$CO_2$]) not only accelerates carbonation but also improves the mechanical properties of the carbonated lime mortars [92,196]. Indeed, several authors observed a significant increase (up to one order of magnitude) in the compressive strength [92,208], as compared with typical values ranging from ~1 up to ~3 MPa for pastes and mortars carbonated in air (i.e., ~0.04 % [$CO_2$]) [46,108,209,210]. These results are striking, as one would expect similar strengths after similar degrees of carbonation for the same pastes/mortars mixes. Apparently, accelerated (or forced) carbonation curing using $CO_2$-rich atmospheres does not only speed up the carbonation process, but also affects the structure of the resulting $CaCO_3$ binder and, in turn, the strength of the material. This was elegantly demonstrated by De Silva et al. [67] who observed that maximum compressive strength of compacted hydrated lime pastes subjected to forced carbonation (2 MPa $CO_2$ pressure) was associated with the formation of large, interconnected rhombohedral calcite crystals. In contrast, carbonation of the same pastes at lower $CO_2$ pressure led to the formation of smaller calcite crystals, not showing an interconnected structure. Considering that the samples carbonated at higher $CO_2$ pressure showed lower portlandite to calcite conversion than those carbonated for the same period of time at lower $CO_2$ pressure, it can be concluded that the morphology of the calcite crystals and the structure of the carbonate matrix formed upon carbonation had a more significant effect on strength than the degree of carbonation. Cizer et al. [69] presented microscopic evidence demonstrating that calcite crystals formed after ACC in mortars, evolved from poorly interlocked scalenohedral to highly interlocked rhombohedral calcite crystals via a dissolution-precipitation mechanisms at a faster rate in 100 % $CO_2$ atmospheres as compared to ambient $pCO_2$. A plausible explanation for this transformation, which progressed over time from the surface to the interior of lime mortar, is the following: upon consumption of available $Ca(OH)_2$, further $CO_2$ dissolution will lead to an acidification of the mortar's pore solution and foster dissolution of scalenohedral calcite crystals. The resulting pore solution saturated with respect to calcite will buffer the pH (i.e., pH of the bicarbonate-carbonate buffer). Upon further drying, precipitation of calcite will take place under close to equilibrium conditions (i.e., low supersaturation and $[Ca^{2+}]/[CO_3^{2-}] \approx 1$) favoring the formation of a limited number of calcite seeds (i.e., low nucleation density) that will grow as large rhombohedral crystals with a compact interlocked structure. This morphology evolution will progress from the surface to the interior, as the surface is directly exposed to $CO_2$, and will be faster and more thorough at high $CO_2$ concentrations. The latter helps to explain why forced carbonation results in plasters and mortars with higher strengths. The above-described calcite morphology evolution also helps to explain why after full carbonation in air, lime mortars show a steady increase in compressive strength over time [92,211].

Similar effects are expected in the case of dolomitic limes. A study by De Silva et al. [107] shows that carbonation at a high $CO_2$ pressure (20 MPa) of compacts prepared with magnesium and calcium hydroxide and their mixtures yielded maximum values of compressive strength for the Mg-rich compacts (>60 MPa). Such carbonated compacts showed large and interlocked nesquehonite and Mg—Ca carbonate phases. Conversely, no reaction or strength gain was observed in Mg-rich compacts when carbonated for 28 days in air at 1 atm. Only the Ca-rich compacts showed an increase in compressive strength under the latter carbonation conditions. These results underline that magnesium hydroxide is poorly reactive at standard atmospheric curing conditions and emphasize that the crystal morphology and texture evolution of the carbonated paste at high $CO_2$ concentrations is critical for strength gain in both magnesian/dolomitic and calcitic limes. These results are also relevant for the understanding of the carbonation curing of MgO cements [20]. However, it should be noted that nesquehonite can evolve into dypingite or hydromagnesite over time (inducing changes in crystal morphology and volume), which might jeopardize the structural integrity of carbonated Mg-rich lime binders [212].

## 7. Kinetics of the carbonation of lime mortars and plasters

### 7.1. Carbonation models

Several models have been proposed for the analysis and prediction of the advancement of the carbonation reaction of hardened cement [43] and lime mortars and plasters [109,213]. These models can be grouped into the following main categories [16]: (i) empirical models, where the relationship between the carbonation depth and its influencing factors is derived from experiments; (ii) statistical models, where the dependent and independent variables are related by mathematical functions, such as multiple linear regression; (iii) numerical models, where several physico-chemical equations, including reaction rates, mass conservation, dissolution and diffusion of $CO_2$ in pore solutions, and energy conservation are computer solved; (iv) machine learning (ML)-based models, which have been recently applied to solve complex non-linear relationships among different variables and parameters involved in the carbonation process.

According to the first type of models (empirical), the progress of the carbonation front in 1D, that is, along the *x* direction normal to the plaster/mortar surface, can be modeled by the second Fick's law of diffusion [47,109]:

$$x = k\sqrt{t} \tag{27}$$

where *t* is the carbonation reaction time and *k* is a rate constant related to the physical-chemical characteristics of the system. Based on this diffusion equation, Van Balen and Van Gemert [109] developed a mathematical model for the evaluation of the uptake of $CO_2$ by a mortar undergoing carbonation while drying progresses. They observed a very fast $CO_2$ uptake during the early stages of carbonation, followed by a

monotonic decrease in the rate of $CO_2$ uptake. The initial fast uptake is consistent with rapid $CO_2$ hydration and subsequent $CaCO_3$ precipitation in the highly alkaline capillary solution (saturated with respect to $Ca(OH)_2$) present in the porous lime mortar. The subsequent monotonic reduction in the carbonation rate is explained by the combined effect of pore volume reduction following conversion of $Ca(OH)_2$ into $CaCO_3$, with a higher molar volume than the former phase, as well as the production of $H_2O$, which hampers the diffusion of $CO_2$ to the reaction front. The reduction in carbonation rate was also assumed to be related to the passivation of the portlandite crystals following surface precipitation of $CaCO_3$ (see, however, Ruiz Agudo et al. [71]). This model assumes that there is a sharp reaction interface between the uncarbonated and carbonated areas. However, it has been experimentally shown that the carbonation front is not a sharp interface, but a diffuse layer with areas of low and high carbonation degree [12,85,204]. The fact that the wake of the carbonation front is not homogeneous, or even continuous, is demonstrated by the observation of the formation Liesegang rings in carbonating lime mortars [73]. Such periodic structures develop in porous systems undergoing diffusion-reaction precipitation [214]. In the case of lime mortars, especially those prepared with aged slaked lime, it is observed that there are alternating bands with high concentration of either $Ca(OH)_2$ or $CaCO_3$, which are clearly distinguished upon application of phenolphthalein (a pH indicator, colorless al pH close to neutrality and with a deep magenta color at pH > 10). Fig. 14a shows an example of the development of such a Liesegang pattern in lime mortars prepared with aged slaked lime putty and quartz sand aggregate (1:3 binder aggregate ratio). The prisms (4 × 4 × 16 cm) were split in half at different elapsed times of carbonation (in air at room *T*) and the fracture surfaces sprayed with a phenolphthalein solution [36,73]. The presence of Liesegang patterns in carbonating lime mortars, evidenced by differential weathering in historic lime mortar structures [215], is a direct proof of the complexity of this process linked to the formation of amorphous precursors (ACC) before the formation of stable calcite [73].

A more detailed numerical model for the carbonation of portlandite at the nano- and micro(pore)scale was recently developed by Varzina et al. [213]. The authors used a lattice Boltzmann framework to model the coupled portlandite dissolution and calcite precipitation during carbonation in air in the presence of an aqueous phase, and modeled reactant diffusion using Fick's second law. Their results show that initially reaction rates are controlled by the dissolution of portlandite, but later, the formation of a porous carbonate layer makes $Ca^{2+}$ and (dissolved) $CO_2$ diffusion through this product layer the rate controlling step. The obtained ion diffusivity across the product carbonate layer was $10^{-13}$ $m^2$ $s^{-1}$, in good agreement with the values of 3.1 × $10^{-12}$ to 8.6 × $10^{-12}$ $m^2$ $s^{-1}$ reported by Galan et al. [203] for accelerated carbonation of portlandite crystals in 100 % $CO_2$ atmosphere. Importantly, the formation of a gap between reactant and product as the reaction progresses, might act as a source of fractures that could detach the product layer from the reactant surface, as experimentally observed by Ruiz-Agudo et al. [71]. This would enable further unrestricted progress of the reaction. In any case, while the results show a diffusion-controlled mechanism, full passivation is not observed. However, the carbonation rate is reduced as the thickness of the carbonate layer increases. Importantly, the model shows that an increase in the concentration of $CO_2$ does increase the carbonation rate, but not so dramatically as could be expected, and this increase only takes place up to a concentration of about 30 % $CO_2$. Yet, higher concentrations of $CO_2$ modify the grow of the carbonate layer: at low $CO_2$ it grows towards the $CO_2$ source, whereas at high $CO_2$ concentrations it also grows in the opposite direction (i.e., towards the reactant portlandite). This would modify the morphology of the carbonate structure, contributing to explaining why lime pastes carbonated at high $CO_2$ concentrations show higher strength, even if the degree of carbonation is not very high. Another important outcome of this computational study is the following: (i) as the product layer grows, a reduction in the size of the pores existing among the calcite particles in this carbonate layer will take place; and (ii) as a result, the solubility of this product phase in the pore solution will be increased, hampering further calcite growth. This so-called "pore-size dependent solubility" effect [213] would prevent closure of the pores between calcite grains of the product layer, enabling a continuous progress of carbonation at reduced rates, even if no cracks develop at the reactant-product interface.

In addition to the previous models specific for lime mortars, several models have been proposed to evaluate the kinetics of carbonation of cement which are reviewed in Qiu [43]. One of them, based on Fick's second law, is the so-called unreacted core-model. It states that the two possible rate-controlling steps in the carbonation of portlandite (in cement) are: (i) diffusion of $CO_2$ to the reaction interface, and (ii) the kinetics of the actual carbonation reaction. Castellote and Andrade [216] demonstrated that experimental carbonation data fit the first case but not the second. The authors conclude that the carbonation of cement is controlled by the diffusion of $CO_2$ along a product shell formed around

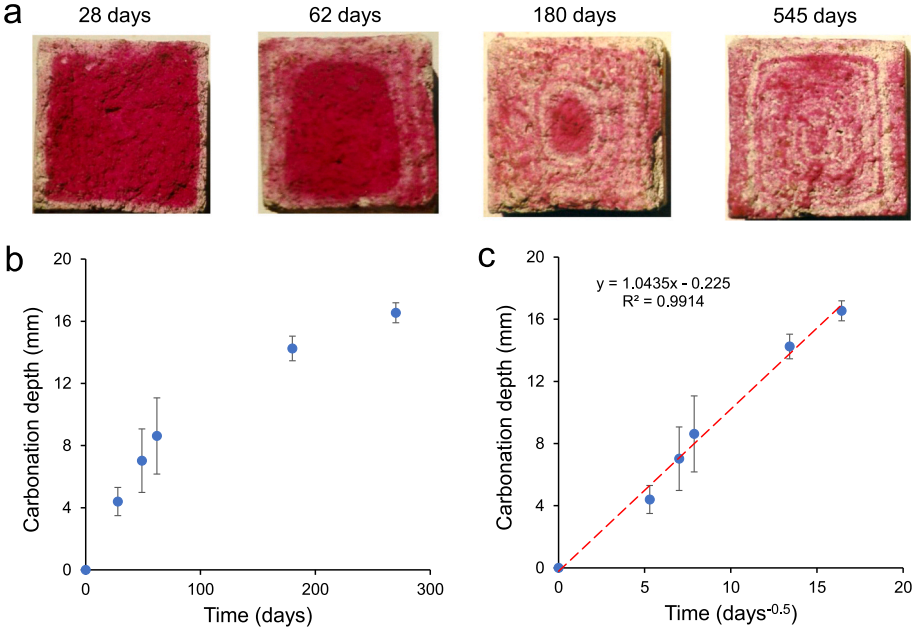


**Fig. 14.** Carbonation evolution of lime mortars. a) Development of Liesegang rings in lime mortars prepared with aged (7 years) slaked lime putty after curing at 60 % RH in air for different periods of time. Standard 4 × 4 × 16 cm mortar prisms (1:3 binder: aggregate ratio) were split and sprayed with phenolphthalein; b) time-evolution of the carbonation depth for the mortars samples depicted in (a); c) the data presented in (b) now represented considering the square root of time. Note the excellent linear fitting to Eq. (27) with a *k* value of 1.043 mm·day$^{-0.5}$. Modified from [73] with permission by Royal Society Publishing.

the unreacted core. Based on Fick's second law, their diffusion-controlled model allows to calculate the fractional conversion of reactant *s*, $X_s$, at a given time *t*, for the case of a cylindrical sample of radius *R*, by using the following equation,

$$X_s = 1 - \left(\frac{r}{R}\right)^2 \quad (28)$$

where *r* is the radius of the unreacted core. The model also enables to calculate the time τ for achieving full carbonation knowing the fractional conversion at a time *t*, given by,

$$\frac{t}{\tau} = X_s + (1 - X_s)ln(1 - X_s) \quad (29)$$

Knowing τ, it is also possible to calculate the effective diffusion coefficient of $CO_2$ across the product layer, *D*, by,

$$\tau = \frac{\rho_s R^2}{4bDC_{CO2}} \quad (30)$$

where $\rho_s$ is the molar fraction of reactant *s*, in the solid, *b* is the stoichiometric coefficient for the carbonation reaction (in the case of portlandite *b* is 1), and $C_{CO2}$ is the concentration of $CO_2$ in the gas phase. Importantly, once *D* is determined for a particular system, the model can be applied to other conditions including variations in $CO_2$ concentration and exposure time. However, this model does not take into account other relevant parameters such as *T* or RH, which are considered in other, more complex models [43,167]. Nonetheless, Castellote and Andrade [216] model, or the more complex ones listed in Qiu [43], have not been used yet to evaluate the kinetics of carbonation of aerial lime mortars.

### 7.2. Experimental carbonation rates of lime mortars

There are several studies that experimentally determined the progress of the carbonation front during setting and hardening of aerial lime mortars. However, only a few report the actual value of *k*, that is, the overall carbonation rate according to Eq. (27). Yet many include numeric values that enable its calculation. Once *k* is known, it is possible to evaluate the time evolution of the carbonation front using Eq. (27).

Table 2 presents *k* values from several studies on lime mortars and plasters carbonation in air at standard *P-T* conditions (a few *k* values corresponding to forced carbonation in $CO_2$-rich atmosphere are included for comparison) [46,47,66,68,92,211,217–223], evidencing that there is a significant scattering in carbonation rate values. Note that except for Ardigoyen and Alvarez [66], *k* values presented in Table 2 are calculated from the analysis of the carbonation depth in split samples sprayed with phenolphthalein (in most cited papers only the depth of the carbonation front at different time intervals is reported). In the case of the lime mortars showing Liesegang pattern development depicted in Fig. 14a, a value of *k* of 1.04 mm·day$^{-1/2}$ is calculated (Fig. 14b–c). Overall, carbonation rate values presented in Table 2 show that full carbonation of an air lime mortar or render with a thickness of about 5 cm can take up to two and a half centuries in the worst-case scenario ($k$ = 0.16 mm·day$^{-1/2}$), and for the average *k* value of 1.23 (±0.89, $N = 28$) mm·day$^{-1/2}$ from the previous studies, the full carbonation of such a mortar/plaster element would take ~4.5 years. This must be considered when designing lime-based masonry units or when preparing laboratory samples for testing, as curing times, for instance, need to be adjusted to the kinetics of lime carbonation. The latter is critical because in some cases test specimen properties, such as compressive and tensile strength, are determined at 28 days, which might be appropriate for cement, but not for slow-setting (carbonating) aerial lime mortars.

The large scattering of *k* values from different studies is likely due to variations in mortar preparation (i.e., different lime or aggregate type and water:binder:aggregate ratios) and curing conditions, all of these factors having an influence on the carbonation rate.

**Table 2**
Carbonation rate (*k*) values of lime mortars calculated from published values of carbonation depth over time determined using phenolphthalein.

| Mortar type, aggregate, binder/aggregate (B/A) ratio, water/binder (W/B) ratio | Curing conditions[a] | *k* value (mm·day$^{-1/2}$) | Ref. |
|---|---|---|---|
| Lime mortar | n.a.[b] | 1.00 | [221] |
| Lime-cement mortar | n.a. | 0.25 | [221] |
| Hemp-lime mortar | 60 % RH | 5.24 | [221] |
| Lime mortar, silicate sand, 1:3 v/v B/A, 0.5–0.54 wt/wt W/B | 25 °C, 60 % RH | 0.95–1.37 | [222] |
| Lime mortar (4 months aged putty), oolitic stone aggregate, 1:3 v/v B/A | 90 % (7 days)/60 % RH | 1.16 | [68] |
| Lime mortar (4 months aged putty), silicate sand, 1:3 v/v B/A | 90 % (7 days)/60 % RH | 1.56 | [68] |
| Lime mortar (4 months aged putty), crushed bioclastic stone aggregate, 1:3 v/v B/A | 90 % (7 days)/60 % RH | 1.23 | [68] |
| Lime mortar, silicate sand, 1:2 v/v B/A, water content 16–18 wt % | 60 % RH, 0.05 % $CO_2$ | 1.53–2.00 | [92] |
| Lime mortar, silicate sand, 1:2 v/v B/A, water content 16–18 wt % | 60 % RH, 5 % $CO_2$ | 6.32–6.66 | [92] |
| Lime mortar, silicate sand, 1:2 v/v B/A, added air-entraining agents | 60 % RH | 1.58–1.96 | [217] |
| Lime mortar, silicate sand, 1:3 v/v B/A, 1.3 v/v W/B | 60 % RH | 1.25–1.30 | [46] |
| Lime mortar, fine aggregate, 1:3 wt/wt B/A, 0.8 wt/wt W/B | 60 % RH | 1.13 | [219] |
| Lime mortar (putty), silicate sand. 1:3 v/v B/A | 50 % or 90 % RH | 2.29 | [220] |
| Lime mortar (aerial+hydraulic), silicate sand, 1:3 v/v B/A | 50 % or 90 % RH | 1.82 | [220] |
| Lime mortar (putty), silicate sand/crushed rock aggregate, 1:3 v/v B/A | 50 % or 90 % RH | 2.10 | [220] |
| Lime mortar (aerial), silicate sand/crushed rock aggregate, 1:3 v/v B/A | 50 % or 90 % RH | 1.40 | [220] |
| Lime mortar, silicate sand (grinding 0′-15′), 1:3 wt/wt B/A, 0.75 wt/wt W/B | 60 % RH, 30 °C | 0.16–0.23 | [223] |
| Lime mortar, silicate sand (grinding 0′-15′), 1:3 wt/wt B/A, 0.75 wt/wt W/B, 4 wt% organics | 60 % RH, 30 °C | 0.40–0.71 | [223] |
| Lime mortar, crushed limestone aggr., 1:3 v/v B/A, 0.9 v/v W/B | 97 % (7 days, 20 °C)/51 % (up to 448 days, 17 °C) RH | 0.20–0.47 | [211] |
| Lime paste, no aggregate, 0.8–1.3 W/B | 60 % RH | 0.66–0.91 | [66] |

[a] Unless stated otherwise, all values correspond to mortars cured in air (~0.03–0.04 % $CO_2$ concentration) at room *T* (20 °C).
[b] Not available.

It is important to indicate that most experimental results on the carbonation of aerial lime mortars show that at the selected testing times (typically <90 days) incomplete carbonation was observed. For instance, Oliveira et al. [46] report a limit for the carbonation level of 70 % irrespective of curing time up to 90 days. This is commonly associated with a passivating effect by the carbonate product layer formed on portlandite crystals. As indicated above, this is very unlikely [71]. It is more likely that the limited carbonation observed is due to low RH conditions and excessive drying, in addition to the limited span of the carbonation curing.

Indeed, from the data reported by Ruiz-Agudo et al. [71] for the carbonation of mm-sized single crystals (room *T*, in air and 93 % RH) a *k* value of 0.0034 mm·day$^{-1/2}$ is obtained, whereas from the model by Varzina et al. [213], simulating carbonation of portlandite single crystals at room *T* in air, a *k* value of 0.012 mm·day$^{-1/2}$ is obtained (i.e., a

carbonated layer of 15 μm is developed within 20 or 1.5 days, respectively). These $k$ values are about two to three orders of magnitude smaller than the average $k$ value determined for lime mortars and plasters carbonated under similar conditions (see above). It is therefore evident that the rate controlling step for carbonation in a lime mortar or plaster is not the diffusion of ions across the carbonate product layer formed on individual portlandite crystals. Conversely, it is very likely that the small (micrometer) size/thickness of individual portlandite crystals in slaked lime leads to their full conversion (within a few days) before a sufficiently thick layer of product carbonate would have developed on such crystals to act as an effective diffusional barrier. This shows that the most likely overall rate-limiting factor for the carbonation of lime mortars and plasters is the actual diffusion of $CO_2$ along the (open and/or partially saturated) pore network in the carbonated profile.

A detailed understanding of the mechanisms and kinetics of lime mortars carbonation is not only relevant for predicting the time evolution of these materials' physical-mechanical properties, but also for predicting their capacity to capture atmospheric $CO_2$ and enable a proper Life Cycle Assessment (LCA) [224]. Note that it has been reported that if a lime-based structure achieves full carbonation, it will contribute to an average capture of ~33 % of the amount of process $CO_2$ emitted during the production of this binder for permanent and safe mineral storage as carbonate phases (EULA, https://www.eula.eu/download/capturing-co2-with-lime/). It is therefore necessary to determine the carbonation rate of a particular lime-based material to evaluate if it will achieve its maximum $CO_2$ capture capacity over its service life.

## 8. Accelerating carbonation

One of the main handicaps for the current use of aerial lime-based mortars and plasters, both in built heritage conservation and modern construction, is the fact that their carbonation is very slow. This makes it difficult to meet building requirements where early strength is needed. To solve this problem, several approaches have been explored to accelerate carbonation and by-pass one or more of the main rate-controlling factors above indicated, namely: (i) $T$, (ii) moisture content/RH, and (iii) $CO_2$ concentration, diffusion through the pore system, and dissolution in pore water. The two first factors can be more or less easily controlled. In general, room $T$ is considered appropriate for optimal carbonation and optimal RH values range from 40 to 80 % [109]. The optimization of $T$ and RH has an impact on carbonation rates, but in practical terms the effects are not so dramatic. Much more important effects are observed by altering the concentration of $CO_2$ and in what manner this gas dissolves in the pore water and reaches the reaction interfaces.

As indicated in the previous sections, increasing $pCO_2$ has a dramatic effect on carbonation rates [61,67]. However, it is not always feasible to increase the $CO_2$ concentration on site where a plaster or mortars is applied. And it is even more difficult to increase the concentration of $CO_2$ where it is more needed, that is, in-depth, within the pore system of a lime mortars or plaster. There are however several studies that present feasible strategies to increase $pCO_2$ within the pore system of a mortar without the need for an external (pressurized) $CO_2$ supply. Compounds such as $NH_4HCO_3$ or $(NH_4)_2CO_3$ lead to the rapid release of $CO_2$ and $NH_3$, fostering carbonation if dosed in the mortar mix. However, they show significant problems for practical application as they induce premature $CaCO_3$ precipitation upon mixing, increasing the fresh lime paste viscosity, and drastically reducing workability [180]. As an alternative to this approach, Baglioni et al. [180] proposed the addition of ethyl or ammonium carbamates to a lime-based conservation grout. During what the authors call "autogenous" setting, the carbamate slowly decomposes at room $T$ releasing $CO_2$ via the reaction,

$$R - O - CO - NR'_2 + H_2O = ROH + CO_2 + HNR'_2 \quad (31)$$

where R is $C_2H_5$ for ethyl carbamate and $NH_4^+$ for ammonium carbamate, and R′ is H.

As a result, in depth carbonation is achieved speeding up the kinetics of lime mortars setting and hardening. The authors observed that carbonation followed a 3D-diffusion model (i.e., D3 model in Table 1). The good fitting of experimental carbonation data of lime grouts dosed with carbamates shows that 3D diffusion of $CO_2$ to the reaction sites (i.e., portlandite-pore solution interfaces) was the rate-determining step.

Medici and Rinaldi [225] tested the addition of poly-amino-phenolic (PAP) compounds, known for their capacity to capture $CO_2$, to accelerate the carbonation of lime mortars. The authors observed a dose-dependent (0.1–0.3 %) acceleration of carbonation in saturated $Ca(OH)_2$ solutions. In parallel they also observed a significant increase in the compressive strength of the carbonated mortars with PAP as compared with the additive-free control. However, dosing the additive at a high concentration (1 %) led to a lower strength than the control mortar. Despite the promising results obtained by using these additives (carbamates and PAP) no follow-up studies or on-site applications have been reported so far to our knowledge.

Ergent et al. [226] proposed the use of diethyl carbonate (DEC, commercially known as DiloCarB®) as a carbonation accelerator. The authors stated that a faster carbonation was achieved in lime mortars dosed with this additive. However, their TG analysis of the consumption of portlandite over time does not show a clear effect on the carbonation rate of mortars with added DEC as compared with the control without additive.

The addition of photoactive anatase ($TiO_2$) nanoparticles was proposed by Karatasios et al. [227] to speed up the carbonation of lime plasters. The authors stated that light irradiation would enable the photooxidation of organic deposits on the mortars surface by the $TiO_2$ nanoparticles in the mortar mix, resulting in the release of $CO_2$ and an acceleration of the carbonation of the lime-binder. However, it is rather unclear if this approach could lead to an acceleration of the carbonation in-depth (i.e., where it is most needed), as the photo-activity of $TiO_2$ would be limited to a very thin surface layer (i.e., the depth that light could penetrate in the mortar).

Another way of speeding up carbonation by increasing $CO_2$ concentration within a mortar mix involves the use of organic additives, fermented plant extracts in particular [223,228–230]. Upon fermentation of the plant extract, $CO_2$ is produced and released within the pore system of the fresh mortar mix. Ultimately, faster and more in-depth carbonation is observed, resulting in a higher compressive strength at early age (28 days). Other natural organic additives have been proposed to speed up lime mortar carbonation. Following the ancient Mesoamerican tradition of adding cactus aqueous extracts to lime mortars and plasters [118], León-Martínez et al. [231] observed a slight increase in the carbonation rate of lime mortars prepared with *Oppunctia ficus-indica* and *Acanthocereus tetragonus* mucilage dosed in a concentrations of 0.25 wt%, but mortars prepared with a higher dose of additive (0.5 wt %) showed little acceleration or even a decrease in the rate of carbonation. Addition of up to 0.4 wt% chitosan to pure lime mortars slightly accelerated carbonation at 100 % $CO_2$ curing conditions, leading to a minor increase in compressive strength [232]. It is unclear though whether the latter acceleration effect will also be observed upon carbonation under ambient conditions.

Arizzi and Cultrone [108] indicate that carbonate aggregate can accelerate carbonation because its angular-shape and roughness favor the formation of communicated pores as opposed to smooth/rounded silicate aggregate (quartz sand). However, although porosity and pore size have an impact on carbonation rates, it is likely that the calcite aggregate will act as a template for $CaCO_3$ heterogeneous nucleation, further speeding up carbonation. Moreover, the newly formed carbonate cement likely grows in crystallographic continuity (i.e., self-epitaxy), and no discontinuity between the aggregate and the carbonate cement is to be expected. As a result, higher strength should be achieved as

compared with mortars prepared using siliceous aggregate (where no crystallographic continuity between the aggregate and the carbonate cement exists), which is in accordance with findings by Arizzi and Cultrone [108] and others [233,234]: a higher strength is achieved as compared with mortars prepared using siliceous aggregate (where no crystallographic continuity between the aggregate and the carbonate cement exists). Hay et al. [208] also reported increased carbonation rates and strength of lime mortars prepared adding ground limestone. As in the previous case, it is assumed that such effects are due to the template action of the ground calcite in the limestone. However, not all carbonate aggregates speed up carbonation: Martinez-Garcia et al. [235] report a reduction in the carbonation rate of lime mortars prepared using ground mussel shell aggregate, as compared with mortars prepared using standard limestone aggregate. Nonetheless, once carbonated, the former mortars reached higher compressive strength than the latter, which is explained considering that the organics in the shell biomineral played a role in the formation of the carbonate binder.

Other possibility to speed up carbonation is to increase the porosity and pore size of the mortar either using a nanosized aggregate, such as ball-milled quarry waste nanoparticles [236], or using additives, such as surfactants with the capacity of acting as air entraining agents (AEA) [217]. The increase in porosity and pore size enables a faster and easier access of diffusing $CO_2$ to reaction sites. However, Silva et al. [217] reported that while an acceleration of the carbonation process was observed with the addition of AEAs, in some cases it was observed that the resistance to weathering (freeze-thaw) was reduced as compared with AEA-free reference aerial lime mortars. Moreover, it should be noted that organic additives such as proteins or polysaccharides in some cases are reported to speed up carbonation [223], but in other cases tend to slow down the carbonation process, yet they typically improve the mechanical properties of the carbonated lime mortars or plaster [97,160,237].

An interesting possibility to enhance in-depth carbonation of lime mortars and plasters could involve the use of silica aerogel particles loaded with $CO_2$, or silica aerogels functionalized with amine compounds for a more effective $CO_2$ capture during $CO_2$ loading, as reported

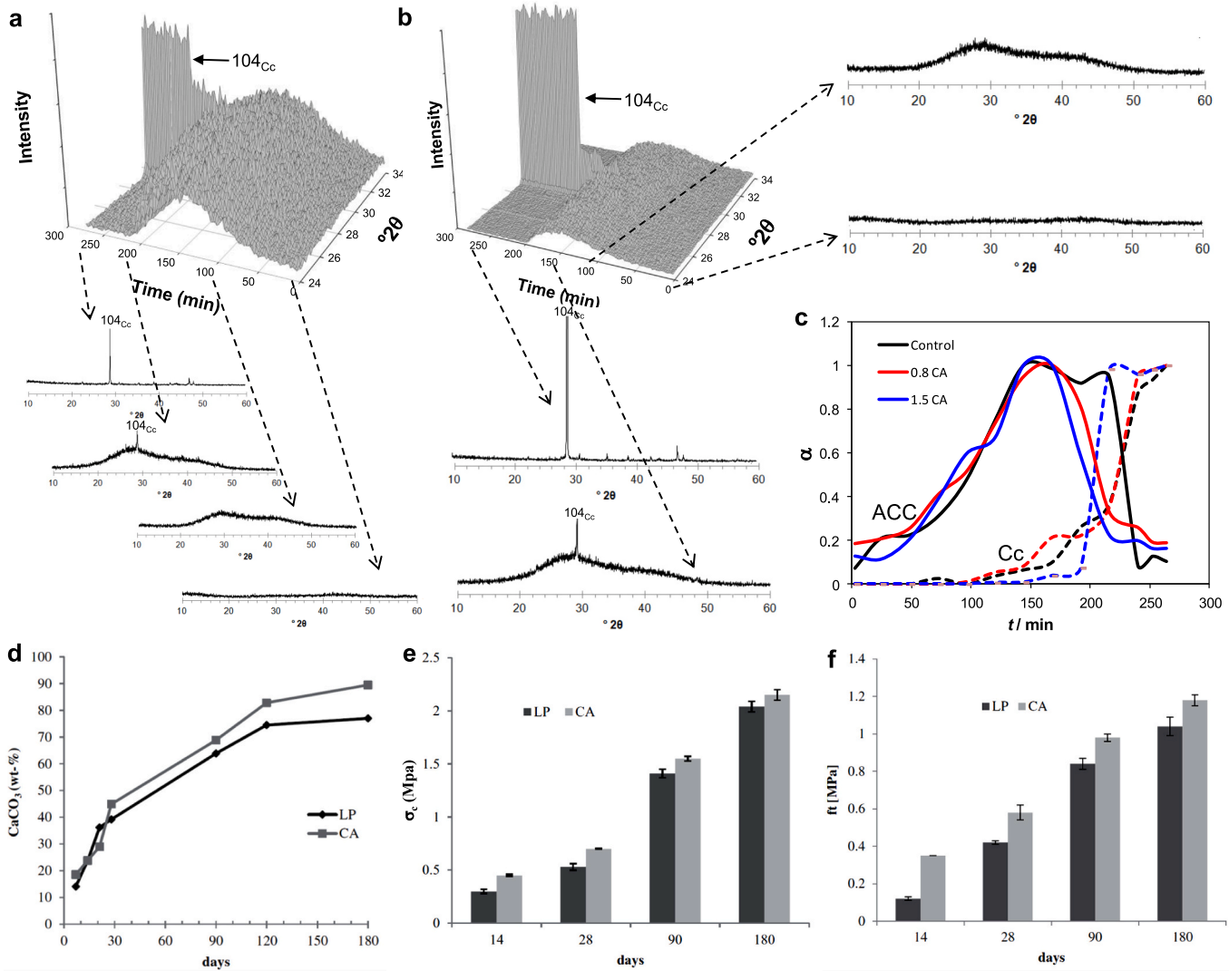


**Fig. 15.** Effect of carbonic anhydrase (CA) enzyme on the carbonation kinetics and physical mechanical properties of lime-based binders. Time-resolved XRD patterns of $Ca(OH)_2$ saturated solution droplets without (a) and with CA (b) exposed to atmospheric $CO_2$. Note the increase in the background intensity due to the formation of ACC and its decrease upon calcite precipitation (best seen in individual XRD patterns, in inset). The 104 Bragg peak of calcite (Cc) is indicated. (c) Time evolution of the fractional amount (α) of ACC (solid lines) and calcite, Cc (dashed lines) in the control (CA-free) and runs with CA dosed in different concentrations (μM); d) time evolution of carbonation for lime pastes with CA and without CA (control, LP); Time evolution of the compressive (e) and flexural (f) strength ($\sigma_c$ and $\sigma_f$, respectively) of lime pasted with CA and without CA (control, LP).
Figure parts a–c reprinted from [151] with permission by Elsevier; parts d–f reprinted from [70] with permission by Taylor & Francis.

by Jassam et al. [238] for the case of cement carbonation curing. Upon mixing with lime during mortar preparation and subsequent setting, $CO_2$ would be released from the silica aerogel within the mortar matrix, contributing to enhanced lime carbonation.

For the case of nanosized portlandite particles (nanolimes), Zhu et al. [239] reported that the addition of graphene quantum dots (GQD) during homogeneous nanolime synthesis, enabled a faster carbonation, not only linked to the high surface area of the nanoparticles, but also to the effect of the adsorbed/incorporated GQD. The latter speeded up the absorption and hydration of $CO_2$ in the presence of humidity, facilitating the conversion of $Ca(OH)_2$ into $CaCO_3$.

Recently, a biomimetic approach has been proposed to accelerate carbonation of lime mortars and plasters. It involves the use of natural enzymes such as carbonic anhydrase (CA) that catalyzes the hydration of $CO_2$ [70,151], as well as their biomimetics, in this case molecular organic framework (MOF), compounds with active metal sites for such a catalysis [50]. In the case of CA, which is key for the biomineralization of $CaCO_3$ by different organisms (e.g., sea-urchins and sea shells), it is observed that this enzyme accelerates the formation of ACC and its transformation into calcite following carbonation in air of a saturated Ca $(OH)_2$ solution (Fig. 15a–c) [151]. Similarly, aerial lime pastes dosed with 1.5 μM CA display a faster carbonation (in air) than reference pastes without this enzyme (Fig. 15d) [70]. Remarkably, both the compression and flexural strength of CA-including lime pastes were higher than those of the CA-free reference pastes regardless of their carbonation time (Fig. 15e-f). It follows that the enzyme not only accelerates carbonation, but also affected the microstructure of the calcite binder, leading to an improvement in the mortars' mechanical properties. Ultimately, this biomimetic approach by-passes one of the most significant rate-limiting step of the carbonation reaction, which is the conversion of $CO_2$ into bicarbonate ions (Eq. (15)). It also leads to binders with improved physical-mechanical properties and nano/microstructural features that somehow resemble those of calcite biominerals (e.g., shells), whose hybrid inorganic-organic nature and hierarchical (nano-micro-meso)structure, impart them a higher hardness and toughness than their individual components [166].

## 9. Conclusions and outlook

Here a general overview of what is known as the carbonation reaction is presented, showing that it is highly relevant not just for the better understanding of the setting and hardening of lime-based mortars and plasters, but also for a range of technological and natural processes, spanning from PCC production and the degradation of reinforced concrete to the long-term control of the climate on Earth.

It is shown that the carbonation reaction is complex from a (geo) chemical point of view, with several interrelated reactions taking place nearly simultaneously that control both the mechanism and the kinetics of this fundamental reaction. Importantly, it is observed that from a chemical (reaction) point of view the rate controlling step is the hydration of $CO_2$ to form bicarbonate and carbonate ions. However, in practice, for systems that are not diffusion-limited, the rate controlling step of the carbonation reaction is the dissolution of the hydroxide parent phase. This is supported by the fact that calculated activation energy values for carbonation of portlandite match those of reaction-controlled kinetics for the dissolution of common minerals.

It is underlined that the carbonation reaction progresses via non-classical crystallization routes, involving several precursors including PNC and amorphous (liquid-like and solid) phases. Moreover, it is now clear that carbonate crystal growth does not necessarily follow a classical route but involves aggregation and attachment of solid nanoparticles (e.g., ACC).

The analysis of the literature reveals that the idea regarding the mechanism of carbonation of lime binders has changed over time. While in the past it was assumed that it was a gas-solid reaction (i.e., solid-state reaction), more recent results obtained using advanced analytical techniques have unambiguously demonstrated that it is a dissolution-precipitation reaction, where the presence of adsorbed water is critical.

Regarding the kinetics of carbonation, a clear distinction has to be made between the carbonation kinetics of $Ca(OH)_2$ crystals, powders and thin films, and the carbonation kinetics of lime-based plasters and mortars. The kinetics of the former can be modeled using classical "solid-state" kinetic models, with deceleratory kinetic models (e.g., F1 and F2) yielding excellent fittings. Conversely, in the case of plasters and mortars, diffusion-limited kinetics rule, and modeling of the carbonation evolution using Fick's second law yields very good fittings, demonstrating that the carbonation front advances with the square root of time. Yet, numerical models using Fick's second law enable to obtain a more accurate picture of the (nano)micro-scale evolution of the carbonation reaction. Importantly, in the case of lime plasters and mortars, rate constants ($k$ values) display a large scattering. This is likely due to the fact that different researchers used different lime-based materials, with variation in the type of binder and aggregate, binder/aggregate ratios, water/binder ratio, and curing conditions. Nonetheless, reported $k$ values show that the carbonation of lime mortars and plasters is very slow, with carbonation of cm-thick sections taking several years.

It is also shown that the formation of a carbonate product layer around portlandite crystals via an ICDP mechanism, does not necessarily result in passivation. Upon reaching a limiting thickness, strain and associated stress due to the molar volume difference between reactant and product phases leads to cracking and detachment of carbonate layers, exposing fresh portlandite surfaces and facilitating the advancement of the carbonation front towards the core of the hydroxide crystals. It is also observed that the carbonate layer is porous, and modeling predicts that pore-closure is unlikely due to pore size solubility effects. As a result, carbonation rates become diffusion controlled by the slow diffusion of reactant/product ions/molecules across this diffusive carbonate barrier.

It is also shown that dolomitic limes undergo NCC during carbonation, with the presence of both ACC after the carbonation of the Ca $(OH)_2$ fraction and AMC following the carbonation of $Mg(OH)_2$. However, while the $Ca(OH)_2$ fraction carbonates in a similar way as in calcitic limes, the $Mg(OH)_2$ fraction is basically unreactive, and undergoes negligible or very little carbonation over time under standard $P$-$T$ conditions.

Future research on the carbonation of lime-based binders should address several key issues that are still not completely understood. One of them refers to fully disclosing the differences in the mechanism and kinetics of carbonation of $Ca(OH)_2$ and $Mg(OH)_2$. In particular, it would be important to fully understand why brucite is so poorly reactive as compared with portlandite. Attention needs also to be paid to understand the role of magnesium ions on the kinetics of both calcium and magnesium carbonate phases formation. Another aspect that should be further studied is the (nano-micro)structure-property relationship of carbonated calcitic and dolomitic limes, and how this is affected by additives, particularly organic (bio)macromolecules. This will provide key information about the secret of ancient masons from different civilizations which produced lime mortars and plasters of outstanding properties and durability using different natural organic additives such as sticky rice (ancient China) or bark extracts (ancient Maya) [240]. It will also be relevant to evaluate the effects of such additives (natural or synthetic) on the carbonation kinetics of lime mortars and plasters. Ultimately, we could learn from Nature and strive to produce, by a biomimetic approach, improved lime-based carbonate binders with structure and properties matching those of carbonate biominerals. This could be achieved by using (natural or synthetic) organic additives similar to those involved in $CaCO_3$ biomineralization.

Finally, a better understanding of the mechanism and kinetics of carbonation of aerial calcitic and dolomitic limes will offer the possibility of modifying key (rate controlling) parameters to speed up the carbonation reaction and improve the physical-chemical and mechanical properties of the set and hardened lime mortars and plasters. This

could be achieved by using a biomimetic approach involving natural and/or synthetic additives, such as carbonic anhydrase enzyme or MOF-based compounds to accelerate carbonation. Another related area of research should focus on disclosing the role of organic additives in modifying the structure of the final $CaCO_3$ crystals in the set and carbonated lime mortars/plasters. It is hypothesized that organics could be occluded in the $CaCO_3$ crystals of carbonated lime mortars, as occurs in $CaCO_3$ biominerals such as mollusk shells, thereby imparting the carbonated matrix similar physical-mechanical properties as those observed in calcite biominerals. The latter, being organic-inorganic hybrid materials, show toughness and damage tolerance orders of magnitude higher than their individual components. Learning from nature, we could strive to develop lime-based materials with improved properties for their use as compatible materials for built heritage conservation, as well as for their use as sustainable binders in modern construction [240].

## CRediT authorship contribution statement

**Carlos Rodriguez-Navarro:** Conceptualization, Methodology, Investigation, Validation, Writing – original draft, Supervision, Project administration, Funding acquisition. **Teodora Ilić:** Investigation, Writing – review & editing. **Encarnación Ruiz-Agudo:** Investigation, Validation, Writing – review & editing, Project administration, Funding acquisition. **Kerstin Elert:** Conceptualization, Investigation, Methodology, Validation, Writing – review & editing.

## Declaration of competing interest

The authors declare that they have no known competing financial interests or personal relationships that could have appeared to influence the work reported in this paper.

## Data availability

All data in this paper are included in the main text.

## Acknowledgements

We acknowledge funding by the Spanish Government grant PID2021-125305NB-I00 funded by MCIN/ AEI /10.13039/ 501100011033 and by ERDF A way of making Europe, Junta de Andalucía research group RNM-179 and grant P20_00675, University of Granada, Unidad Científica de Excelencia UCE-PP2016-05, and European Commission, H2020 Programme, Marie Skłodowska-Curie Action European Training network – Innovative Training Network (ETN-ITN), SUBlime (grant agreement # 955986). Funding for open access charge: Universidad de Granada/CBUA.

## References

[1] Ö. Cizer, K. Van Balen, J. Elsen, D. Van Gemert, Real-time investigation of reaction rate and mineral phase modifications of lime carbonation, Constr. Build. Mater. 35 (2012) 741–751.
[2] R.S. Boynton, Chemistry and Technology of Lime and Limestone, Wiley, New York, 1980.
[3] K. Elert, C. Rodriguez-Navarro, E.S. Pardo, E. Hansen, O. Cazalla, Lime mortars for the conservation of historic buildings, Stud. Conserv. 47 (2002) 62–75.
[4] J. Lanas, J.P. Bernal, M.A. Bello, J.A. Galindo, Mechanical properties of natural hydraulic lime-based mortars, Cem. Concr. Res. 34 (2004) 2191–2201.
[5] A. El-Turki, R.J. Ball, G.C. Allen, The influence of relative humidity on structural and chemical changes during carbonation of hydraulic lime, Cem. Concr. Res. 8 (2007) 1233–1240.
[6] H.F. Taylor, Cement Chemistry, Thomas Telford, London, 1997.
[7] Ö. Cizer, K. Van Balen, D. Van Gemert, Competition between hydration and carbonation in hydraulic lime and lime-pozzolana mortars, Adv. Mater. Res. 133-134 (2010) 241–246.
[8] M.D. Jackson, E.N. Landis, P.F. Brune, M. Vitti, H. Chen, Q. Li, M. Kunz, H. R. Wenk, P.J.M. Monteiro, A.R. Ingraffea, Mechanical resilience and cementitious processes in Imperial Roman architectural mortar, Proc. Natl. Acad. Sci. 111 (2014) 18484–18489.
[9] P. Hewlett, M. Liska (Eds.), Lea's Chemistry of Cement and Concrete, Butterworth-Heinemann, New York, 2019.
[10] J. Elsen, M.D. Jackson, E. Ruiz-Agudo, Historic concrete science: *opus caementicium* to "natural cements", Elements 18 (2022) 301–307.
[11] W.F. Cole, B. Kroone, Carbonate minerals in hydrated Portland cement, Nature 84 (1959) BA57.
[12] A. Morandeau, M. Thiery, P. Dangla, Investigation of the carbonation mechanism of CH and CSH in terms of kinetics, microstructure changes and moisture properties, Cem. Concr. Res. 56 (2014) 153–170.
[13] W. Ashraf, Carbonation of cement-based materials: challenges and opportunities, Constr. Build. Mater. 120 (2016) 558–570.
[14] B. Šavija, M. Luković, Carbonation of cement paste: understanding, challenges, and opportunities, Constr. Build. Mater. 117 (2016) 285–301.
[15] S. Steiner, B. Lothenbach, T. Proske, A. Borgschulte, F. Winnefeld, Effect of relative humidity on the carbonation rate of portlandite, calcium silicate hydrates and ettringite, Cem. Concr. Res. 135 (2020), 106116.
[16] Z. Chen, J. Lin, K. Sagoe-Crentsil, W. Duan, Development of hybrid machine learning-based carbonation models with weighting function, Constr. Build. Mater. 321 (2022) 126359.
[17] Z. Xu, Z. Zhang, J. Huang, K. Yu, G. Zhong, F. Chen, W. Yang, Y. Wang, Effects of temperature, humidity and $CO_2$ concentration on carbonation of cement-based materials: a review, Constr. Build. Mater. 346 (2022), 128399.
[18] S. Monkman, Y. Shao, Assessing the carbonation behavior of cementitious materials, J. Mater. Civ. Eng. 18 (2006) 768–776.
[19] S. Kashef-Haghighi, S. Ghoshal, $CO_2$ sequestration in concrete through accelerated carbonation curing in a flow-through reactor, Ind. Eng. Chem. Res. 49 (2010) 1143–1149.
[20] D. Zhang, Z. Ghouleh, Y. Shao, Review on carbonation curing of cement-based materials, J. $CO_2$ Util. 21 (2017) 119–131.
[21] Z. Liu, W. Meng, Fundamental understanding of carbonation curing and durability of carbonation-cured cement-based composites: a review, J. CO2 Util. 44 (2021), 101428.
[22] V.G. Papadakis, C.G. Vayenas, M.N. Fardis, Fundamental modeling and experimental investigation of concrete carbonation, ACI Mater. J. 88 (1991) 363–373.
[23] J. Cowie, F.P. Glasser, The reaction between cement and natural waters containing dissolved carbon dioxide, Adv. Cem. Res. 4 (1992) 119–134.
[24] A.V. Saetta, B.A. Schrefler, R.V. Vitaliani, The carbonation of concrete and the mechanism of moisture, heat and carbon dioxide flow through porous materials, Cem. Concr. Res. 23 (1993) 761–772.
[25] L.J. Parrott, Damage caused by carbonation of reinforced concrete, Mater. Struct. 23 (1990) 230–234.
[26] C. Dow, F.P. Glasser, Calcium carbonate efflorescence on Portland cement and building materials, Cem. Concr. Res. 33 (2003) 147–154.
[27] A. Goudie, H.A. Viles, Salt Weathering Hazard, Wiley, New York, 1997.
[28] E. Doehne, C.A. Price, Stone Conservation: An Overview of Current Research, Getty Conservation Institute, Los Angeles (CA), 2010.
[29] C. Rodriguez-Navarro, E. Doehne, Salt weathering: influence of evaporation rate, supersaturation and crystallization pattern, Earth Surf. Process. Landf. 24 (1999) 191–209.
[30] G.W. Scherer, Crystallization in pores, Cem. Concr. Res. 29 (1999) 1347–1358.
[31] G.W. Scherer, Stress from crystallization of salt, Cem. Concr. Res. 34 (2004) 1613–1624.
[32] L.A. Rijniers, H.P. Huinink, L. Pel, K. Kopinga, Experimental evidence of crystallization pressure inside porous media, Phys. Rev. Lett. 94 (2005), 075503.
[33] M. Schiro, E. Ruiz-Agudo, C. Rodriguez-Navarro, Damage mechanisms of porous materials due to in-pore salt crystallization, Phys. Rev. Lett. 109 (2012), 265503.
[34] R.J. Flatt, N. Aly Mohamed, F. Caruso, H. Derluyn, J. Desarnaud, B. Lubelli, R. M. Espinosa Marzal, L. Pel, C. Rodriguez-Navarro, G.W. Scherer, N. Shahidzadeh, M. Steiger, Predicting salt damage in practice: a theoretical insight into laboratory tests, RILEM Tech. Lett. 2 (2017) 108–118.
[35] V. Fassina, R. Arbizzani, A. Naccari, Salt efflorescences on the marble slabs of S. Maria dei Miracoli church: a survey on their origin and the methodology of their removal, in: Proc. 8th Int. Congr. Deterioration and Conservation of Stone, Berlin, 1996, pp. 523–534.
[36] O. Cazalla, C. Rodriguez-Navarro, E. Sebastian, G. Cultrone, M.J. De la Torre, Aging of lime putty: effects on traditional lime mortar carbonation, J. Am. Ceram. Soc. 83 (2000) 1070–1076.
[37] E.F. Hansen, C. Rodríguez-Navarro, K. Van Balen, Lime putties and mortars, Stud. Conserv. 53 (2008) 9–23.
[38] W. Ashraf, J. Olek, S. Sahu, Phase evolution and strength development during carbonation of low-lime calcium silicate cement (CSC), Constr. Build. Mater. 210 (2019) 473–482.
[39] X. Wang, M.Z. Guo, T.C. Ling, Review on $CO_2$ curing of non-hydraulic calcium silicates cements: mechanism, carbonation and performance, Cem. Concr. Compos. 133 (2022), 104641.
[40] P. Juilland, E. Gallucci, R. Flatt, K. Scrivener, Dissolution theory applied to the induction period in alite hydration, Cem. Concr. Res. 40 (2010) 831–844.
[41] W. Ashraf, J. Olek, Carbonation behavior of hydraulic and non-hydraulic calcium silicates: potential of utilizing low-lime calcium silicates in cement-based materials, J. Mater. Sci. 51 (2016) 6173–6191.
[42] K. Svensson, A. Neumann, F. Feitosa Menezes, C. Lempp, H. Pöllmann, Carbonation of natural wollastonite at non-ambient conditions relevant for

CCS—the possible use as cementitious material in wellbores, Appl. Sci. 9 (2019) 1259.
[43] Q. Qiu, A state-of-the-art review on the carbonation process in cementitious materials: fundamentals and characterization techniques, Constr. Build. Mater. 247 (2020), 118503.
[44] K. Wan, Q. Xu, Y. Wang, G. Pan, 3D spatial distribution of the calcium carbonate caused by carbonation of cement paste, Cem. Concr. Compos. 45 (2014) 255–263.
[45] R.M.H. Lawrence, A Study of Carbonation in Non-hydraulic Lime Mortars, University of Bath, Bath, UK, 2006 (PhD Thesis).
[46] M.A. Oliveira, M. Azenha, P.B. Lourenco, A. Meneghini, E.T. Guimaraes, F. Castro, D. Soares, Experimental analysis of the carbonation and humidity diffusion processes in aerial lime mortar, Constr. Build. Mater. 148 (2017) 38–48.
[47] E. Despotou, A. Shtiza, T. Schlegel, F. Verhelst, Literature study on the rate and mechanism of carbonation of lime in mortars, Mauerwerk 20 (2016) 124–137.
[48] J.C. Walker, P.B. Hays, J.F. Kasting, A negative feedback mechanism for the long-term stabilization of Earth's surface temperature, J. Geophys. Res. 86 (1981) 9776–9782.
[49] R.A. Berner, A.C. Lasaga, R.M. Garrels, Carbonate-silicate geochemical cycle and its effect on atmospheric carbon dioxide over the past 100 million years, Am. J. Sci. 283 (1983) 641–683.
[50] F. Di Lorenzo, C. Ruiz-Agudo, A. Ibañez-Velasco, R. Gil-San Millán, J.A. R. Navarro, E. Ruiz-Agudo, C. Rodriguez-Navarro, The carbonation of wollastonite: a model reaction to test natural and biomimetic catalysts for enhanced $CO_2$ sequestration, Minerals 8 (2018) 209.
[51] L. Monasterio-Guillot, A. Fernandez-Martinez, E. Ruiz-Agudo, C. Rodriguez-Navarro, Carbonation of calcium-magnesium pyroxenes: physical-chemical controls and effects of reaction-driven fracturing, Geochim. Cosmochim. Acta 304 (2021) 258–280.
[52] D. Daval, I. Martinez, J. Corvisier, N. Findling, B. Goffe, F. Guyot, Carbonation of Ca-bearing silicates, the case of wollastonite: experimental investigations and kinetic modeling, Chem. Geol. 265 (2009) 63–78.
[53] W. Seifritz, CO2 disposal by means of silicates, Nature 345 (1990) 486.
[54] K.S. Lackner, C.H. Wendt, D.P. Butt, E.L. Joyce Jr., D.H. Sharp, Carbon dioxide disposal in carbonate minerals, Energy 20 (1995) 1153–1170.
[55] A. Sanna, M. Uibu, G. Caramanna, R. Kuusik, M.M. Maroto-Valer, A review of mineral carbonation technologies to sequester $CO_2$, Chem. Soc. Rev. 43 (2014) 8049–8080.
[56] G. Gadikota, Carbon mineralization pathways for carbon capture, storage and utilization, Commun. Chem. 4 (2021) 23.
[57] M. Erans, S.A. Nabavi, V. Manović, Carbonation of lime-based materials under ambient conditions for direct air capture, J. Clean. Prod. 242 (2020), 118330.
[58] T. Aono, Studies on the reactions between gas and solid. Part II. Absorption of $CO_2$ by CaO and $Ca(OH)_2$, Bull. Chem. Soc. Japan 6 (1931) 319–324.
[59] J.E. Gillott, Carbonatation of $Ca(OH)_2$ investigated by thermal and x-ray diffraction methods of analysis, J. Appl. Chem. 17 (1967) 185–189.
[60] O. Matsuda, H. Yamada, On the carbonation of slaked lime, Gyps. Lime 97 (1968) 3–10.
[61] D.R. Moorehead, Cementation by the carbonation of hydrated lime, Cem. Concr. Res. 16 (1986) 700–708.
[62] S.M. Shih, C.S. Ho, Y.S. Song, J.P. Lin, Kinetics of the reaction of $Ca(OH)_2$ with $CO_2$ at low temperature, Ind. Eng. Chem. Res. 38 (1999) 1316–1322.
[63] G. Cultrone, E. Sebastián, M.O. Huertas, Forced and natural carbonation of lime-based mortars with and without additives: mineralogical and textural changes, Cem. Concr. Res. 35 (2005) 2278–2289.
[64] K. Van Balen, Carbonation reaction of lime, kinetics at ambient temperature, Cem. Concr. Res. 35 (2005) 647–657.
[65] D.T. Beruto, F. Barberis, R. Botter, Calcium carbonate binding mechanisms in the setting of calcium and calcium–magnesium putty-limes, J. Cult. Herit. 6 (2005) 253–260.
[66] M. Arandigoyen, J.I. Alvarez, Carbonation process in lime pastes with different water/binder ratio, Mater. Constr. 56 (2006) 5–18.
[67] P. De Silva, L. Bucea, D.R. Moorehead, V. Sirivivatnanon, Carbonate binders: reaction kinetics, strength and microstructure, Cem. Concr. Compos. 28 (2006) 613–620.
[68] R.M.H. Lawrence, T.J. Mays, P. Walker, D. D'ayala, Determination of carbonation profiles in non-hydraulic lime mortars using thermogravimetric analysis, Thermochim. Acta 444 (2006) 179–189.
[69] Ö. Cizer, C. Rodriguez-Navarro, E. Ruiz-Agudo, J. Elsen, D. Van Gemert, K. Van Balen, Phase and morphology evolution of calcium carbonate precipitated by carbonation of hydrated lime, J. Mater. Sci. 47 (2012) 6151–6165.
[70] Ö. Cizer, E. Ruiz-Agudo, C. Rodriguez-Navarro, Kinetic effect of carbonic anhydrase enzyme on the carbonation reaction of lime mortar, Int. J. Archit. Herit. 12 (2018) 779–789.
[71] E. Ruiz-Agudo, K. Kudłacz, C.V. Putnis, A. Putnis, C. Rodriguez-Navarro, Dissolution and carbonation of portlandite [$Ca(OH)_2$] single crystals, Environ. Sci. Technol. 47 (2013) 11342–11349.
[72] C. Rodriguez-Navarro, Binders in historical buildings: traditional lime in conservation, Semin. SEM 9 (2012) 91–112.
[73] C. Rodriguez-Navarro, O. Cazalla, K. Elert, E. Sebastian, Liesegang pattern development in carbonating traditional lime mortars, Proc. R. Soc. London A 458 (2002) 2261–2273.
[74] C. Rodriguez-Navarro, K. Kudłacz, Ö. Cizer, E. Ruiz-Agudo, Formation of amorphous calcium carbonate and its transformation into mesostructured calcite, CrystEngComm 17 (2015) 58–72.
[75] C. Rodriguez-Navarro, K. Elert, R. Ševčík, Amorphous and crystalline calcium carbonate phases during carbonation of nanolimes: implications in heritage conservation, CrystEngComm 18 (2016) 6594–6607.
[76] R. Veiga, Air lime mortars: what else do we need to know to apply them in conservation and rehabilitation interventions? A review, Constr. Build. Mater. 157 (2017) 132–140.
[77] J.I. Alvarez, R. Veiga, S. Martínez-Ramírez, M. Secco, P. Faria, P.N. Maravelaki, M. Ramesh, I. Papayanni, J. Valek, RILEM TC 277-LHS report: a review on the mechanisms of setting and hardening of lime-based binding systems, Mater. Struct. 54 (2021) 75.
[78] C. Groot, R. Veiga, I. Papayianni, R. Van Hees, M. Secco, J.I. Alvarez, P. Faria, M. Stefanidou, RILEM TC 277-LHS report: lime-based mortars for restoration–a review on long-term durability aspects and experience from practice, Mater. Struct. 55 (2022) 245.
[79] W.D. Kingery, P.B. Vandiver, M. Prickett, The beginnings of pyrotechnology, part II: production and use of lime and gypsum plaster in the Pre-Pottery Neolithic Near East, J. Field Archaeol. 15 (1988) 219–243.
[80] D. Carran, J. Hughes, A. Leslie, C. Kennedy, A short history of the use of lime as a building material beyond Europe and North America, Int. J. Archit. Herit. 6 (2012) 117–146.
[81] G. Artioli, M. Secco, A. Addis, The Vitruvian legacy: mortars and binders before and after the Roman world, EMU Notes Miner. 20 (2019) 151–202.
[82] D.E. Friesem, I. Abadi, D. Shaham, L. Grosman, Lime plaster cover of the dead 12,000 years ago–new evidence for the origins of lime plaster technology, Evol. Hum. Sci. 1 (2019), e9.
[83] A.D. Cowper, Lime and Lime Mortars, Building Research Station, HM Stationary Office, London, 1927.
[84] A. Moropoulou, A. Bakolas, K. Bisbikou, Investigation of the technology of historic mortars, J. Cult. Herit. 1 (2000) 45–58.
[85] R.M. Lawrence, T.J. Mays, S.P. Rigby, P. Walker, D. D'Ayala, Effects of carbonation on the pore structure of non-hydraulic lime mortars, Cem. Concr. Res. 37 (2007) 1059–1069.
[86] C. Rodriguez-Navarro, E. Ruiz-Agudo, A. Luque, A.B. Rodriguez-Navarro, M. Ortega-Huertas, Thermal decomposition of calcite: mechanisms of formation and textural evolution of CaO nanocrystals, Am. Mineral. 94 (2009) 578–593.
[87] C. Rodriguez-Navarro, K. Kudlacz, E. Ruiz-Agudo, The mechanism of thermal decomposition of dolomite: new insights from 2D-XRD and TEM analyses, Am. Mineral. 97 (2012) 38–51.
[88] M.A. Shand, The Chemistry and Technology of Magnesia, John Wiley & Sons, Hoboken, NJ, 2006.
[89] C. Rodriguez-Navarro, E. Hansen, W.S. Ginell, Calcium hydroxide crystal evolution upon aging of lime putty, J. Am. Ceram. Soc. 81 (1998) 3032–3034.
[90] E. Ruiz-Agudo, C. Rodriguez-Navarro, Microstructure and rheology of lime putty, Langmuir 26 (2010) 3868–3877.
[91] C. Rodriguez-Navarro, E. Ruiz-Agudo, M. Ortega-Huertas, E. Hansen, Nanostructure and irreversible colloidal behavior of $Ca(OH)_2$: implications in cultural heritage conservation, Langmuir 21 (2005) 10948–10957.
[92] B.A. Silva, A.F. Pinto, A. Gomes, A. Candeias, Effects of natural and accelerated carbonation on the properties of lime-based materials, J. CO2 Util. 49 (2021), 101552.
[93] T. Ogino, T. Suzuki, K. Sawada, The formation and transformation mechanism of calcium carbonate in water, Geochim. Cosmochim. Acta 51 (1987) 2757–2767.
[94] S. Martinez-Ramirez, S. Sanchez-Cortes, J.V. Garcia-Ramos, C. Domingo, C. Fortes, M.T. Blanco-Varela, Micro-Raman spectroscopy applied to depth profiles of carbonates formed in lime mortar, Cem. Concr. Res. 33 (2003) 2063–2068.
[95] M. Singh, S.V. Kumar, S.A. Waghmare, P.D. Sabale, Aragonite–vaterite–calcite: polymorphs of $CaCO_3$ in 7th century CE lime plasters of Alampur group of temples, India, Constr. Build. Mater. 112 (2016) 386–397.
[96] R. Ravi, S. Thirumalini, N. Taher, Analysis of ancient lime plasters–reason behind longevity of the Monument Charminar, India a study, J. Build. Eng. 20 (2018) 30–41.
[97] S. Thirumalini, R. Ravi, M. Rajesh, Experimental investigation on physical and mechanical properties of lime mortar: effect of organic addition, J. Cult. Herit. 31 (2018) 97–104.
[98] K.A. Gour, R. Ramadoss, T. Selvaraj, Revamping the traditional air lime mortar using the natural polymer–Areca nut for restoration application, Constr. Build. Mater. 164 (2018) 255–264.
[99] C. Rodriguez-Navarro, C. Jimenez-Lopez, A. Rodriguez-Navarro, M.T. Gonzalez-Muñoz, M. Rodriguez-Gallego, Bacterially mediated mineralization of vaterite, Geochim. Cosmochim. Acta 71 (2007) 1197–1213.
[100] M.B. Toffolo, The significance of aragonite in the interpretation of the microscopic archaeological record, Geoarchaeology 36 (2021) 149–169.
[101] F. Lippmann, Crystal Chemistry of Sedimentary Carbonate Minerals, Springer, Berlin, 1973.
[102] N. Oriols, N. Salvadó, T. Pradell, N. Jiménez, M. Cotte, V. Gonzalez, S. Butí, Carbonation of fresco mural paintings with a dolomitic mortar, Cem. Concr. Res. 157 (2022), 106828.
[103] R.M. Dheilly, A. Bouguerra, B. Beaudoin, J. Tudo, M.I. Queneudec, Hydromagnesite development in magnesian lime mortars, Mater. Sci. Eng. A 268 (1999) 127–131.
[104] E. Königsberger, L.C. Königsberger, H. Gamsjäger, Low temperature thermodynamic model for the system $Na_2CO_3$–$MgCO_3$–$CaCO_3$–$H_2O$, Geochim. Cosmochim. Acta 63 (1999) 3105–3119.
[105] J. Lanas, J.L. Alvarez, Dolomitic lime: thermal decomposition of nesquehonite, Thermochim. Acta 421 (2004) 123–132.

[106] G. Cultrone, A. Arizzi, E. Sebastián, C. Rodriguez-Navarro, Sulfation of calcitic and dolomitic lime mortars in the presence of diesel particulate matter, Environ. Geol. 56 (2008) 741–752.
[107] P. De Silva, L. Bucea, V. Sirivivatnanon, Chemical, microstructural and strength development of calcium and magnesium carbonate binders, Cem. Concr. Res. 39 (2009) 460–465.
[108] A. Arizzi, G. Cultrone, The influence of aggregate texture, morphology and grading on the carbonation of non-hydraulic (aerial) lime-based mortars, Q. J. Eng. Geol. Hydrogeol. 46 (2013) 507–520.
[109] K. Van Balen, D. Van Gemert, Modeling lime mortar carbonation, Mater. Struct. 27 (1994) 393–398.
[110] M. Arandigoyen, J.P. Bernal, M.B. López, J.I. Alvarez, Lime-pastes with different kneading water: pore structure and capillary porosity, Appl. Surf. Sci. 252 (2005) 1449–1459.
[111] L.B. Sickels, Organic additives in mortars, Edinb. Architect. Res. 8 (1981) 7–20.
[112] L. Rampazzi, M.P. Colombini, C. Conti, C. Corti, A. Lluveras-Tenorio, A. Sansonetti, M. Zanaboni, Technology of Medieval mortars: an investigation into the use of organic additives, Archaeometry 58 (2016) 115–130.
[113] L. Ventola, M. Vendrell, P. Giraldez, L. Merino, Traditional organic additives improve lime mortars: new old materials for restoration and building natural stone fabrics, Constr. Build. Mater. 25 (2011) 3313–3318.
[114] F. Yang, B. Zhang, Q. Ma, Study of sticky rice–lime mortar technology for the restoration of historical masonry construction, Acc. Chem. Res. 43 (2010) 936–944.
[115] E.H. Morris, J. Charlot, A.A. Morris, The Temple of the Warriors at Chichen Itza, Yucatan, Carnegie Institution, Washington D.C., 1931.
[116] E.R. Littmann, Ancient Mesoamerican mortars, plasters, and stuccos: the use of bark extracts in lime plasters, Am. Antiq. 25 (1960) 593–597.
[117] D. Magaloni, R. Pancella, Y. Fruh, J. Cañetas, V. Castaño, Studies on the Mayan mortars technique, MRS Proc. 352 (1995) 483–489.
[118] C. Rodriguez-Navarro, E. Ruiz-Agudo, A. Burgos-Cara, K. Elert, E.F. Hansen, Crystallization and colloidal stabilization of $Ca(OH)_2$ in the presence of nopal juice (*Opuntia ficus indica*): implications in architectural heritage conservation, Langmuir 33 (2017) 10936–10950.
[119] C. Rodriguez-Navarro, A. Burgos-Cara, F. Di Lorenzo, E. Ruiz-Agudo, K. Elert, Nonclassical crystallization of calcium hydroxide via amorphous precursors and the role of additives, Cryst. Growth Des. 20 (2020) 4418–4432.
[120] D.M. Kern, The hydration of carbon dioxide, J. Chem. Educ. 37 (1960) 14–23.
[121] V.A. Juvekar, M.M. Sharma, Absorption of $CO_2$ in a suspension of lime, Chem. Eng. Sci. 28 (1973) 825–837.
[122] J.R. Burns, R.J.J. Jachuck, Monitoring of $CaCO_3$ production on a spinning disc reactor using conductivity measurements, AICHE J. 51 (2005) 1497–1507.
[123] W. Dreybrodt, J. Lauckner, Liu Zaihua, U. Svensson, D. Buhmann, The kinetics of the reaction $CO_2 + H_2O \rightarrow H^+ + HCO_3^-$ as one of the rate limiting steps for the dissolution of calcite in the system $H_2O$-$CO_2$-$CaCO_3$, Geochim. Cosmochim. Acta 60 (1996) 3375–3381.
[124] W. Dreybrodt, L. Eisenlohr, B. Madry, S. Ringer, Precipitation kinetics of calcite in the system $CaCO_3$-$H_2O$-$CO_2$: the conversion to $CO_2$ by the slow process $H^+ + HCO_3^- \rightarrow CO_2 + H_2O$ as a rate limiting step, Geochim. Cosmochim. Acta 61 (1997) 3897–3904.
[125] P. Somasundaran, G.E. Agar, The zero point of charge of calcite, J. Colloid Interface Sci. 24 (1967) 433–440.
[126] Z. Liu, W. Dreybrod, Dissolution kinetics of calcium carbonate minerals in $H_2O$-$CO_2$ solutions in turbulent flow: the role of the diffusion boundary layer and the slow reaction $H_2O + CO_2 \rightarrow H^+ + HCO_3^-$, Geochim. Cosmochim. Acta 61 (1997) 2879–2889.
[127] V.H. Veley, The inertness of quicklime, J. Chem. Soc. Trans. 63 (1893) 821–833.
[128] J.R. Johnstone, F.P. Glasser, Carbonation of single crystals of portlandite in cement paste, in: 9th ICCCC, vol. 5, 1992, pp. 370–376 (New Dehli).
[129] F. Pontiga, J.M. Valverde, H. Moreno, F.J. Duran-Olivencia, Dry gas–solid carbonation in fluidized beds of $Ca(OH)_2$ and nanosilica/$Ca(OH)_2$ at ambient temperature and low $CO_2$ pressure, Chem. Eng. J. 222 (2013) 546–552.
[130] G. Montes-Hernandez, A. Pommerol, F. Renard, P. Beck, E. Quirico, O. Brissaud, In situ kinetic measurements of gas-solid carbonation of $Ca(OH)_2$ by using an infrared microscope coupled to a reaction cell, Chem. Eng. J. 161 (2010) 250–256.
[131] E.T. Stepkowska, Hypothetical transformation of $Ca(OH)_2$ into $CaCO_3$ in solid-state reactions of portland cement, J. Therm. Anal. Calorim. 80 (2005) 727–733.
[132] D.T. Beruto, R. Botter, Liquid-like $H_2O$ adsorption layers to catalyze the $Ca(OH)_2$/$CO_2$ solid–gas reaction and to form a non-protective solid product layer at 20°C, J. Eur. Ceram. Soc. 20 (2000) 497–503.
[133] A. Putnis, Mineral replacement reactions, Rev. Mineral. Geochem. 70 (2009) 87–124.
[134] V. Nikulshina, M.E. Gálvez, A. Steinfeld, Kinetic analysis of the carbonation reactions for the capture of $CO_2$ from air via the $Ca(OH)_2$–$CaCO_3$–CaO solar thermochemical cycle, Chem. Eng. J. 129 (2007) 75–83.
[135] V. Manovic, E.J. Anthony, Lime-based sorbents for high-temperature $CO_2$ capture—a review of sorbent modification methods, Int. J. Environ. Res. Public Health 7 (2010) 3129–3140.
[136] V. Materic, S.I. Smedley, High temperature carbonation of $Ca(OH)_2$, Ind. Eng. Chem. Res. 50 (2011) 5927–5932.
[137] J.W. Gibbs, On the equilibrium of heterogeneous substances (first part), Trans. Connecticut Acad. Arts Sci. 3 (1876) 108–248.
[138] J.W. Gibbs, On the equilibrium of heterogeneous substances (concluded), Trans. Connecticut Acad. Arts Sci. 16 (1878) 343–524.
[139] M. Volmer, A. Weber, Keimbildung in übersättigten Gebilden, Z. Phys. Chem. 119 (1926) 277–301.
[140] R. Becker, W. Doring, Kinetische Behandlung der Keimbildung in übersättigen Dämpfen, Ann. Phys. 24 (1935) 719–752.
[141] B. Mutaftschiev, The Atomistic Nature of Crystal Growth, Springer, Berlin, 2001.
[142] D. Gebauer, M. Kellermeier, J.D. Gale, L. Bergström, H. Cölfen, Pre-nucleation clusters as solute precursors in crystallisation, Chem. Soc. Rev. 43 (2014) 2348–2371.
[143] J.W. Mullin, Crystallization, 4th edition, Butterworth, Oxford, 2001.
[144] J.J. De Yoreo, P.G. Vekilov, Principles of crystal nucleation and growth, Rev. Mineral. Geochem. 54 (2003) 57–93.
[145] Q. Li, Y.S. Jun, The apparent activation energy and pre-exponential kinetic factor for heterogeneous calcium carbonate nucleation on quartz, Commun. Chem. 1 (2018) 56.
[146] H. Cölfen, S. Mann, Higher-order organization by mesoscale self-assembly and transformation of hybrid nanostructures, Angew. Chem. Int. Ed. 42 (2003) 2350–2365.
[147] J.H. Harding, C.L. Freeman, D.M. Duffy, Oriented crystal growth on organic monolayers, CrystEngComm 16 (2014) 1430–1438.
[148] D. Gebauer, A. Völkel, H. Cölfen, Stable prenucleation clusters, Science 322 (2008) 1819–1822.
[149] A.F. Wallace, L.O. Hedges, A. Fernandez-Martinez, P. Raiteri, J.D. Gale, G. A. Waychunas, S. Whitelam, J.F. Banfield, J.J. De Yoreo, Microscopic evidence for liquid-liquid separation in spersaturated $CaCO_3$ solutions, Science 341 (2013) 885–889.
[150] E. Ruiz-Agudo, A. Burgos-Cara, C. Ruiz-Agudo, A. Ibañez-Velasco, H. Cölfen, C. Rodriguez-Navarro, A non-classical view on calcium oxalate precipitation and the role of citrate, Nat. Commun. 8 (2017) 768.
[151] C. Rodriguez-Navarro, Ö. Cizer, K. Kudłacz, A. Ibañez-Velasco, C. Ruiz-Agudo, K. Elert, A. Burgos-Cara, E. Ruiz-Agudo, The multiple roles of carbonic anhydrase in calcium carbonate mineralization, CrystEngComm 21 (2019) 7407–7423.
[152] J.J. De Yoreo, P.U.P.A. Gilbert, N.A.J.M. Sommerdijk, R.L. Penn, S. Whitelam, D. Joester, H. Zhang, J.D. Rimer, A. Navrotsky, J.F. Banfield, A.F. Wallace, F. M. Michel, F.C. Meldrum, H. Cölfen, P.M. Dove, Crystallization by particle attachment in synthetic, biogenic and geologic environments, Science 349 (2015), aaa6760-1.
[153] R. Demichelis, P. Raiteri, J.D. Gale, D. Quigley, D. Gebauer, Stable prenucleation mineral clusters are liquid-like ionic polymers, Nat. Commun. 2 (2011) 590.
[154] F. Sebastiani, S.L. Wolf, B. Born, T.Q. Luong, H. Cölfen, D. Gebauer, M. Havenith, Water dynamics from THz spectroscopy reveal the locus of a liquid–liquid binodal limit in aqueous $CaCO_3$ solutions, Angew. Chem. Int. Ed. 56 (2017) 490–495.
[155] M. Sleutel, A.E. Van Driessche, Role of clusters in nonclassical nucleation and growth of protein crystals, Proc. Natl. Acad. Sci. 111 (2014) E546–E553.
[156] M.H. Nielsen, S. Aloni, J.J. De Yoreo, In situ TEM imaging of $CaCO_3$ nucleation reveals coexistence of direct and indirect pathways, Science 345 (2014) 1158–1162.
[157] J. Ihli, W.C. Wong, E.H. Noel, Y.Y. Kim, A.N. Kulak, H.K. Christenson, M.J. Duer, F.C. Meldrum, Dehydration and crystallization of amorphous calcium carbonate in solution and in air, Nat. Commun. 5 (2014) 3169.
[158] A. Gal, W. Habraken, D. Gur, P. Fratzl, S. Weiner, L. Addadi, Calcite crystal growth by a solid-state transformation of stabilized amorphous calcium carbonate nanospheres in a hydrogel, Angew. Chem. Int. Ed. 52 (2013) 4867–4870.
[159] X. Zhang, A.S. Lea, A.M. Chaka, J.S. Loring, S.T. Mergelsberg, E. Nakouzi, O. Qafoku, J.J. De Yoreo, H.T. Schaef, K.M. Rosso, In situ imaging of amorphous intermediates during brucite carbonation in supercritical $CO_2$, Nat. Mater. 21 (2022) 345–351.
[160] K. Zhang, Y. Zhang, Y. Liu, L. Wang, L. He, T. Dong, R. Lu, Y. Zhang, F. Yang, Influence of polar amino acids on the carbonation of lime mortars, Herit. Sci. 10 (2022) 190.
[161] I. Matsushita, T. Suzuki, T. Moriga, T. Ashida, I. Nakabayashi, J. Metson, XPS study on the carbonation process of $Ca(OH)_2$, J. Ceram. Soc. Japan 101 (1993) 725–727.
[162] H.W. Wang, L.L. Daemen, M.C. Cheshire, M.K. Kidder, A.G. Stack, L.F. Allard, J. Neuefeind, D. Olds, J. Liub, K. Page, Synthesis and structure of synthetically pure and deuterated amorphous (basic) calcium carbonates, Chem. Commun. 53 (2017) 2942–2945.
[163] Y. Politi, D.R. Batchelor, P. Zaslansky, B.F. Chmelka, J.C. Weaver, I. Sagi, S. Weiner, L. Addadi, Role of magnesium ion in the stabilization of biogenic amorphous calcium carbonate: a structure−function investigation, Chem. Mater. 22 (2010) 161–166.
[164] A.L. Harrison, G.M. Dipple, I.M. Power, K.U. Mayer, Influence of surface passivation and water content on mineral reactions in unsaturated porous media: implications for brucite carbonation and $CO_2$ sequestration, Geochim. Cosmochim. Acta 148 (2015) 477–495.
[165] C. Rodriguez-Navarro, A. Burgos Cara, K. Elert, C.V. Putnis, E. Ruiz-Agudo, Direct nanoscale imaging reveals the growth of calcite crystals via amorphous nanoparticles, Cryst. Growth Des. 16 (2016) 1850–1860.
[166] C. Rodriguez-Navarro, E. Ruiz-Agudo, J. Harris, S.E. Wolf, Nonclassical crystallization in vivo et in vitro (II): nanogranular features in biomimetic minerals disclose a general colloid-mediated crystal growth mechanism, J. Struct. Biol. 196 (2016) 260–287.
[167] B. Marchese, Non-crystalline $Ca(OH)_2$ in ancient non-hydraulic lime mortars, Cem. Concr. Res. 10 (1980) 861–864.
[168] R.G. Newton, J.H. Sharp, The chemical composition of lime plasters, Cem. Concr. Res. 17 (1987) 77–80.

[169] J. Adams, D. Dollimore, D.L. Griffiths, Thermal analytical investigation of unaltered $Ca(OH)_2$ in dated mortars and plasters, Thermochim. Acta 324 (1998) 67–76.
[170] D. Ferretti, Z.P. Bažant, Stability of ancient masonry towers: moisture diffusion, carbonation and size effect, Cem. Concr. Res. 36 (2006) 1379–1388.
[171] B. Xu, M.B. Toffolo, E. Boaretto, K.M. Poduska, Assessing local and long-range structural disorder in aggregate-free lime binders, Ind. Eng. Chem. Res. 55 (2016) 8334–8340.
[172] B. Lubelli, T.G. Nijland, R.P.J. Van Hees, Self-healing of lime based mortars: microscopy observations on case studies, Heron 56 (2011) 75–91.
[173] L.M. Seymour, J. Maragh, P. Sabatini, M. Di Tommaso, J.C. Weaver, A. Masic, Hot mixing: mechanistic insights into the durability of ancient Roman concrete, Sci. Adv. 9 (2023), eadd1602.
[174] J. Lanas, J.P. Bernal, M.A. Bello, J.I. Alvarez, Mechanical properties of masonry repair dolomitic lime-based mortars, Cem. Concr. Res. 36 (2006) 951–960.
[175] A. Arizzi, G. Cultrone, The difference in behaviour between calcitic and dolomitic lime mortars set under dry conditions: the relationship between textural and physical–mechanical properties, Cem. Concr. Res. 42 (2012) 818–826.
[176] X. Zhang, F.P. Glasser, K.L. Scrivener, Reaction kinetics of dolomite and portlandite, Cem. Concr. Res. 66 (2014) 11–18.
[177] G. Ponce-Antón, M.C. Zuluaga, L.A. Ortega, J.A. Mauleon, Multi-analytical approach for chemical-mineralogical characterization of reaction rims in the lime mortars from Amaiur Castle (Navarre, Spain), Microchem. J. 152 (2020), 104303.
[178] E. Ruiz-Agudo, F. Mees, P. Jacobs, C. Rodriguez-Navarro, The role of saline solution properties on porous limestone salt weathering by magnesium and sodium sulfates, Environ. Geol. 52 (2007) 269–281.
[179] A. Khawam, D.R. Flanagan, Solid-state kinetic models: basics and mathematical fundamentals, J. Phys. Chem. B 110 (2006) 17315–17328.
[180] P. Baglioni, L. Dei, F. Piqué, G. Sarti, E. Ferroni, New autogenous lime-based grouts used in the conservation of lime-based wall paintings, Stud. Conserv. 42 (1997) 43–54.
[181] P. Baglioni, D. Chelazzi, R. Giorgi, E. Carretti, N. Toccafondi, Y. Jaidar, Commercial Ca $(OH)_2$ nanoparticles for the consolidation of immovable works of art, Appl. Phys. A Mater. Sci. Process. 114 (2014) 723–732.
[182] R. Camerini, G. Poggi, D. Chelazzi, F. Ridi, R. Giorgi, P. Baglioni, The carbonation kinetics of calcium hydroxide nanoparticles: a Boundary Nucleation and Growth description, J. Colloid Interface Sci. 547 (2019) 370–381.
[183] F.A. Pisu, D. Chiriu, P.C. Ricci, C.M. Carbonaro, Defect related emission in calcium hydroxide: the controversial band at 780 $cm^{-1}$, Crystals 10 (2020) 266.
[184] H. Yagi, A. Iwazawa, R. Sonobe, T. Matsubara, H. Hikita, Crystallization of calcium carbonate accompanying chemical absorption, Ind. Eng. Chem. Res. 23 (1984) 153–158.
[185] J. García-Carmona, J. Gómez-Morales, R. Rodríguez-Clemente, Morphological control of precipitated calcite obtained by adjusting the electrical conductivity in the $Ca(OH)_2$-$H_2O$-$CO_2$ system, J. Cryst. Growth 249 (2003) 561–571.
[186] G. Montes-Hernandez, F. Renard, N. Geoffroy, L. Charlet, J. Pironon, Calcite precipitation from $CO_2$-$Ca(OH)_2$ slurry under high pressure of $CO_2$, J. Cryst. Growth 308 (2007) 228–236.
[187] J.R. Clarkson, T.J. Price, C.J. Adams, Role of metastable phases in the spontaneous precipitation of calcium carbonate, J. Chem. Soc. Faraday Trans. 88 (1992) 243–249.
[188] C. Tai, F.-B. Chen, Polymorphism of $CaCO_3$ precipitated in a constant-composition environment, AICHE J. 44 (1998) 1790–1798.
[189] J.D. Rodriguez-Blanco, S. Shaw, L.G. Benning, The kinetics and mechanisms of amorphous calcium carbonate (ACC) crystallization to calcite, via vaterite, Nanoscale 3 (2011) 265–271.
[190] R.M. Dheilly, J. Tudo, Y. Sebaïbi, M. Quéneudec, Influence of storage conditions on the carbonation of powdered $Ca(OH)_2$, Constr. Build. Mater. 16 (2002) 155–161.
[191] T. Yang, B. Keller, E. Gagyari, K. Hametner, D. Günther, Direct observation of the carbonation process on the surface of calcium hydroxide crystals in hardened cement paste using an atomic force microscope, J. Mater. Sci. 38 (2003) 1909–1916.
[192] E. Dubina, L. Korat, L. Black, J. Strupi-Šuput, J. Plank, Influence of water vapour and carbon dioxide on free lime during storage at 80 °C, studied by Raman spectroscopy, Spectrochim. Acta A 111 (2013) 299–303.
[193] G.L. Pesce, I.W. Fletcher, J. Grant, M. Molinari, S.C. Parker, R.J. Ball, Carbonation of hydrous materials at the molecular level: a time of flight-secondary ion mass spectrometry, Raman and density functional theory study, Cryst. Growth Des. 17 (2017) 1036–1044.
[194] B. Chen, M.L. Laucks, E.J. Davis, Carbon dioxide uptake by hydrated lime aerosol particles, Aerosol Sci. Technol. 38 (2004) 588–597.
[195] J.H. Park, S.H. Kim, J.C. Kim, B.Y. Choi, S.K. Kwak, O.H. Han, Y.I. Kim, S.W. Lee, Role of intercalated water in calcium hydroxide interlayers for carbonation reaction, Chem. Eng. J. 420 (2021) 130422.
[196] D. Ergenç, R. Fort, Accelerating carbonation in lime-based mortar in high $CO_2$ environments, Constr. Build. Mater. 188 (2018) 314–325.
[197] C. Rodriguez-Navarro, E. Ruiz-Agudo, Nanolimes: from synthesis to application, Pure Appl. Chem. 90 (2018) 523–550.
[198] K. Vance, G. Falzone, I. Pignatelli, M. Bauchy, M. Balonis, G. Sant, Direct carbonation of $Ca(OH)_2$ using liquid and supercritical $CO_2$: implications for carbon-neutral cementation, Ind. Eng. Chem. Res. 54 (2015) 8908–8918.
[199] J. Yu, X. Zeng, G. Zhang, J. Zhang, Y. Wang, G. Xu, Kinetics and mechanism of direct reaction between $CO_2$ and $Ca(OH)_2$ in micro fluidized bed, Environ. Sci. Technol. 47 (2013) 7514–7520.
[200] A.C. Lasaga, Chemical kinetics of water-rock interactions, J. Geophys. Res. 89 (1984) 4009–4025.
[201] H.H. Wickman, J.N. Korley, Colloid crystal self-organization and dynamics at the air/water interface, Nature 393 (1998) 445–447.
[202] M.Y. Lin, H. Lindsay, D.A. Weitz, R.C. Ball, R. Klein, P. Meakin, Universality in colloid aggregation, Nature 339 (1989) 360–362.
[203] I. Galan, F.P. Glasser, D. Baza, C. Andrade, Assessment of the protective effect of carbonation on portlandite crystals, Cem. Concr. Res. 74 (2015) 68–77.
[204] M. Thiery, G. Villain, P. Dangla, G. Platret, Investigation of the carbonation front shape on cementitious materials: effects of the chemical kinetics, Cem. Concr. Res. 37 (2007) 1047–1058.
[205] Y. Pu, L. Li, Q. Wang, X. Shi, C. Luan, G. Zhang, L. Fu, A.E.F. Abomohra, Accelerated carbonation technology for enhanced treatment of recycled concrete aggregates: a state-of-the-art review, Constr. Build. Mater. 282 (2021) 122671.
[206] S. Sánchez Moral, J. García-Guinea, L.D. Luque Ripoll, R. González-Martín, P. López-Arce, Cinética de carbonatación de morteros experimentales de cal de tipo romano, Mater. Constr. 54 (2004) 23–37.
[207] D. Wang, J. Xiao, Z. Duan, Strategies to accelerate $CO_2$ sequestration of cement-based materials and their application prospects, Constr. Build. Mater. 314 (2022), 125646.
[208] R. Hay, G. Kashwani, K. Celik, Carbonation, strength development, and characterization of calcined limestone as a potential construction material, Cem. Concr. Res. 139 (2021), 106263.
[209] A. Moropoulou, A. Bakolas, P. Moundoulas, E. Aggelakopoulou, S. Anagnostopoulou, Strength development and lime reaction in mortars for repairing historic masonries, Cem. Concr. Compos. 27 (2005) 289–294.
[210] E. Ontiveros-Ortega, R. Rodríguez-García, A. González-Serrano, L. Molina, Evolution of mechanical properties in aerial lime mortars of traditional manufacturing, the relationship between putty and powder lime, Constr. Build. Mater. 191 (2018) 575–589.
[211] L. Garijo, X. Zhang, G. Ruiz, J.J. Ortega, Age effect on the mechanical properties of natural hydraulic and aerial lime mortars, Constr. Build. Mater. 236 (2020) 117573.
[212] S.A. Walling, J.L. Provis, A discussion of the papers "Impact of hydrated magnesium carbonate additives on the carbonation of reactive MgO cements" and "Enhancing the carbonation of MgO cement porous blocks through improved curing conditions", by C. Unluer & A. Al-Tabbaa, Cem. Concr. Res. 79 (2016) 424–426.
[213] A. Varzina, Ö. Cizer, L. Yu, S. Liu, D. Jacques, J. Perko, A new concept for pore-scale precipitation-dissolution modelling in a lattice Boltzmann framework–application to portlandite carbonation, Appl. Geochem. 123 (2020) 104786.
[214] H.K. Henish, Crystal Growth in Gels, Pennsylvania State University Press, University Park, Pennsylvania, USA, 1970.
[215] J. Delgado Rodrigues, Liesegang rings in differential deterioration patterns of lime mortars, J. Cult. Herit. 21 (2016) 819–822.
[216] M. Castellote, C. Andrade, Modelling the carbonation of cementitious matrixes by means of the unreacted-core model, UR-CORE, Cem. Concr. Res. 38 (2008) 1374–1384.
[217] B.A. Silva, A.F. Pinto, A. Gomes, A. Candeias, Suitability of different surfactants as air-entraining admixtures for lime mortars, Constr. Build. Mater. 256 (2020) 118986.
[218] S.H. Kang, Y.H. Kwon, J. Moon, Quantitative analysis of $CO_2$ uptake and mechanical properties of air lime-based materials, Energies 12 (2019) 2903.
[219] S.H. Kang, Y.H. Kwon, J. Moon, Controlling the hydration and carbonation in lime-based materials: advantage of slow carbonation in $CO_2$ curable construction materials, Constr. Build. Mater. 249 (2020) 118749.
[220] F.G. Branco, M.D.L. Belgas, C. Mendes, L. Pereira, J.M. Ortega, Characterization of fresh and durability properties of different lime mortars for being used as masonry coatings in the restoration of ancient constructions, Sustainability 13 (2021) 4909.
[221] F.P. Campo, C. Tua, L. Biganzoli, S. Pantini, M. Grosso, Natural and enhanced carbonation of lime in its different applications: a review, Environ. Technol. Rev. 10 (2021) 224–237.
[222] M.I. Romero-Hermida, A.M. Borrero-López, V. Flores-Alés, F.J. Alejandre, J. M. Franco, A. Santos, L. Esquivias, Characterization and analysis of the carbonation process of a lime mortar obtained from phosphogypsum waste, Int. J. Environ. Res. Public Health 18 (2021) 6664.
[223] S. Jayasingh, T. Selvaraj, S. Raneri, Evaluating the impact of organic addition and aggregate gradation on air lime mortar: new compatible green material for heritage application, Int. J. Architect. Herit. 16 (2022) 681–691.
[224] J. Diaz-Basteris, J.C.S. Rivero, B. Menéndez, Life cycle assessment of restoration mortars and binders, Constr. Build. Mater. 326 (2022) 126863.
[225] F. Medici, G. Rinaldi, Poly-amino-phenolic additives accelerating the carbonation of hydrated lime in mortar, Environ. Eng. Sci. 19 (2002) 271–276.
[226] D. Ergenç, R. Fort, A. Santos Silva, R. Veiga, D. Sanz Arauz, The effects of DiloCarB as carbonation accelerator on the properties of lime mortars, Mater. Struct. 51 (2018) 10.
[227] I. Karatasios, M.S. Katsiotis, V. Likodimos, A.I. Kontos, G. Papavassiliou, P. Falaras, V. Kilikoglou, Photo-induced carbonation of lime-$TiO_2$ mortars, Appl. Catal. B 95 (2010) 78–86.
[228] S. Jayasingh, T. Selvaraj, Effect of natural herbs on hydrated phases of lime mortar, J. Archit. Eng. 26 (2020), 04020021.
[229] M. Shivakumar, T. Selvaraj, M.P. Dhassaih, Preparation and characterization of ancient recipe of organic lime putty-evaluation for its suitability in restoration of Padmanabhapuram Palace, India, Sci. Rep. 11 (2021) 13261.

[230] A. Manoharan, C. Umarani, Properties of air lime mortar with bio-additives, Sustainability 14 (2022) 8355.
[231] F.M. León-Martínez, P.D.J. Cano-Barrita, F. Castellanos, K.B. Luna-Vicente, S. Ramírez-Arellanes, C. Gómez-Yáñez, Carbonation of high-calcium lime mortars containing cactus mucilage as additive: a spectroscopic approach, J. Mater. Sci. 56 (2021) 3778–3789.
[232] M. Carmona-Carmona, P. Acedo-Fuentes, A. Romero-Casado, J.M. Meneses-Rodríguez, M. Trujillo-Gómez, J.J. Tejado-Ramos, Chitosan as a carbonation catalyst in lime mortars, Res. Eng. Des. 17 (2023), 100912.
[233] J. Lanas, J.I. Alvarez-Galindo, Masonry repair lime-based mortars: factors affecting the mechanical behavior, Cem. Concr. Res. 33 (2003) 1867–1876.
[234] S. Scannell, M. Lawrence, P. Walker, Impact of aggregate type on air lime mortar properties, Energy Procedia 62 (2014) 81–90.
[235] C. Martinez-Garcia, B. Gonzalez-Fonteboa, D. Carro-Lopez, F. Martinez-Abella, Carbonation evolution of lime putty coatings with mussel shell aggregate, Constr. Build. Mater. 264 (2020) 120165.
[236] I. Rigopoulos, L. Kyriakou, M.A. Vasiliades, T. Kyratsi, A.M. Efstathiou, I. Ioannou, Improving the carbonation of air lime mortars at ambient conditions via the incorporation of ball-milled quarry waste, Constr. Build. Mater. 301 (2021), 124073.
[237] H. Liu, Y. Zhao, C. Peng, S. Song, A. López-Valdivieso, Lime mortars–the role of carboxymethyl cellulose on the crystallization of calcium carbonate, Constr. Build. Mater. 168 (2018) 169–177.
[238] T.M. Jassam, K. Kien-Woh, B. Lau, M.M.M. Yaseer, Novel cement curing technique by using controlled release of carbon dioxide coupled with nanosilica, Constr. Build. Mater. 223 (2019) 692–704.
[239] J. Zhu, X. Li, Y. Zhang, J. Wang, B. Wei, Graphene-enhanced nanomaterials for wall painting protection, Adv. Funct. Mater. 28 (2018) 1803872.
[240] C. Rodriguez-Navarro, L. Monasterio-Guillot, M. Burgos-Ruiz, E. Ruiz-Agudo, K. Elert, Unveiling the secret of ancient Maya masons: Biomimetic lime plasters with plant extracts, Sci. Adv. 9 (2023) eadf6138.